https://doi.org/10.15388/vu.thesis.366
https://orcid.org/0000-0001-6629-7562

VILNIUS UNIVERSITY
CENTER FOR PHYSICAL SCIENCES AND TECHNOLOGY

Kazimieras Badokas

Remote epitaxy of GaN via graphene on GaN/sapphire templates by MOVPE

DOCTORAL DISSERTATION

Technological Science,
Materials Engineering (T 008)

VILNIUS 2022

The dissertation was prepared between 2018 and 2022 at the Institute of Photonics and Nanotechnology, Vilnius University. The research was supported by the Research Council of Lithuania (doctoral scholarships for academic achievements, No.: P-DAP-19-61, P-DAP-20-154). The research was also partially funded by the European Social Fund according to the activity "Improvement of researchers' qualification by implementing world-class R&D projects" of Measure No. 09.3.3-LMT-K-712, Contract No. LMT-K-712-01-0076.

Academic supervisor – Dr. Tadas Malinauskas (Vilnius University, Technological Sciences, Materials Engineering – T 008).

This doctoral dissertation will be defended in a public meeting of the Dissertation Defense Panel:

Chairman – Prof. Habil. Dr. Sigitas Tamulevičius (Kaunas University of Technology, Technological Sciences, Materials Engineering – T 008).
Members:
Dr. Renata Butkutė (Center for Physical Sciences and Technology, Technological Sciences, Materials Engineering – T 008),
Dr. Irmantas Kašalynas (Center for Physical Sciences and Technology, Physical Sciences, Physics – N 002),
Dr. Šarūnas Meškinis (Kaunas University of Technology, Technological Sciences, Materials Engineering – T 008),
Dr. Pawel Prystawko (Institute of High Pressure Physics of the Polish Academy of Sciences, Physical Sciences, Physics – N 002).

The dissertation shall be defended at a public meeting of the Dissertation Defense Panel at 2 PM on September 21, 2022, in meeting room D401 of the National Center for Physical Sciences and Technology.
Address: Sauletekio av. 3, Vilnius 10257, Lithuania.
Tel.: +370 264 9211; e-mail: office@ftmc.lt.

The text of this dissertation can be accessed at the library of Vilnius University, as well as on the website of Vilnius University:
www.vu.lt/lt/naujienos/ivykiu-kalendorius

https://doi.org/10.15388/vu.thesis.366
https://orcid.org/0000-0001-6629-7562

VILNIAUS UNIVERSITETAS
FIZINIŲ IR TECHNOLGIJOS MOKSLŲ CENTRAS

Kazimieras Badokas

Nuotolinė GaN epitaksija per grafeną ant GaN/safyro padėklų MOVPE metodu

DAKTARO DISERTACIJA

Technologijos mokslai,
Medžiagų inžinerija (T 008)

VILNIUS 2022

Disertacija rengta 2018–2022 metais Vilniaus universiteto Fotonikos ir nanotechnologijų institute. Mokslinius tyrimus rėmė Lietuvos mokslo taryba (paramos už studijų rezultatus registracijų Nr.: P-DAP-19-61, P-DAP-20-154). Eksperimentinė veikla iš dalies finansuota Europos socialinio fondo lėšomis (projekto Nr. 09.3.3-LMT-K-712), pagal dotacijos sutartį su Lietuvos mokslo taryba, sutarties Nr. LMT-K-712-01-0076.

Mokslinis vadovas – Dr. Tadas Malinauskas (Vilniaus universitetas, technologijos mokslai, medžiagų inžinerija – T 008).

Gynimo taryba:
Pirmininkas – Prof. habil. dr. Sigitas Tamulevičius (Kauno technologijos universitetas, technologijos mokslai, medžiagų inžinerija – T 008).
Nariai:
Dr. Renata Butkutė (Fizinių ir technologijos mokslų centras, technologijos mokslai, medžiagų inžinerija – T 008),
Dr. Irmantas Kašalynas (Fizinių ir technologijos mokslų centras, gamtos mokslai, fizika – N 002),
Dr. Šarūnas Meškinis (Kauno technologijos universitetas, technologijos mokslai, medžiagų inžinerija – T 008),
Dr. Pawel Prystawko (Lenkijos Mokslų akademijos Aukštų slėgių fizikos institutas, gamtos mokslai, fizika – N 002).

Disertacija ginama viešame Gynimo tarybos posėdyje 2022 m. rugsėjo mėn. 21 d. 14 val. Nacionalinio fizinių ir technologijos mokslų centro posėdžių salėje D401.
Adresas: Saulėtekio al. 3, Vilnius 10257, Lietuva.
Tel. Nr.: +370 264 9211, el. paštas: office@ftmc.lt.

Disertaciją galima peržiūrėti Vilniaus universiteto bibliotekoje ir VU interneto svetainėje adresu:
https://www.vu.lt/naujienos/ivykiu-kalendorius

ABBREVIATIONS

2D – two dimensional

V/III – flux ratio between group-V and group-III elements

AFM – atomic force microscopy (microscope)

CCD – charge-coupled device

CVD – chemical vapor deposition

DI – deionized

EBSD – electron backscatter diffraction

EDX – energy-dispersive X-ray spectroscopy

ELOG – epitaxial lateral overgrowth

EM – electromagnetic

FFT – fast Furrier transform

FIB – focused ion beam

FWHM – full width at half maximum

GO – graphene oxide

hBN – hexagonal boron nitride

HEMT – high electron mobility transistor

IoT – internet of things

IPA – isopropyl alcohol

LD – laser diode

LED – light-emitting diode

MBE – molecular beam epitaxy

$MgCp_2$ – bis(cyclopentadienyl)magnesium

MO – metalorganics

MOCVD – metalorganic chemical vapor deposition

MOVPE – metalorganic vapor phase epitaxy

MQW – multiple quantum wells

NBE – near-band-edge

ND – neutral density

*n*GaN – *n*-type gallium nitride

*p*GaN – *p*-type gallium nitride

PL – photoluminescence

PMMA – poly(methylmethacrylate)

POV – point of view

RMS – root mean square

RTA – rapid thermal annealing

SE – secondary electrons

SEM – scanning electron microscopy (microscope)

SLM – standard liter per minute

TEM – transmission electron microscopy (microscope)

TMDC – transition metal dichalcogenide

TMG – trimethylgallium

TRT – thermal release tape

*u*GaN – undoped gallium nitride

vdW – van der Waals

XRD – X-ray diffraction

CONTENTS

INTRODUCTION

Gallium nitride-based light-emitting devices have greatly influenced our lives throughout the days and nights for decades now [1]. LEDs in general lighting and backlighting systems have become ubiquitous, thanks to the pioneering of efficient blue-emitting diodes by Akasaki, Amano, and Nakamura around the 90s [2–4]. Moreover, GaN is currently on track to broad adoption in consumer power electronics [5]. The wide bandgap and high electron mobility, amongst other advantages, make GaN-based battery chargers smaller, more efficient, and capable of maintaining the desired characteristics even at elevated temperatures. That is why GaN is sometimes even called “the silicon of the future” [6].

The industry of flexible devices, wearables, and electronic skins (e-Skins) is also a good fit for III-Vs [7,8]. Sufficiently thin membranes of otherwise bulk semiconductor materials enable the fabrication of flexible devices – be it displays, sensors, power generators, or similar. However, to realize the full potential of such applications, thin membranes of GaN and other semiconductors should be stackable. Lift-off and transfer of thin membranes of dissimilar materials could be realized by peeling off the epitaxial films and stacking them just like bricks of Lego – an idea initially demonstrated for 2D materials [9] that can be extended to thin 3D membranes, as illustrated in Figure 1.

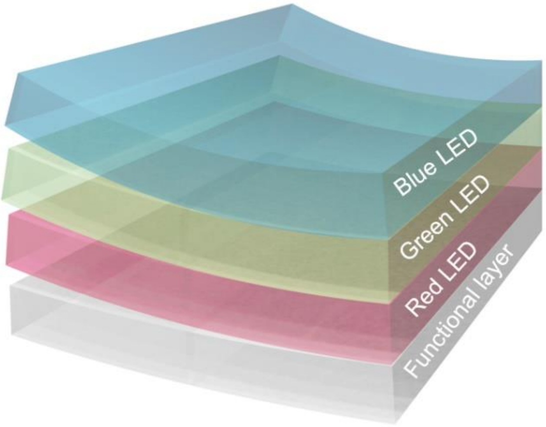

Figure 1. Illustration of flexible and stackable layers of sufficiently thin different-material semiconductor membranes.

Essentially all GaN-based devices have to be fabricated on substrates. Some substrates are cheap, while others are costly. Native substrates (bulk GaN) are the latter (Figure 2). Bulk GaN is lattice and thermal expansion matched to the epitaxial layer – translating into the best quality GaN-based devices. However, occasionally, epitaxial substrates become unnecessary or even interfere with the intended operation of the device after the active layers are formed. The lift-off of the grown films is a complicated solution due to the strong covalent bonding between the epitaxial layer and substrate.

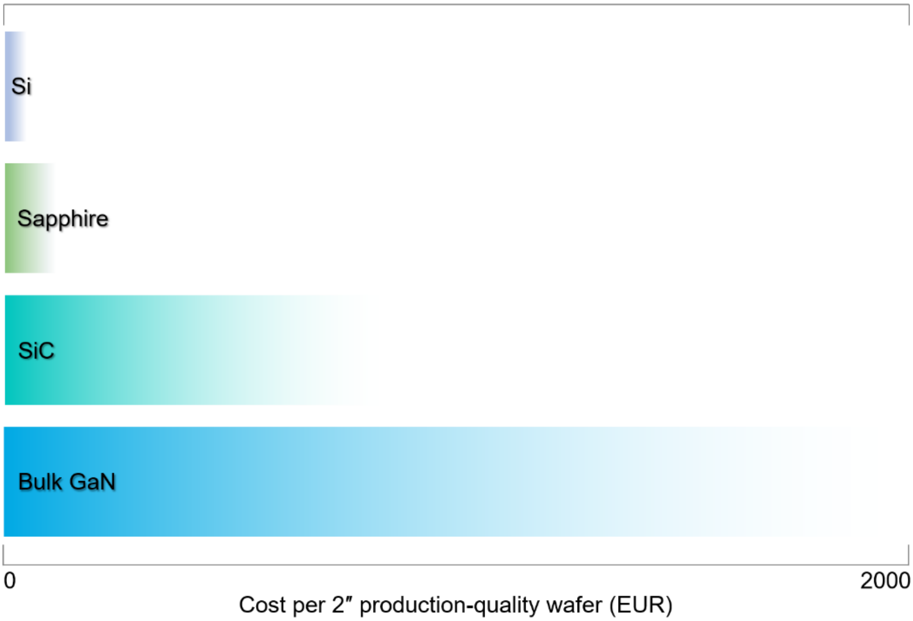

Figure 2. Cost per production-quality (non-dummy) 2-inch wafers from commercial suppliers as of spring 2022. Note that the exact price and suppliers are undisclosed due to the confidentiality of quotations.

Graphene – a "wonder" [10] monolayer of carbon – could be used to cover epitaxial substrate turning it into sort of a "copy machine" [11]. Essentially, graphene has a van der Walls surface, translating into the lack of dangling bonds. Thus, the growing crystalline epitaxial layer attaches to the monolayer graphene very weakly. The main advantage of such mild bonding is the facile epilayer release from the substrate after growth [12,13].

Another benefit of using graphene as an interlayer is its ability to transmit the "seeding" [14] potential from the substrate beneath for epitaxy. The seeding effect governs the atomic interactions between the substrate and the epitaxial layer through the monolayer [13]. Of course, if it is not too thick [14]. Because of the graphene-mediated interaction, epitaxial relation is preserved between the substrate and the epitaxial layer, manifesting in high-quality membrane fabrication and its possible subsequent release from the substrate (Figure 3). The concept of the seeded crystal growth through graphene was coined in 2017 as “remote epitaxy” [13], in contrast to the van der Walls epitaxy on purely van der Walls surface materials.

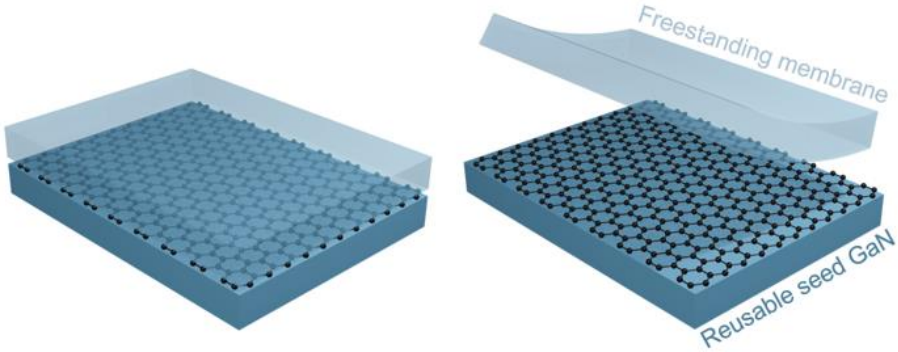

Figure 3. Graphene turns the substrate into a copy machine – an illustration of high-quality freestanding membrane exfoliation leaving behind a regrowth-ready bulk substrate.

In recent years, epitaxy on graphene-covered substrates and its benefits have been demonstrated for many diverse materials such as perovskites [15], GaAs [16], transition metal dichalcogenides [17] and oxides [18]. Distinct epitaxial substrates with both transferred as well as on-substrate formed graphene were demonstrated, including freestanding GaN [19], sapphire [20], and SiC [21]. However, there was a lack of experiments adopting wet-transferred graphene and GaN/sapphire templates for GaN remote epitaxy by the MOVPE process [22].

This work addressed the MOVPE process capabilities for the growth of GaN on wet-transferred graphene covering GaN/sapphire templates, which would ultimately extend to new functionalities and cost savings while preserving a high quality of GaN epitaxial technology.

NOVELTY AND AIM

At the time of the planning of scientific experiments, most of the peer-reviewed works were aimed at the demonstration of epitaxy on graphene-covered substrates involving bulk GaN and the transfer of epitaxial graphene from SiC (also known as the dry transfer of epitaxial graphene). Both materials were relatively costly when the idea for this work was conceived, and they still are. However, one of the primary targets of remote epitaxy is cost reduction achieved by implementing reusable substrates [11]. At the same time, a few additional improvements became clear to help drive the process price tag down even more.

First, expensive and limited-size bulk GaN substrates could be replaced with GaN/sapphire templates by growing a thick GaN epitaxial layer by the MOVPE process on a 2-inch diameter sapphire substrate. This approach significantly reduces the cost of the template, up to 10 times or even more. It also expands the substrate size availability, as the industry now uses sapphire substrates of at least 6-inch in diameter. Second, a less obvious benefit is the *in-house* control of GaN properties, such as surface morphology.

Finally, the wet transfer of graphene is also significantly cheaper. Transfer-ready, CVD graphene is available in various sizes of at least 1 square inch (Figure 4), while epitaxial graphene on SiC usually comes in smaller sizes and is significantly more expensive. Of course, the most notable tradeoff is its quality, as was already demonstrated in the scientific literature [23].

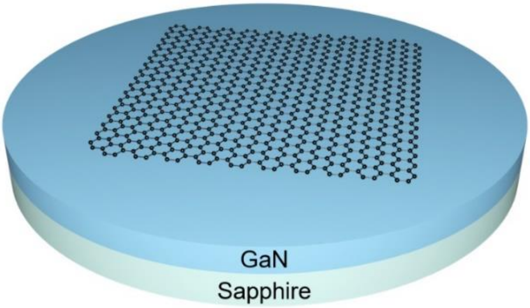

Figure 4. Illustration of wet-transferred graphene and a GaN/sapphire template as a cost-effective alternative. Similar structure templates were used in this work.

Nevertheless, the industry itself should ultimately decide the balance between cost and quality of the process. The main goal of this work was to investigate the suitability of GaN/sapphire templates covered with wet-transferred graphene for the remote epitaxy of GaN by the MOVPE process. The insights and thorough investigation of template preparation, graphene transfer, nucleation, GaN film growth, and peeling-off of the membrane should be valuable for further remote epitaxy development and refinement.

The following tasks were performed to achieve the main goal in this work:

1. GaN/sapphire template fabrication and evaluation of its suitability for remote epitaxy of GaN by MOVPE process.

2. Wet and dry transfer of graphene and its quality evaluation.

3. Determination of suitable MOVPE process recipe for high-quality GaN epitaxial layer fabrication utilizing remote epitaxy.

4. Exfoliation of GaN membrane fabricated by remote epitaxy of GaN by MOVPE process.

5. Evaluation of the suitability of multiple graphene layers for remote epitaxy of GaN by MOVPE process.

LAYOUT

This thesis is composed of an introduction to the topic and this work itself; an overview of the novelty, aim, and tasks; a comment on the layout; a description of thesis statements; an outline of the publications, presentations, and training during the approximate period of PhD studies; details about personal contribution to this work; a chapter (No. 2) providing the background about the materials and experimental techniques used in this study; a chapter (No. 3) outlining the experimental results, including methodical information, in the order of which the experiments were conducted (for the most part); an outlook for the future; conclusions; references; a short comment on the technological aspects of experimental work; acknowledgments; a summary in Lithuanian; and articles included in this work (if possible).

This dissertation is based on two peer-reviewed publications [P1] and [P2] by Badokas *et al.* and closely resembles these publications. Part of the experimental results and insights were discussed in the coursework reports and thesis of the bachelor's student D. Augulis, who was supervised by K. Badokas (2021–2022). All the detailed contributions are outlined in the relevant chapter of this work.

The permission to reuse published material was granted from *IOP Publishing* regarding the article [P1]. The article [P2] was published in an open-access journal under the *Creative Commons Attribution License (CC BY)*, permitting the reuse of the published material.

THESIS STATEMENTS

1. GaN/sapphire template covered with wet-transferred graphene allows remote epitaxy of GaN by MOVPE process and facilitates the exfoliation of the high-quality GaN membrane.

2. Remote epitaxy of high-quality GaN and graphene preservation is achieved by a two-step MOVPE process consisting of GaN seed growth at 700 °C and subsequent lateral coalescence at 1075 °C.

PUBLICATIONS, PRESENTATIONS, AND WORKSHOPS

The author of this dissertation has co-authored 12 peer-reviewed publications listed in the *WoS* database, as well as presented or significantly contributed to more than 30 conference presentations during his scientific career. The most significant publications, presentations, and relevant workshops from 2018 to 2022 are listed in the following subchapters.

Publications included in this work

[P1] K. Badokas, A. Kadys, D. Augulis, J. Mickevičius, I. Ignatjev, M. Skapas, B. Šebeka, G. Juška, and T. Malinauskas, "MOVPE growth of GaN via graphene layers on GaN/sapphire templates", Nanomaterials **12**(5), 785 (2022).

[P2] K. Badokas, A. Kadys, J. Mickevičius, I. Ignatjev, M. Skapas, S. Stanionytė, E. Radiunas, G. Juška, and T. Malinauskas, "Remote epitaxy of GaN via graphene on GaN/sapphire templates", J. Phys. D **54**, 205103 (2021).

Publications not directly related to this work

[p1] D. Dobrovolskas, A. Kadys, A. Usikov, T. Malinauskas, K. Badokas, I. Ignatjev, S. Lebedev, A. Lebedev, Y. Makarov, and G. Tamulaitis, "Luminescence of structured InN deposited on graphene interlayer", J. Lumin. **232**, 117878 (2021).

[p2] V. Novickij, R. Stanevičienė, R. Gruškienė, K. Badokas, J. Lukša, J. Sereikaitė, K. Mažeika, N. Višniakov, J. Novickij, and E. Servienė, "Inactivation of bacteria using bioactive nanoparticles and alternating magnetic fields", Nanomaterials **11**(2), 342 (2021).

[p3] T. Čeponis, K. Badokas, L. Deveikis, J. Pavlov, V. Rumbauskas, V. Kovalevskij, S. Stanionyte, G. Tamulaitis, and E. Gaubas, "Evolution of scintillation and electrical characteristics of AlGaN double-response sensors during proton irradiation", Sensors **19**(15), 3388 (2019).

[p4] D.-I. Moon, B. Kim, R. Peterson, K. Badokas, M.-L. Seol, D. G. Senesky, J.-W. Han, and M. Meyyappan, “A single input multiple output (SIMO) variation-tolerant nanosensor”, ACS Sens. **3**(9), 1782–1788 (2018).

Presentations related to this work

[C1] K. Badokas, A. Kadys, D. Augulis, J. Mickevičius, I. Ignatjev, M. Skapas, B. Šebeka, G. Juška, and T. Malinauskas, “GaN epitaxy on graphene-covered substrate”, Graphene Week, Munich, Germany, September 5–9, 2022, poster presentation by K. Badokas.

[C2] K. Badokas, D. Augulis, A. Kadys, J. Mickevičius, I. Ignatjev, B. Šebeka, M. Skapas, G. Juška, and T. Malinauskas, “MOVPE of GaN on graphene-covered GaN/sapphire templates”, Open Readings, Vilnius, Lithuania, March 15–18, 2022, oral presentation (online) by K. Badokas.

[C3] D. Augulis, K. Badokas, A. Kadys, B. Šebeka, I. Ignatjev, J. Mickevičius, and T. Malinauskas, “Exfoliation of GaN thin films grown by MOVPE via graphene”, Open Readings, Vilnius, Lithuania, March 15–18, 2022, poster presentation by former student D. Augulis under K. Badokas supervision.

[C4] K. Badokas, A. Kadys, D. Augulis, I. Ignatjev, G. Juška, J. Mickevičius, and T. Malinauskas, “MOVPE epitaxy of group-III nitrides via few-layer graphene on GaN/sapphire templates”, MRS Fall Meeting, Boston, MA, USA, virtual event, November 29–December 08, 2021, oral presentation (online) by K. Badokas.

[C5] K. Badokas, A. Kadys, D. Augulis, I. Ignatjev, G. Juška, J. Mickevičius, and T. Malinauskas, “Remote epitaxy of GaN via few-layer graphene”, Advanced Materials and Technologies, Palanga, Lithuania, August 23–27, 2022, poster and oral presentations by K. Badokas, best poster presentation award received.

[C6] D. Augulis, K. Badokas, A. Kadys, S. Strumskis, I. Ignatjev, G. Juška, J. Mickevičius, and T. Malinauskas, "The influence of graphene surface treatment on remote epitaxy of gallium nitride", Open Readings, Vilnius, Lithuania, March 16–19, 2021, poster presentation by former student D. Augulis under K. Badokas supervision.

[C7] K. Badokas, A. Kadys, T. Grinys, M. Kolenda, S. Stanionytė, M. Skapas, J. Mickevičius, and T. Malinauskas, "Remote epitaxy of GaN via graphene", APROPOS 17, September 30–October 01, 2020, Vilnius, Lithuania, invited talk given by supervisor Dr. T. Malinauskas.

[C8] K. Badokas, A. Kadys, I. Ignatjev, G. Juška, J. Mickevičius, P. Ščajev, and T. Malinauskas, "Galio nitrido MOCVD epitaksija per grafeną", LNFK-43, October 03–05, 2019, Kaunas, Lithuania, oral presentation by K. Badokas.

[C9] K. Badokas, A. Kadys, I. Ignatjev, G. Juška, J. Mickevičius, P. Ščajev, and T. Malinauskas, "Graphene as an interlayer for MOCVD epitaxy of GaN", Graphene Week, September 23–27, 2019, Helsinki, Finland, poster presentation by K. Badokas.

[C10] K. Badokas, A. Kadys, I. Ignatjev, G. Juška, J. Mickevičius, P. Ščajev, and T. Malinauskas, "MOCVD epitaxy of GaN via graphene", Advanced Materials and Technologies, August 19–23, 2019, Palanga, Lithuania, poster presentation by K. Badokas.

[C11] K. Badokas, A. Kadys, T. Grinys, M. Kolenda, S. Stanionytė, M. Skapas, J. Mickevičius, and T. Malinauskas, "MOCVD epitaxy of GaN via graphene", EW-MOVPE 18, April 16–19, 2019, Vilnius, Lithuania, poster presentation and conference co-organization by K. Badokas.

[C12] K. Badokas, A. Kadys, and T. Malinauskas, "MOCVD epitaxy of III-nitrides via graphene", Graphene Study, March 03–08, 2019, Obergurgl, Austria, poster presentation by K. Badokas.

[C13] K. Badokas, “Group-III nitrides and graphene: an introduction”, EUIMWP PhD and ECI meeting under COST action, January 31–February 01, 2019, Ljubljana, Slovenia, oral presentation by K. Badokas.

[C14] K. Badokas and T. Malinauskas, “MOCVD growth of III-nitride semiconductors by van der Waals epitaxy via graphene”, Graphene Study, July 01–06, 2018, Hindås, Sweden, poster presentation by K. Badokas.

Presentation not directly related to this work

[c1] K. Badokas, T. Malinauskas, D. Paipulas, A. Kadys, T. Grinys, and E. Gaubas, “GaN p-i-n diodes for radiation detection”, IWN, November 11–16, 2018, Kanazawa, Japan, poster presentation by K. Badokas.

Relevant training

[W1] Graphene Study (Winter), March 03–08, 2019, Obergurgl, Austria.

[W2] Graphene Study (Summer), July 01–06, 2018 Hindås, Sweden.

Training and meetings not directly related to this work

[w1] 69th Lindau Nobel Laureate Meeting, June 30–July 5, 2019, Lindau, Germany.

[w2] Silicon photonics workshop organized by *LioniX*, February 26–March 1, 2019, Enschede, Netherlands.

CONTRIBUTION

The author of this thesis was responsible for the majority of the experimental work and analysis of results. However, it would hardly be possible to own and master such a variety of experimental techniques. Thus, part of the work was delegated to or conducted in collaboration with colleagues as follows:

- Conceptualization, planning, and major discussions – K. Badokas, Dr. A. Kadys, and Dr. T. Malinauskas.

- Preparation of manuscripts for publications – K. Badokas, Dr. J. Mickevičius, and Dr. T. Malinauskas.

- Graphene transfer – K. Badokas and D. Augulis (under K. Badokas supervision).

- MOVPE growths – Dr. A. Kadys, K. Badokas, and D. Augulis (under Dr. A. Kadys supervision).

- Raman shift measurements – Dr. I. Ignatjev, K. Badokas, and D. Augulis (mostly spectra analysis, under K. Badokas supervision).

- TEM measurements – Dr. M. Skapas, K. Badokas, and Dr. A Selskis (sample preparation for TEM).

- SEM measurements – K. Badokas, D. Augulis (under K. Badokas supervision), and E. Radiunas.

- AFM measurements – G. Juška, D. Augulis (under K. Badokas supervision), and K. Badokas (mainly data analysis).

- Metal deposition – K. Badokas (sputtering), Dr. T. Grinys (e-beam), Dr. B. Šebeka (electrochemistry), and D. Augulis (all experiments under K. Badokas supervision).

- XRD measurements – Dr. T. Malinauskas, Dr. S. Stanionytė, and D. Augulis (under Dr. T. Malinauskas supervision).

- Photoluminescence measurements – Dr. J. Mickevičius.

- Hall effect measurements – Dr. A. Kadys.

1. BACKGROUND

1.1. Materials

Gallium nitride and graphene were the primary materials investigated in this work. Both of these materials have already attracted significant attention from the research community as well as the industry. Extensive investigation over the years has generated lots of information about the properties and the fabrication *know-how*. This subchapter is dedicated to an overview of the basic properties and fabrication techniques of GaN and graphene.

1.1.1. Gallium nitride

Gallium nitride is one of the most widely used compound semiconductors of all group-III nitrides. GaN has a direct wide bandgap of around 3.4 eV, making it suitable for both electronic and photonic applications. GaN compounds are fabricated primarily by the MOVPE process. Although, the MBE process is also used. A commonly used wurtzite crystal structure has lattice constants a = 3.19 Å and c = 5.19 Å [24] (Figure 5). GaN growth in polar *c*-direction is the most common approach. However, crystal growth in semi- and non-polar directions attracts significant attention as well. The quantum-confined Stark effect can be reduced or totally avoided resulting in an increase in device efficiency [25].

Currently, GaN is widely used as a light-emitting material in blue and white LEDs (in combination with appropriate phosphors). The compositional modification by the addition of indium enables the controlled shift of emission wavelengths to the green spectral region as well as the formation of InGaN quantum wells for enhanced device efficiency.

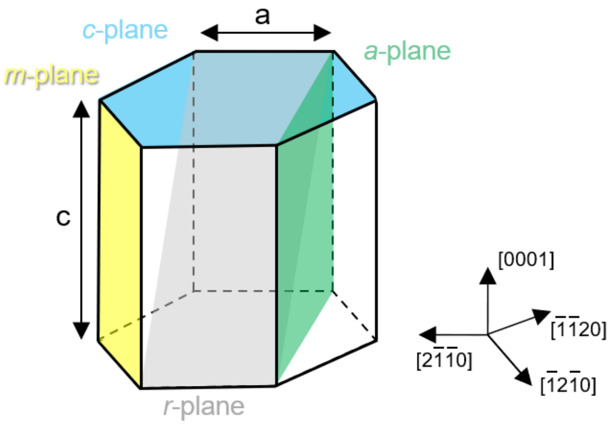

Figure 5. Hexagonal crystal structure of GaN. Common planes, lattice constants, and crystallographic directions are marked accordingly.

Compared to the widely popular silicon, gallium nitride possesses a wider bandgap (1.1 eV for Si compared to 3.4 eV for GaN) and demonstrates higher electron mobility (considering GaN HEMTs). These advantages make GaN-based battery chargers smaller and more efficient in contrast to Si-based ones dominating the market for decades. The time will tell if GaN-based chargers will replace Si-based ones. However, GaN-based electronics will at least remain a complementary technology to Si for high-power applications. The wide bandgap of GaN also means that devices can withstand elevated temperatures and harsh operational environments [26].

GaN is also a piezoelectric material meaning that GaN crystals respond to mechanical stress with voltage induction across the active layer of the device, which can be utilized for specific applications [27]. The “ambient mechanical energy” [28] of various motions can be harvested by piezoelectric generators and stored or used to power low-power ubiquitous IoT sensors and small-scale wearable devices. Flexible GaN thin film-based piezoelectric generators were already demonstrated, highlighting the potential of GaN-based power generation [28].

The rapid development of 5G data transmission infrastructure also pushes conventional silicon-based technology to its limits. A new generation of high-power and high-frequency transistors is anticipated to help develop the recently booming small satellite communication network. GaN-based HEMTs are already implemented in similar technologies and are expected to play one of the key roles in future space and telecommunication devices [29,30].

GaN potential is extensively explored for numerous sensing applications as well. These include, but are not limited to: humidity [31], pressure [32], pH [33], and gas [34]. More exotic uses include GaN-based memristors – devices engineered as artificial neural networks [35]. Thus, despite being best known in the industry of LEDs, gallium nitride and its compounds have considerable potential in many distinct areas. Scalable preparation of freestanding and transferable membranes as well as further cost reduction at the manufacturing side, are likely to catalyze even wider adoption of GaN-based consumer devices.

1.1.2. Graphene

In inorganic compounds, carbon atoms could be arranged in various ways translating into diverse structures – namely, allotropes of carbon. For example, one of the best-known allotropes of carbon is diamond, primarily used as a fashion accessory. Diamond also has its rather niche applications in science and technology [36]. Graphite is a widely popular pencil material. Interestingly, it was also utilized as a neutron moderator in older nuclear reactors [37]. There are also fullerenes – a class of ball-like carbon structures composed of an ordered sphere-like arrangement of tens of carbon atoms [38]. The carbon nanotubes are structured as rolled sheets of one carbon layer taken out from graphite. Such carbon nanotubes have many applications. One of the examples is gas sensing [39]. A pristine single sheet of carbon taken out from the surface of graphite makes up a two-dimensional, Nobel Prize-winning material – graphene [40].

Graphene is one of the many discovered allotropes of carbon. It is composed of a single layer of hexagonally-arranged carbon atoms (Figure 6) [41]. To better understand how thin a sheet of graphene is, the following example could be considered. A carbon layer has a specific surface area of one side equal to 1315 m^2/g [42]. A soccer field has an area of around 8000 m^2 for international matches [43]. Thus, it would take only a few grams of graphene sheet to completely cover the entire football field with it [44].

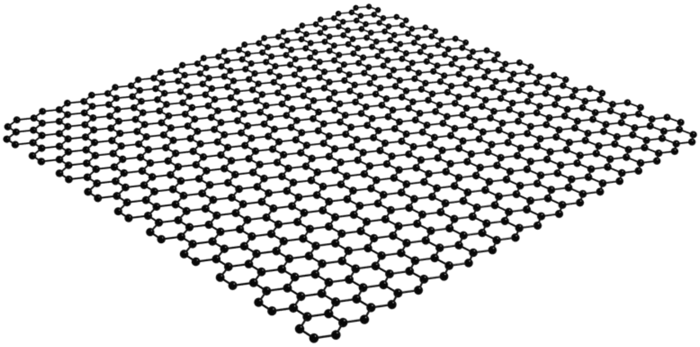

Figure 6. Structure of monolayer graphene as a representation of connected carbon atoms.

Graphene was first theoretically described in scientific literature as early as 1947 while exploring the “band theory of graphite” [45]. The name graphene was suggested only later [46]. After that, from time to time, there were experiments conducted to produce graphene sheets, but single sheet isolation proved to be unsuccessful. It was even thought that such a thin monolayer of carbon could be unstable under ambient conditions, rendering it practically impossible to isolate monolayer graphene at all. But the situation in carbon science suddenly changed for the better. In 2004, graphene layers from the bulk graphite were separated by the most straightforward technique – the adhesive tape method [40]. After six years, scientists were awarded the Nobel Prize in Physics for “the ground-breaking experiments regarding the two-dimensional material graphene” [47].

The interest in graphene and related layered 2D materials was highlighted by the European Union’s Flagship research initiative (*Graphene Flagship*), launched back in 2013. A billion euros investment in the science of graphene was expected to unleash the potential and take the novel technology from laboratories to consumers [48].

The electronic properties of graphene have been extensively investigated since 2004. Monolayer, when pristine, is a zero-gap material [41]. Regarding its band structure, valence and conduction bands of graphene maintain the shape of conical surfaces. These surfaces contact each other at a particular point called the Dirac point. Thus, no bandgap is introduced into the monolayer graphene system. In the absence of external influence, the valence band of graphene is fully occupied, and the conduction band is fully depleted of electrons. However, the situation can be modified in a controlled manner by placing monolayer graphene into a field-effect transistor configuration [41,49]. The electrically controlled bias of such a device can shift the Fermi level either to the valance or to the conduction bands. In this way, charge carriers are introduced, modifying the conductivity of monolayer graphene.

In low-temperature measurements, charge carrier mobility in graphene reached at least 200 000 $cm^2V^{-1}s^{-1}$, considering suspended graphene sheets [50]. In typical practical applications, charge carrier mobility values are lower, as the present supporting substrates could contribute to the charge carrier scattering process. However, graphene is still well suited for high-speed, high-frequency electronics [51]. The conductivity of graphene is susceptible to the adsorption of other species to its surface, making the monolayer suitable for high-sensitivity gas detection [52].

Monolayer graphene has no color, and its light absorption is as low as approximately 2.3 % in the visible spectrum [53]. As a zero-gap material, graphene is not well suited as an emitter. However, it was demonstrated that the bandgap in graphene could be induced with an electric field if the bilayer graphene structure is fabricated [54]. Also, some optoelectronic applications can take advantage of both the interband and the intraband optical transitions in graphene [55].

The particular sigma-type (σ) bonding between carbon atoms situated nearby results in the surprising mechanical strength of monolayer graphene. Because of this strength, graphene attracts significant attention both as a free-standing material and a reinforcement component in various composites [56]. The “intrinsic strength” of the defect-free graphene is related to the “maximum stress” (for example, “nanoindentation”) of the suspended graphene membrane before it breaks apart [57]. The strength of the graphene monolayer could be illustrated by considering the following situation: a 1 m^2 suspended hammock made from pristine monolayer graphene would be able to hold a mass of around 4 kg without breaking apart (Figure 7). As the mass of an average cat is approximately 4 kg, the practically transparent pristine monolayer graphene hammock would be able to hold a cat [58].

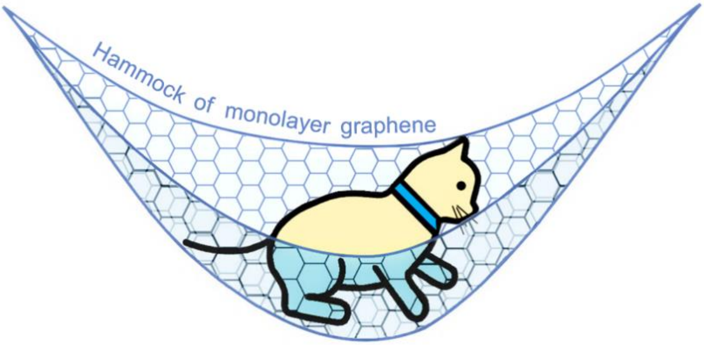

Figure 7. Illustration of remarkable strength of graphene – hypothetically, an almost invisible hammock made from the monolayer would be able to hold an average cat. An image was produced according to the NobelPrize.org press release illustration [58].

The high in-plane thermal conductivity of graphene was reported, exceeding the value of 1000 $Wm^{-1}K^{-1}$ [59]. In comparison, copper is known to have a thermal conductivity of approximately 400 $Wm^{-1}K^{-1}$, meaning that a single sheet of graphene conducts heat at least a few times better than copper metal [60]. However, graphene has a significantly large anisotropy for heat conductivity depending on heat conduction direction. The anisotropy could be explained by relatively weak van der Waals interactions between neighboring planes or other surrounding materials. The difference in thermal conductivity according to the direction makes graphene suitable for uses in both heat-sinking applications, where high conductivity is desirable as well as thermoelectric applications, where relatively low thermal conductivity is required [59].

Extraordinary thermal and mechanical properties make graphene a suitable material for composites, where it can be used to strengthen the structural elements and help dissipate heat. For example, a well-known commercial aircraft manufacturer was reported to be working on graphene composites for a leading edge structure, as the leading edge of the wing of an aircraft must withstand mechanical stress and effectively dissipate heat due to friction in high-speed conditions [61]. A shoemaking company has been offering graphene-enhanced rubber in its shoes, as the addition of graphene was reported to increase the durability of the shoe and allow a better grip of the outsole [62].

The perfect monolayer graphene is considered one of the thinnest physical barriers for any molecules to pass. The electron cloud surrounding the monolayer restricts mass permeation except for hydrogen [63]. Proton permeability through graphene was demonstrated. In the case of molecular hydrogen, H_2 was shown to dissociate near the monolayer surface, resulting in the proton flipping through the graphene in a two-step process [64]. The mass transport restriction of graphene for any atoms other than hydrogen is an essential feature for epitaxy on graphene-covered substrates.

Since the first isolation of monolayer graphene in 2004, numerous fabrication methods have been well researched, developed, and improved [65]. The top-down approaches include mechanical exfoliation of monolayers [66], oxidation of graphite, and the exfoliation of GO [67], as well as liquid-phase exfoliation [68]. The mechanical exfoliation method was well suited to the initial demonstration of lifted-off monolayers and is still suitable for some very specific applications. Mechanical exfoliation is a slow process and results in a very low yield of 2D material. However, the quality of graphene fabricated by the latter method is relatively good. On the other hand, GO and liquid phase exfoliation fabrication results in high-yield production at the quality expense [65].

Bottom-up synthesis of graphene is the primary choice whenever scalable production and high-quality monolayers are necessary. The production of graphene by bottom-up approaches includes two main methods: CVD growth of graphene on metal foils [69] and carbonization (also named simply “graphitization” or “graphitization of the surface of SiC”) [70] (Figure 8). In this work, graphene layers prepared by both bottom-up production methods were used.

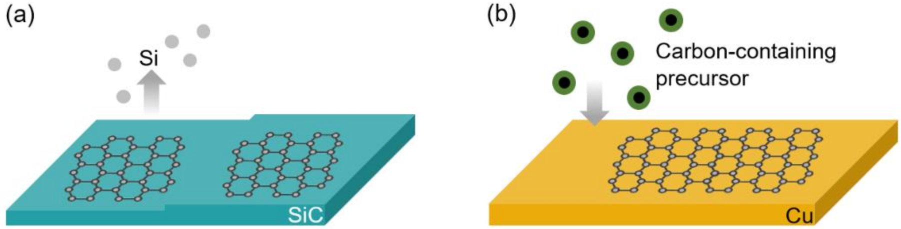

Figure 8. Schematic representation of bottom-up fabrication of graphene by: SiC substrate carbonization (a) and chemical vapor deposition on Cu foil from the carbon-containing source (b).

Epitaxial graphene on SiC is formed by thermal treatment of SiC substrate at high temperature (usually > 1000 °C) in an inert gas atmosphere or in a vacuum. Si atoms tend to sublimate from the surface of SiC if the right conditions are set, leaving only C atoms behind. Such an approach to carbon layer formation by SiC heating was initially demonstrated back in 1965 [71]. Currently, the fabrication of epitaxial graphene on SiC is a method of choice when high-quality graphene monolayers are necessary. However, this fabrication technique requires very expensive and limited-size SiC crystals making it rather pricey [65]. Graphitized SiC substrates were recently demonstrated to be suitable for GaN remote epitaxy on their own by utilizing the „graphene buffer layer on SiC as a release layer" [21]. In case graphene on other substrates is necessary, the dry transfer approach can be used to transfer it. Such transfer requires a particular metal layer (for example, Ni) deposited on epitaxial graphene on a SiC wafer [72]. A dry transfer method of epitaxial graphene on SiC will be discussed in depth in the Experimental chapter of this work.

CVD graphene growth on copper foil is a relatively good-quality, large area, and inexpensive graphene production method. It is based on carbon source decomposition at high temperatures and an assembly of carbon atoms into a graphene structure on the metal foil surface [73]. Cu foil is the primary choice for CVD synthesis, as Cu has a relatively low solubility of carbon atoms, and it has demonstrated a required catalytic effect for graphene formation [65,74].

Monolayer graphene formed on the surface of metal foil usually has to be transferred elsewhere. The transfer of CVD-grown graphene is a relatively well-explored topic – the wet transfer technique is used. In such transfer, graphene is usually spin-coated with PMMA (or similar polymer) supporting layer, and the metal foil is etched away. Afterward, graphene can be placed onto an arbitrary substrate by transfer in water. A wet transfer method of CVD graphene will be discussed in depth in the Experimental chapter of this work.

Wet transfer graphene from two commercial suppliers was used for the remote epitaxy experiments: *Graphenea*, Inc. and *ACS Materials*, LLC. Graphene on SiC substrate was purchased from *Graphensic* Ab.

1.2. Methods

Although only the MOVPE growth was employed to fabricate GaN/sapphire templates and GaN films, diverse characterization methods were used to evaluate the quality of GaN and graphene as well as to reveal the underlying formation mechanisms. This subchapter is dedicated to an overview of the basic principles of GaN growth on graphene-covered substrates, the MOVPE process, and characterization methods – TEM, SEM, AFM, Raman spectroscopy, photoluminescence, and XRD.

1.2.1. Metalorganic vapor phase epitaxy

Metalorganic vapor phase epitaxy, also commonly known as metalorganic chemical vapor deposition, is a technology targeted at thin-film crystalline epilayer production at scale. The MOVPE process is now at the heart of ubiquitous photonic and electronic device manufacturing. The development of MOVPE technology, at least for III-V compounds, began in the late 1960s. The works were pioneered by Manasevit *et al.* [75]. A few years after the successful demonstration of "single-crystal gallium arsenide on insulating substrates" [76], epitaxy of diverse III-V compounds was also reported [77]. The potential of MOVPE technology was highlighted in the successful fabrication of photonic devices, such as "room-temperature $Ga_{(1-x)}Al_xAs$/GaAs double-heterostructure lasers" [78].

MOVPE process efficiency and relatively good epilayer uniformity were the main driving factors for the technological improvements partially by "trial and error" throughout the following years [79]. As MOVPE equipment was very complex, the process parameters together with the reactor design had to be constantly improved. One of the achievements was the introduction of a rotating-disk reactor design [79], followed by the implementation of multi-wafer capability [80]. After all the improvements made early on, scalable and relatively cost-effective device production was achieved, especially for the GaAs and related compound semiconductors that helped shape the world of photonics and electronics that we have today.

The fabrication of high-quality GaN-based epilayers by the MOVPE process still had challenges to overcome in the early 1990s. Primarily the low quality of the deposited GaN and insufficient *p*-type conductivity. The introduction of aluminum nitride [4] or low-temperature GaN nucleation [2] layers in

MOVPE growth of GaN led by Akasaki, Amano, and, independently, Nakamura translated into the substantial improvement in crystalline quality of the GaN epilayers. Moreover, upgrades in MOVPE reactor design by introducing a “subflow” of gases also improved the technology of that time [2]. Finally, successful Mg doping in *p*-type GaN layers was demonstrated, giving the green light for efficient blue-emitting diodes [81]. Altogether, these innovations were the final steps toward the wide commercialization of blue LEDs, which are nowadays fabricated by the MOVPE process at an industrial scale. The impact of GaN fabrication technology was highlighted by the Nobel Prize in Physics in 2014, awarded for “the invention of efficient blue light-emitting diodes which has enabled bright and energy-saving white light sources” [82].

Two types of MOVPE reactors are commonly used. Depending on the direction of flow of gaseous species, reactors are either horizontal or vertical type. The latter MOVPE system was used in this study. It was *AIXTRON* brand close-coupled showerhead reactor, with the capacity of carrying three wafers, each 2-inch diameter in size.

From an engineering point of view, the MOVPE reactor is composed of several main components: a cooled showerhead, a susceptor, heating elements for the susceptor, and a gas distribution system, including bubbler cylinders submerged into controlled-temperature baths. The reactor is also equipped with additional systems, occupying most space in a lab. Those are primarily used to transfer the substrates, supply the power for the heating elements and maintain proper coolant flow during the MOVPE process. The schematic representation of the MOVPE reactor used in this work to grow GaN templates and epilayers is shown in Figure 9.

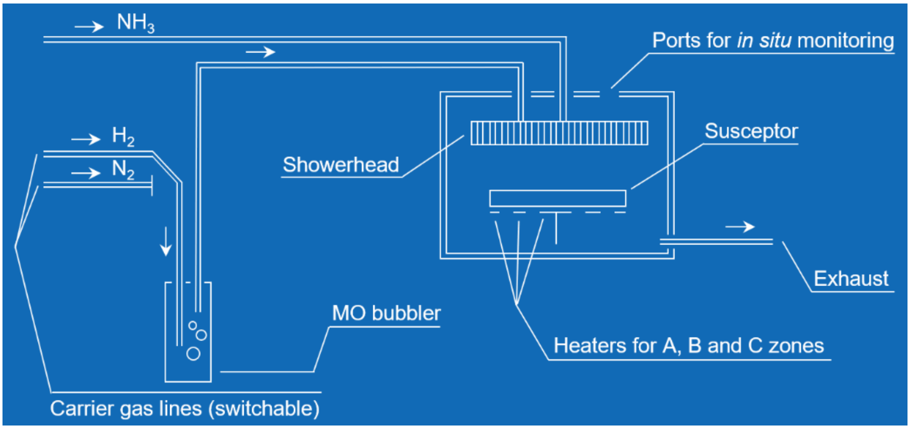

Figure 9. Schematics of showerhead-type vertical MOVPE reactor configured for GaN growth using H_2 as MO carrier gas. An MOVPE system of this type was used in this study.

First of all, the MOVPE process requires specific carrier gas to transport the metalorganics. Nitrogen and hydrogen were available as carrier gases in this work. TMG was used as a metalorganic source of Ga. MO is generally stored in a liquid phase inside a specially designed storage cylinder called the bubbler. The selected carrier gas enters the bubbler through the inlet manifold and produces MO-saturated vapor. Subsequently, MO and carrier gas are introduced to the reactor chamber right above the heated susceptor. The distance between the showerhead and the susceptor was kept constant at 11 mm in this work. Numerous mass flow controllers are responsible for precisely controlling the amount of gas introduced to the growth chamber. The showerhead is composed of many precisely drilled holes for the gaseous species introduction. Also, there are few ports for *in situ* monitoring by laser reflectometry system. In this work, the precursor for N was NH_3. Group-III and group-V precursors do not mix until the introduction to the reaction chamber, and the showerhead is constantly cooled to avoid the prereactions at its surface. The heating of the susceptor is controlled by three independent heating elements responsible for three heating zones – A, B, and C. The susceptor rotates during the entire growth process. The rotation speed was set to 1 rev./s and kept constant in the MOVPE processes related to this work. The gaseous species extraction system is responsible for maintaining the desired pressure in the reaction chamber and extracting the MOVPE process byproducts.

During MOVPE growth, many complex chemical and physical reactions occur [83]. The general reactions include the decomposition of gas-phase precursors due to pyrolysis, the adsorption of group-III and group-V elements, the kinetic process on the surface (i. e., surface diffusion and desorption), and nuclei formation at the energetically favorable sites as well as subsequent film growth.

1.2.2. Remote and van der Waals epitaxy

The epitaxy of GaN on van der Waals surface of graphene is still a topic of debate, at least when it comes to naming it. Recently, it was defined as “direct van der Walls epitaxy”, “graphene-assisted epitaxy”, “remote epitaxy”, “quasi-van der Waals epitaxy”, and “thru-hole epitaxy”, to name a few descriptions throughout the literature [13,19,84–88]. Note that the use of some names appeared in non-peer-reviewed publications and should be considered with caution. The uncertainty on process labeling might be attributed to the still inconclusive results reported. For example, graphene was described to exhibit suppressed nucleation [89] and decomposition due to the influence of the underlying substrate [90]. However, the findings of this work and successful demonstration of exfoliation and theoretical evidence [14,19,20,P1,P2] lead to a conclusion that two distinct GaN growth modes on graphene should be considered – vdW and remote epitaxy.

The mechanism of van der Waals growth was proposed decades ago as a way to overcome the obstacles posed by the high lattice mismatch of the substrate and epilayer [91]. In such a case, the nucleation and growth of crystalline layers are guided not by the formation of covalent bonds but rather by the relatively weak van der Waals interactions, as depicted in Figure 10. The main disadvantage of vdW epitaxy is that without periodic interaction guidance, each seed is arbitrarily aligned [14]. The lack of azimuthal alignment translates into textured epilayers and, subsequently, poor quality of the device.

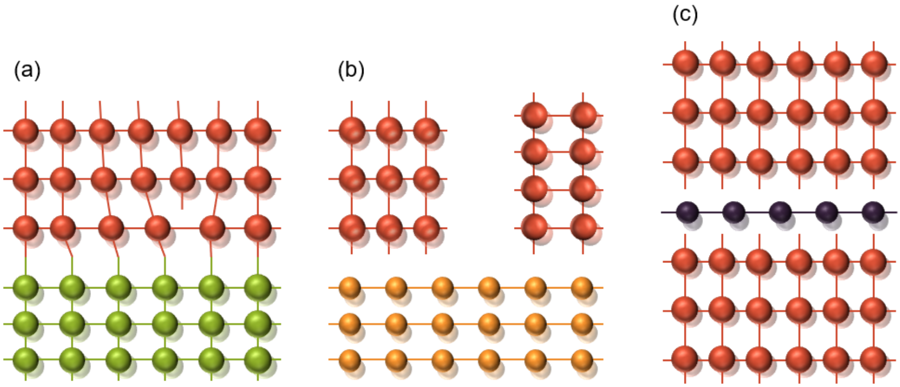

Figure 10. Schematic representation of crystal formation on different substrates. Conventional deposition on lattice-mismatched substrate results in poor quality epilayer (a), epitaxy on van der Waals surface allows strain-free epitaxy; however, it lacks proper guidance for the epilayer (b). Remote epitaxy on 2D material solves the latter problem by enabling the interaction through the interlayer while prohibiting covalent bond formation (c). An illustration is made partially adapted from literature [91,92].

However, monolayer graphene was shown to be "partially transparent to wetting" [93], meaning that the atomic interactions through it are possible [94]. The exact mechanism influencing remote interaction between the substrate and the epilayer is still debatable. For example, "charge transfer" [95] via graphene was recently proposed, considering monolayer graphene. The transparency of 2D material covering the sufficiently ionic substrate translates to another kind of growth mode – remote epitaxy. The ionicity of 3D material must be carefully considered to determine whether remote epitaxy is possible, as the transmittance of the potential field must be sufficient [14]. The differences between vdW and remote epitaxies in epilayer formation are schematically represented in Figure 11.

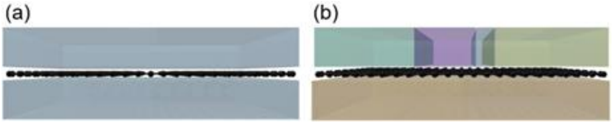

Figure 11. GaN epitaxy on monolayer graphene covered GaN representing remote epitaxy mode on GaN substrate (a) and GaN epitaxy on an insufficiently ionic substrate covered with monolayer graphene resulting in vdW epitaxy mode (b). Different orientations of crystallites are color-coded.

Moreover, graphene on GaN was shown to permit atomic interactions for up to two monolayers [14]. The expected growth modes as a function of the number of graphene layers for GaN on GaN are illustrated in Figure 12. The possible advantages of remote epitaxy on bilayer graphene were also explored in this work.

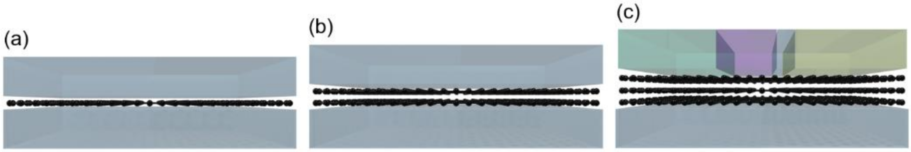

Figure 12. GaN epitaxy on GaN substrate covered with varying number of graphene layers: monolayer graphene (a), bilayer graphene (b), and trilayer graphene (c). Different orientations of crystallites are color-coded.

MOVPE and MBE are the epitaxial growth techniques suitable for GaN and related compound epilayer formation by remote epitaxy [22]. However, the MOVPE process is commonly employed, partially due to its broad adoption in III-N device manufacturing.

1.2.3. Transmission and scanning electron microscopy

The curiosity to see the world hidden from the naked eye, either by being too small or too far, drove humanity to invent magnifying devices. Antonie van Leeuwenhoek pioneered microscopy, while Galileo Galilei managed to look deep into the night sky around the 17th century. However, as scientific experiments advanced, the fundamental hurdle of microscopy was encountered. It was the diffraction limit formulated by Ernst Abbe [96]. This limit relates to the resolution of a microscope with the lights in use to observe an object of interest. Currently, the resolution of ordinary optical microscopes is down to 200 nm. Far too low to watch the world at the atomic scale.

Scanning electron microscopy and transmission electron microscopy both are microscopic analysis techniques utilizing electron interaction with a sample instead of light as a source of information [97]. A high electron-accelerating voltage of up to a few hundred kilovolts combined with the concept of de Broglie wavelength enables the observation of sub-nanometer features using SEM and sub-atomic features using TEM. At the heart of the microscope is the electron gun. For example, the very sharp Schottky-type tungsten tip is heated by passing a high current through it and promoting the emission of electrons. The electrons are then guided to the preferred direction by maintaining a potential difference between the gun and surrounding electrodes (or the walls of the electron gun chamber). The beam of electrons is subsequently focused by a series of EM coils and guided to the surface of a sample under investigation. In the case of SEM, the image is acquired by scanning the surface point by point and mapping the intensity of the signal at each scanned point of the investigated area.

Numerous types of specific information about the sample can be obtained from its interaction with an accelerated electron beam [98], as is illustrated in Figure 13. The primary information carriers in SEM are secondary emitted electrons and backscattered ones. The latter electrons come out of the sample after interacting with the nuclei of atoms in the specimen. The signal generated from the detection of backscattered electrons carries the information on elemental composition because of the size of nuclei correlation with the scattering intensity. For example, higher atomic number elements would backscatter electrons more intensely, producing brighter areas in a scanned image compared to lower atomic number atoms. Another essential signal carrier in SEM analysis is secondary emitted electrons. The material itself produces the secondary emitted electrons after the specimen interaction with an electron beam. The secondary emitted electrons typically have lower energy than backscattered ones. Thus, they are emitted from the vicinity of the surface of a sample and are interpreted as the carriers of the topographic information of the sample. In this work, secondary emitted electron detection was used to acquire the images provided. Moreover, energy-dispersive X-ray spectra rely on X-rays produced after electron beam-sample interaction. EDX is used to determine the precise material composition of the specimen. *Apollo CamScan 300* and *HITACHI SU8230* SEM equipment operating at variable voltages was used in this study.

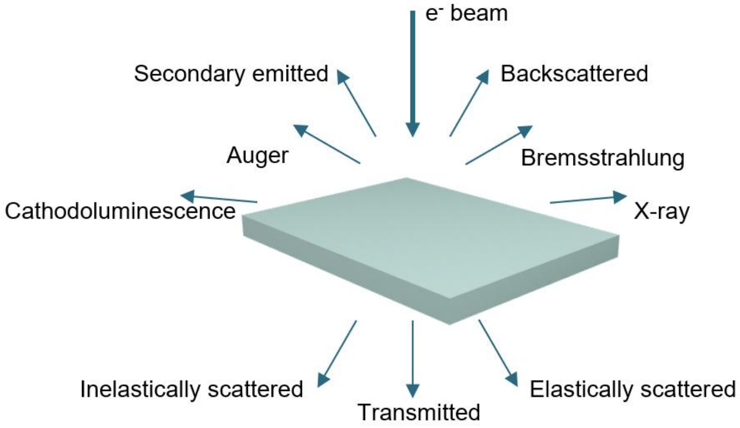

Figure 13. The result of electron beam interaction with the bulk specimen under investigation.

The beam manipulation and focusing system above the specimen holder in TEM are similar to that of SEM. The main difference lies in signal generation. In TEM analysis, images are constructed from the transmitted electrons [99].

The specimens must be prepared for TEM imaging as they must be sufficiently thin to transmit the electron flux. Typically, less than 100 nm of sample thickness is necessary to obtain an image. Thus, the specimens investigated in this work had to be prepared in a separate procedure. As only a small portion of the sample can be studied at once, TEM imaging always presents some uncertainty that the researchers must be aware of. For example, a relatively small volume may represent the outlier data. The volume of interest of graphene samples was selected further from the edges of graphene, where fewer inhomogeneities occur during monolayer cut and transfer, to minimize the likelihood of an error in this work. Also, TEM imaging was used only as a supplementary investigation technique to confirm the data obtained by other means of investigation.

The preparation of samples started with metal deposition before sample cutting with Ga ions in a FIB device. Outlined is a relatively standard sample preparation procedure usually implemented when thin samples from the bulk are necessary [100,101]. The metal layer on top is used to avoid slope formation and leave a steep GaN wall edge, as the Ga ion beam retains a spatial Gaussian distribution profile of ions and otherwise would result in an uneven edge. Afterward, the volume around the sample was ablated using a focused Ga ion beam. Trenches of approximately 20 μm width were formed.

Further ablation followed trench formation by tilting the sample until it was partially detached at the bottom. A specimen was then placed onto the sample holder and further thinned to periodic 50 nm zones while keeping the thicker areas in between as supporting columns. The final TEM investigation-ready specimen is shown in image Figure 14. For the sample preparation in this study, FIB equipment *Helios NanoLab 650* with Ga ion source was used. More details could be found in the literature [102].

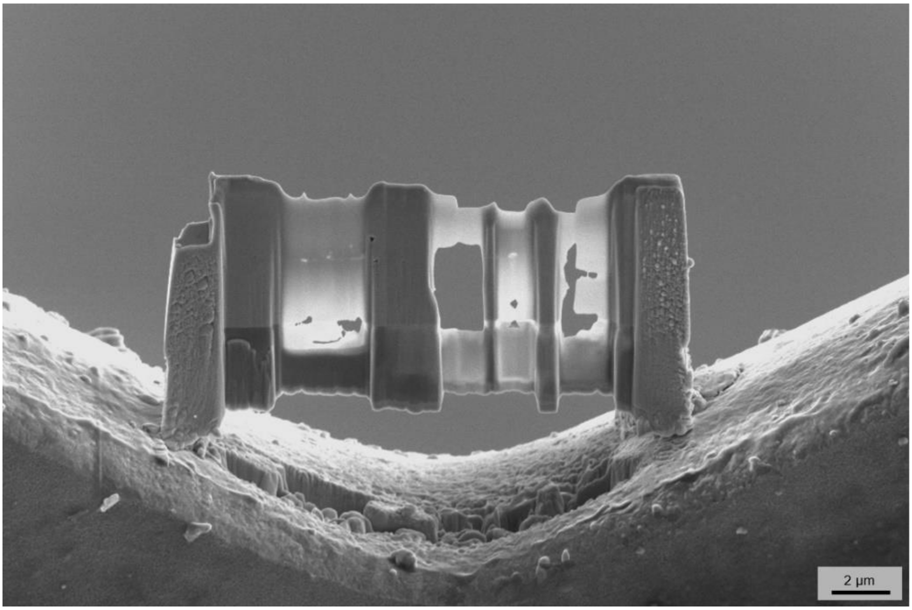

Figure 14. TEM imaging-ready sample (GaN/graphene/GaN/sapphire) on holder after FIB preparation at the Center for Physical Sciences and Technology.

TEM images were acquired using *FEI Tecnai G2 F20 X-TWIN* equipment operating at 200 kV.

1.2.4. Atomic force microscopy

Atomic force microscopy is the surface probing technique. The primary information about the specimen comes from the surface-tip interactions and is governed by the topography of the sample in the imaging mode [99]. The AFM technique was introduced by Binning *et al.* in the 1980s [103] and has been a vastly popular surface characterization method since then. It was even shown to be capable of individual atom manipulation [104].

Nanonics MultiView 1000 AFM system was used to evaluate the surface roughness in this work. The cantilever with a sharp tip made of CrAu alloy was positioned near the sample surface to conduct the measurements. The surface of the samples was raster-scanned while keeping the height constant through a feedback loop (*intermittent mode*) and mapping the changes in the height of a sample. Acquired AFM scans were analyzed using freely distributed WSxM software [105]. Root mean square values of surface feature height were calculated, representing the average specimen surface height deviations from the mean height [106]. In this case, the smaller the surface RMS value, the smoother the surface was. Surface smoothness was a vital parameter to consider, especially before graphene transfer.

1.2.5. Raman spectroscopy

Raman spectroscopy is a light scattering technique used to probe molecular vibrations, molecular rotations, and intermolecular interactions. Raman scattering was demonstrated experimentally in the late 1920s by Sir Chandrasekhara Venkata Raman [107]. Initially, the newly observed phenomenon was denoted as “a new type of secondary radiation or modified scattered radiation” [107]. The process was later named after its inventor. The potential impact of this technique was also highlighted by awarding Sir C. V. Raman with Nobel Prize in Physics in 1930 [108].

In the Raman scattering event, incident light photons interact with molecules inelastically, contrary to Rayleigh scattering. The latter is an elastic process meaning that the photon energy is strictly conserved. However, Raman scattered photons could change the energy and the direction of travel. A constant energy characteristic of the scattering medium is either lost or acquired in the light scattering event. A redshift of photons is denoted as Stokes Raman scattering (resulting energy of scattered light is calculated as $h\nu_0 - h\nu_{vib(1)}$, where $h\nu_0$ represents the energy of incoming photon and $h\nu_{vib(1)}$ is the energy difference between the ground and the first vibrational states of a scattering medium) and blueshift – anti-Stokes Raman scattering (resulting energy is calculated as $h\nu_0 + h\nu_{vib(1)}$) [109]. The simplified graphical representation of the light scattering process and the possible pathways is shown in Figure 15.

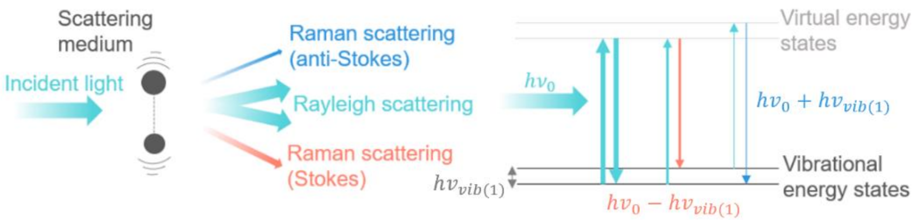

Figure 15. Light scattering process. Simplified light scattering process of a diatomic molecule (on the left). A corresponding energy diagram of the light scattering process (on the right). The thickness of the arrows represents exaggerated relative intensities of scattered light.

In the early days of the experiments, Raman spectra were challenging to measure as the intensity of light scattered by the sample is generally very low compared to the power of the excitation source. However, Raman spectroscopy is a widely implemented spectroscopic technique nowadays.

In spectral analysis, it is convenient to calculate Raman shift in wavenumbers:

$$\Delta\tilde{\nu} = \frac{1}{\lambda_0} - \frac{1}{\lambda_R}, \tag{1}$$

where $\Delta\nu$ is the Raman shift expressed in wavenumbers, λ_0 is the wavelength of excitation light and λ_R is the wavelength of scattered light. For convenience, when λ is measured in nm, the result of equation (1) should be multiplied by 10^7 to calculate the Raman shift value in cm^{-1}, which is the standard unit of Raman shift in spectroscopy. However, Raman shifts are computed and represented automatically and by specialized software in modern Raman spectroscopy-dedicated systems, as was the case in this work.

Raman spectroscopy is employed for many research and development applications. For example, characterization of strain in semiconductors [110], defect analysis in semiconductors [111], determination of the composition of semiconductors [112], as well as life sciences [113] and cosmology [114]. Importantly, it is a versatile tool for graphene characterization as Raman spectroscopy is accurate, non-destructible, and scalable for both laboratory research and commercial uses [115]. From a historical point of view, Raman spectroscopy has been used to study graphite since the 1970s [116]. Soon after discovering graphene, Raman spectroscopy became the method of choice for the investigation of both monolayer “graphene and graphene layers” [117].

Raman spectrum of graphene layers (as well as bulk graphite) typically demonstrates three distinctive features in an approximate range of 1300–2800 cm^{-1}. The first Raman-related feature is a defect-related mode D appearing at around 1340 cm^{-1}. The appearance of D mode is expected in the presence of lattice defects. Thus, in case defect-free graphene lattice is under investigation, D mode is not visible as it is induced by the “breathing vibration” of “aromatic carbon rings” [118]. Such vibration is Raman forbidden in a perfect monolayer [118].

The following first-order mode is an in-plane vibrational mode manifesting itself at around 1588 cm^{-1} and denoted G. The G mode in the graphene Raman spectrum is related to the “stretching vibration” of two neighboring sp^2 hybridized carbon atoms [118]. Finally, the second-order overtone of D mode appears at around 2680 cm^{-1} and is named 2D [118]. This mode is always present in the Raman spectrum of graphene as the most intense one, in case monolayer graphene is present. Although the mechanism of the 2D mode is not directly related to the G mode, historically, it was named G’. The latter notation can still be found in the literature [119]. The typical Raman spectrum of graphene and visualization of G and 2D mode-resulting vibrations is represented in Figure 16. Note that particular Raman shifts of some modes are dependent on the excitation wavelength [120].

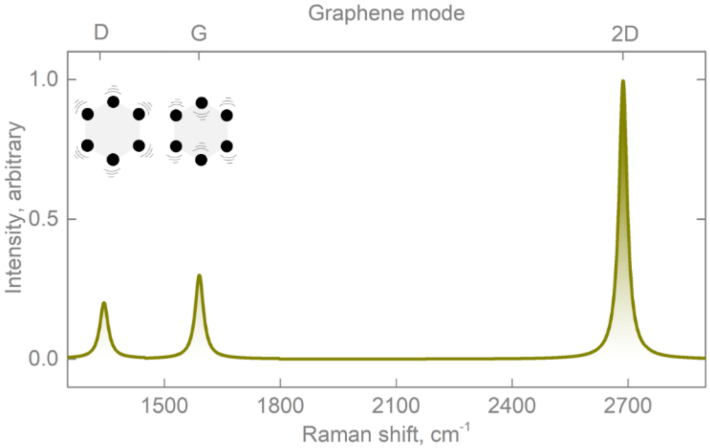

Figure 16. Representative Raman spectra. Representative Raman spectra of defective graphene. Three prominent features D, G, and 2D are identified. The corresponding motion of carbon atoms in aromatic ring configuration is shown.

In this work, samples were investigated using two Raman spectroscopy systems:

1. Confocal Raman imaging microscope *Renishaw inVia* with a 532 nm laser excitation source. Further details can be found in Badokas *et al.* [P1].

2. Confocal Raman imaging microscope *WITEC alpha 300R* with a 532 nm laser excitation source. Further details can be found in Badokas *et al.* [P2].

The table-top spectroscopy setup includes various components [121]. A specimen is positioned on a movable microscope stage, and the region of interest is selected using a microscope. The ROI selection can be made by either looking through the ocular of the microscope or in a user interface of the control program. Excitation light comes from a laser. The beam of the laser is focused on the selected ROI. The scattered light is collected with the same microscope used to focus the laser light. Rayleigh scattering rejection (notch) filters must be in place to transmit only the relatively weak Raman scattered light by blocking the intense laser light.

In some cases, holographic notch filters could be used. An adjustable slit is in place to control the intensity of the Raman signal. Diffraction grating disperses the scattered light focused on a CCD for signal acquisition. In practice, equipment design and optical elements vary from system to system. However, the principal components are represented in Figure 17 and closely reassemble the equipment used in this work.

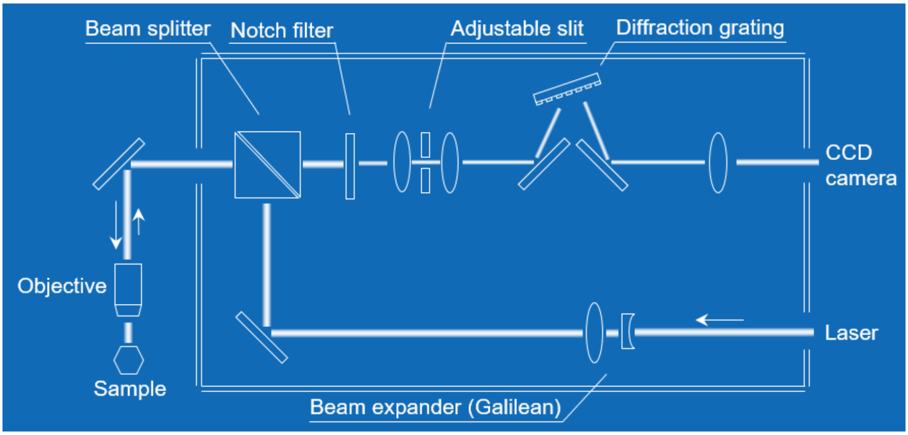

Figure 17. Schematics of Raman spectroscopy setup closely reassembling the one used in this study. An illustration is made according to the schematics from literature [121].

1.2.6. Photoluminescence

Photoluminescence is a process of light emission of the material, usually a semiconductor, after its excitation with light. Photoluminescence excitation spectrum can be used to determine the approximate bandgap of the material, its composition, internal strain, impurities, and related properties [122,123]. A typical experimental setup consists of an excitation source (laser emitting higher photon energy than the bandgap of material under investigation), guiding optics, a monochromator, and a CCD camera or a photomultiplier.

The experimental setup used in this study is outlined in Figure 18. Measurements were performed at room temperature. A continuous-wave He-Cd laser emitting at 325 nm was used for GaN sample excitation. The luminescence spectra were analyzed and recorded by a double monochromator *Jobin Yvon HRD-1* and a photomultiplier *Hamamatsu*.

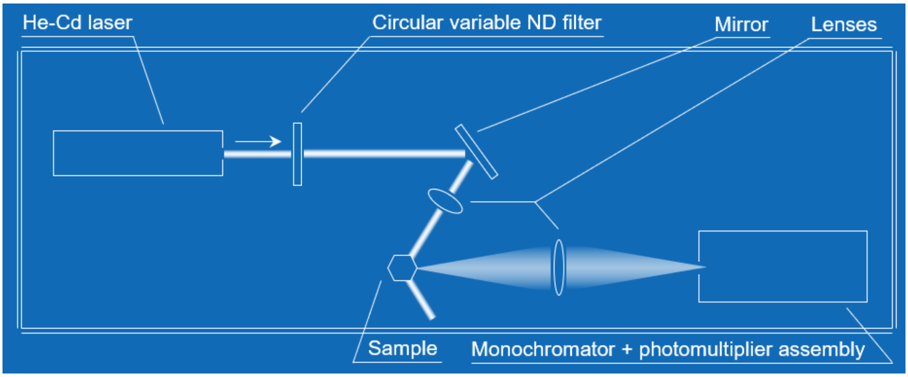

Figure 18. Schematics of photoluminescence measurement setup closely reassembling the one used in this study.

1.2.7. X-ray diffraction

X-ray diffraction is an essential tool to determine the crystallographic structure of the material. Max von Laue first observed the diffraction phenomenon after X-ray interaction with crystalline material, and in the year 1912 was awarded Nobel Prize in Physics [124]. However, the methodology of X-ray diffraction was developed mainly by W. H. Bragg and W. L. Bragg. Scientists also shared Nobel Prize in Physics three years later [125].

Quantitatively the X-ray diffraction is described with the Bragg equation:

$$2d \sin \theta = n\lambda, \tag{2}$$

where d is the distance measured between atomic planes, θ is an angle of incidence of X-ray, n is an integer number representing the diffraction order, and λ is the wavelength used to probe the specimen. The diffraction signal is most intense at θ angles satisfying the Bragg equation (equation (2)), as the atoms in atomic planes act as X-ray diffracting points. Note that the angle 2θ is usually measured experimentally [126]. The principle of X-ray diffraction as the wave reflection from the atomic planes is represented in Figure 19.

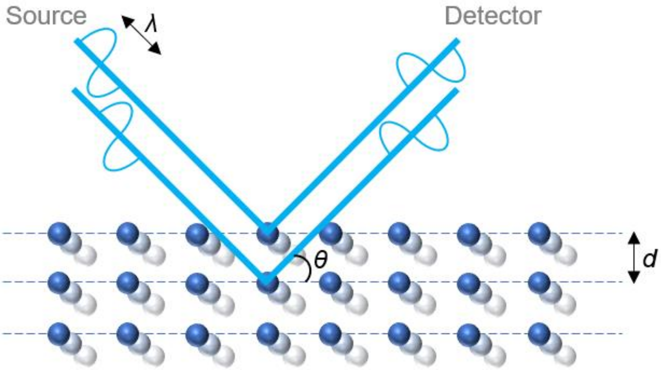

Figure 19. Representation of interference after X-ray diffraction from a periodic array of atoms. Annotation corresponds to the Bragg equation.

In practice, numerous types of scans are available depending on the type of sample (powder or bulk crystal) and the type of information (material composition, strain, orientation, defectivity, and similar) intended to be acquired. For example, pole figures could be measured to determine precisely the orientation of crystallites in space [127]. The map of a polar figure is acquired by rotating the sample azimuthally (around the surface normal direction) as well as changing its tilt while keeping the X-ray source and detector at a certain angle. The rocking curve measurements determine the diffraction peak broadening caused by crystal lattice distortions. In this work, ω scans were used to calculate an FWHM value of diffraction peaks. In such scans, the detector and the X-ray source are kept stationary at an angle of interest while the sample is rotated about the tilt (ω angle) axis. Furthermore, the twist of *m*-planes of GaN (Figure 5) could be evaluated by performing φ-scan. This is done by utilizing the in-plane diffraction geometry and determining the FWHM of such a diffraction peak [128].

In this work, X-ray measurements were conducted using *Rigaku SmartLab* equipment.

2. EXPERIMENTAL

The MOVPE process and membrane exfoliation had to be thoroughly investigated and optimized whenever possible to prepare the ground for novel GaN functionalities and achieve cost savings while preserving the high crystalline quality of the epitaxial layer. This chapter outlines all the main experiments and investigation results in the order that they were conducted (for the most part), emphasizing the preparation of template, the graphene transfer, suitability of monolayer in high-temperature growth, investigation of epitaxial GaN thin films on graphene, exfoliation of the membrane, transfer of more than one layer of graphene and, consequently, the GaN film epitaxy on more than one layer of graphene.

2.1. Preparation of template

For the remote epitaxy of GaN by MOVPE process on the graphene-covered GaN, the first challenge was to fabricate GaN/sapphire template. The approach of template fabrication was chosen as the most economically viable solution, considering the high cost of bulk GaN substrate available, as was discussed in the Introduction chapter. It also became a perfect starting point for getting *hands-on* experience with complex MOVPE process equipment.

Each workday of epitaxy started with the rather tedious but necessary care of the MOVPE reactor. The process chamber had to be baked at 1300 °C in a hydrogen atmosphere for 30 minutes to ensure that most of the contaminants from previous growths were etched away. The baking was followed by mechanical scrubbing and vacuuming of the susceptor and showerhead. The planned MOVPE growth of GaN proceeded when the visual inspection of dust particles was successfully passed. As the growth process in the MOVPE reactor used in this study was fully automatic, an operator only needed to write a program in a dedicated software environment outlining all the steps (e.g., when to purge gas lines, which bubbler to choose, what gas flow rate to maintain, and similar settings). Some of the parameters in a recipe were known from previous experience, and some were equipment-unique or previously calibrated. The remaining settings were chosen for each designed structure specifically.

For the following graphene transfer experiments, GaN layers were grown by MOVPE process on the 2-inch (5.08 cm) *c*-plane (surface normal direction [0001]) sapphire substrates with a surface miscut angle of 0.25–0.35° toward the *m*-axis, as it was beneficial for GaN nucleation [129]. For the MOVPE growths, the first process was the rector chamber purge with N_2 gas, as it ensured the removal of any dust residues left during wafer handling in the glove box. Afterward, the temperature was ramped to over 1000 °C, and the sapphire substrate was annealed under an H_2 gas atmosphere for 10 min. This process ensured that most of the contaminants were removed from the surface of sapphire, and oxygen was also partially removed to permit the formation of a nitride layer. Eventually, the GaN film was grown using a multi-step growth recipe, including the deposition of the low-temperature nucleation and the subsequent GaN film growth at an elevated temperature of 1075 °C.

A set of samples were fabricated, including unintentionally doped and slightly Si-doped (resulting in *n*-type) GaN films. It was previously observed that slightly Si-doped samples exhibited smoother surface morphology than the undoped (or unintentionally doped – *u*GaN) ones. To confirm the previous observation, around 5 µm of both doped and undoped GaN films on sapphire were prepared by the MOVPE process and investigated by AFM (Figure 20). Hall effect measurements revealed carrier densities of approximately 10^{16} cm^{-3} and 10^{17} cm^{-3} for *u*GaN and *n*GaN samples, respectively.

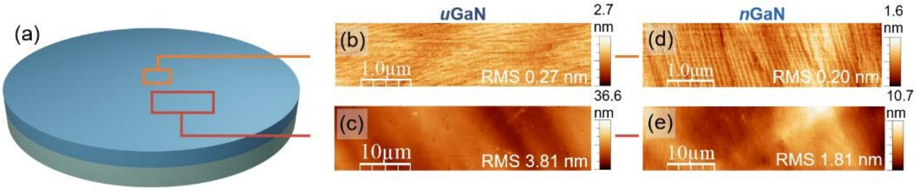

Figure 20. Schematic representation of GaN/sapphire template (a). AFM scans of unintentionally doped (b) and (c), and Si-doped (d) and (e) surfaces of GaN/sapphire template. Surface RMS values are indicated in each AFM scan accordingly.

As expected, the surface smoothness of the *n*GaN representative sample was slightly better, with a surface RMS value of 0.20 nm. In comparison, the *u*GaN sample exhibited a surface RMS value of 0.27 nm in a 1 µm × 5 µm scan area. A larger surface area scan revealed an even more significant difference (Figure 20). RMS value of doped GaN surface was 1.81 nm, while undoped GaN – 3.81 nm. It should be noted that dust particles on the surface might have impacted the RMS value obtained from the 10 µm × 50 µm area scan. Nevertheless, an overall smoother *n*GaN recipe was chosen to fabricate the

GaN/sapphire template for subsequent graphene transfer. The origin of Si doping influence on the surface of GaN film is out of the scope of this thesis.

Usually, MOVPE equipment was well under load for various growths. Thus, thorough planning of experiments was crucial. Sometimes, prepared GaN/sapphire templates had to be kept for an extended period before graphene transfer and the final GaN epitaxial layer deposition. In that case, the GaN/sapphire template *renewal* procedure was carried out, covering the GaN/sapphire template with approximately 100 nm of additional GaN film. This step was intended to clean the surface oxide layer formed, if any.

The final version of the GaN sapphire template was composed of a relatively thick Si-doped GaN film grown using a multi-step protocol (as outlined earlier) at the reactor pressure of 150 mbar, while keeping the V/III flux ratio of 700. GaN template thickness was estimated to be around 3.1 µm. The thickness of the template was later confirmed by TEM imaging (discussed later in the subchapter GaN growth on monolayer graphene). The surface of the final GaN template was relatively smooth, exhibiting a surface RMS value of 0.2–0.3 nm (not shown here).

2.2. Transfer of monolayer graphene

A transfer of graphene was arguably one of the critical steps for a successful remote epitaxy. It was also a relatively well-explored topic – many groups have employed dry and wet procedures for some time. As the author of this thesis had no technological capabilities or *know-how* in manufacturing graphene, monolayers had to be supplied from elsewhere. A few companies provided graphene commercially at the time of initial experiments. Thus, it was decided to evaluate three suppliers (named Graphene A, Graphene B, and Graphene C) and determine the best graphene suiting the needs of this work, as the transfer protocols and process cost varied significantly.

Graphene A was transferred by first soaking the sponge made of fabric holding the PMMA/graphene *sandwich* in place. The sponge was moistened by applying DI water droplets at the corners of the sponge. The soaked PMMA/graphene/sponge structure was dipped into room temperature DI water, and PMMA/graphene was left to float freely for a few hours. The dipping was particularly challenging as layer roll-up and air bubble trapping had to be prevented. DI water was left to a standstill overnight before the transfer of graphene to reduce the risk of air bubble trapping, as it was expected to produce tears in the monolayer during the PMMA cleaning step.

Next, the GaN/sapphire template was put beneath the floating PMMA/graphene. The floating structure was *fished* as close to the center of the template as possible. Eventually, the PMMA/graphene was left to dry naturally for 10 min and then baked in the controlled environment oven for half an hour at 100 °C in the air atmosphere. The PMMA was etched away by dipping the graphene-covered template into preheated (40 °C temperature) acetone and later into preheated (40 °C temperature) IPA solutions. Acetone and IPA baths were stirred by hand from time to time for around 45 min during the PMMA etching step. The sample was rinsed with DI water and dried by gently blowing with N_2 gas to ensure minimal surface contamination. As a final step, it was further dried in the controlled environment oven for 15 min at 50 °C in the air atmosphere. The stop-motion picture of the transfer process is provided in Figure 21.

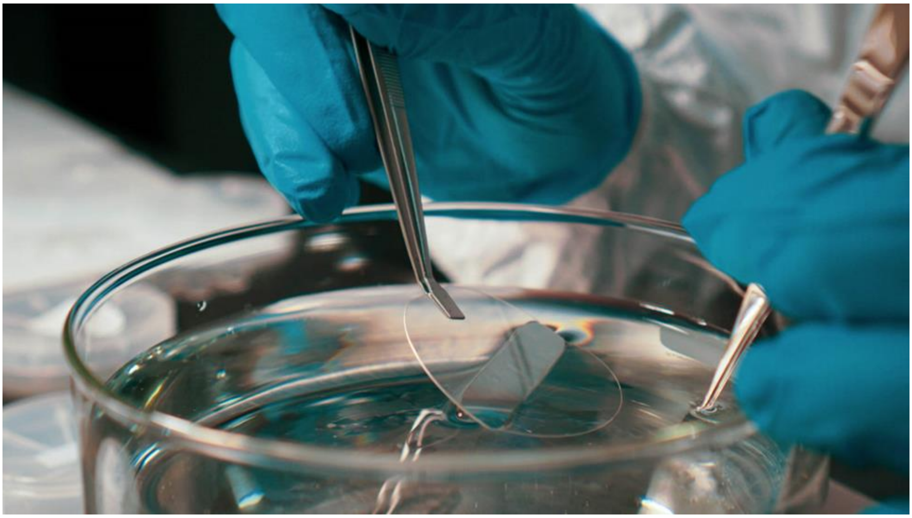

Figure 21. Picture of monolayer graphene transfer onto GaN/sapphire template by the author of this work during the wet transfer procedure.

Graphene B was provided in 1 in^2 (6.45 cm^2) and 1 cm^2 films. According to the supplier, it was CVD synthesis monolayer graphene with no less than 95 % surface coverage. As a transfer-ready product, graphene was *sandwiched* between special paper (or thin plastic) film and PMMA polymer film, acting as handling and supporting layers. In the remote epitaxy of GaN experiments, graphene was transferred as a 1 in^2 or 1 cm^2 sheet (as provided by the supplier), or a 1 in^2 sheet was cut into slices of 1.3 cm × 0.8 cm or 1.3 cm × 1.3 cm. A wet transfer procedure was employed to transfer the graphene. The process was very similar to the Graphene A transfer and PMMA cleaning. Although slightly different.

Firstly, the PMMA/graphene was placed into DI water and left floating on the surface of the water freely for around 5 to 10 min. The GaN template was carefully put beneath the floating polymer/graphene slice with tweezers. By pulling the template out of the water, graphene/PMMA was placed as close to the center part of the GaN/sapphire template as possible. The template with graphene was then left to dry in the air until all the water had evaporated. It took approximately half an hour for the graphene/PMMA to fully flatten and firmly adhere to the GaN/sapphire template.

Secondly, the sample was put in a controlled environment oven and heated at a temperature of 150 °C under an N_2 atmosphere for 30 min. Eventually, the oven chamber was evacuated. The sample was further stored for 24 h at room temperature in a vacuum. The latter step was necessary to avoid the graphene/PMMA detachment and was recommended by the manufacturer.

Finally, the polymer supporting the graphene was dissolved by keeping the sample in preheated acetone solution for 45 min at 40 °C and subsequently rinsing in preheated isopropyl alcohol for another 45 min at 40 °C. Both solutions were gently stirred by hand from time to time to dissolve the PMMA more effectively. To ensure that minimal surface contamination was achieved, the sample was rinsed with DI water and dried by gently blowing N_2 gas. The dried sample was annealed for approximately 8 hours in a controlled environment oven at 300 °C under a vacuum condition. This step was necessary to guarantee that most organic surface residues were decomposed and desorbed, exposing the pristine monolayer graphene.

Samples were investigated using optical microscopy to confirm the high quality of the transfer procedure and spot errors. As graphene was known to absorb around 2.3 % of visible light, contrasting areas were observed under the microscope, revealing the successful transfer or large tears and wrinkles (Figure 22). For the most part, only the samples that passed the inspection were used for the MOVPE growth of GaN.

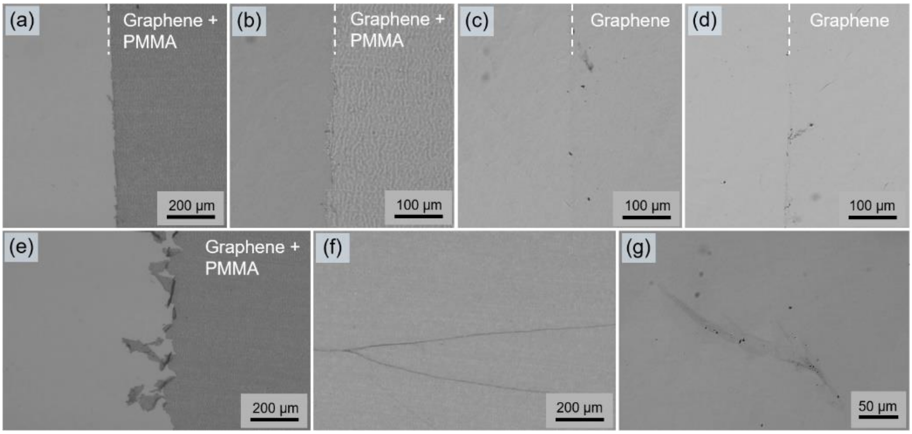

Figure 22. Representation of quality control implemented by investigation of the graphene transfer under an optical microscope. Graphene/template boundary after the transfer (a), initial annealing (b), rinse in acetone (c), and rinse in an IPA solution as well as DI water (d). The edge of graphene in case cutting with scissors was used (e), wrinkles, and possible few-layer zones were observed in (f) and (g).

The Graphene C sample was acquired as epitaxial, second-grade graphene on Si-face 4H-SiC semi-insulating substrate without an intentional off-cut. The size of the SiC wafer was 7 mm × 7 mm. The monolayer graphene covered around 90 % of the area, with possible two-layer zones present, as was evaluated by the manufacturer (primarily by provided AFM data). The transferring procedure started with the deposition of a thin 20 nm Ni layer by e-beam evaporation and subsequent magnetron sputtering of a 500 nm Ni layer. Different techniques of Ni deposition were used to create better adhesion. Afterward, a slightly larger size (compared to SiC substrate) thermal release tape (releasing the sample at 150 °C) was placed on top of the metal handling layer. The SiC substrate was held to the table by a double-sided tape while pulling upwards on the thermal release tape from all four corners with tweezers. In that way, minimal bending and cracking were expected to appear. However, this step proved to be hard to master, as the pull-up usually resulted in the cracking of the metal handler and possible fracturing of the graphene layer.

The TRT/Ni/graphene structure was transferred to the GaN/sapphire template and slightly adhered to the surface by gently rubbing it with a soft Q-tip. Afterward, the whole structure was placed on the 150 °C preheated hot plate, and TRT immediately released graphene with the handler. A ferric chloride solution was used to remove the Ni layer. The graphene-covered substrate was rinsed in acetone, IPA, and DI water (using the rinsing protocol described earlier to transfer Graphene A sample). Further details and tips for the transfer of epitaxial graphene can be found in the literature [12].

A set of samples (Graphene A and Graphene B) were initially subjected to investigation by AFM. Only the edge of monolayer graphene on the template was examined as it was the most efficient. As expected, the Graphene B sample demonstrated a relatively smooth surface and a height increase of a few nm towards the graphene edge (Figure 23). However, in the Graphene A sample, the surface was relatively rough (measured surface RMS value was 9.4 nm) with no clear distinction between graphene-covered and graphene-free areas. The previous observation was attributed to the residual contamination of the surface. Thus, the AFM results favored using Graphene B. Otherwise, the transfer and PMMA cleaning procedure of Graphene A had to be improved.

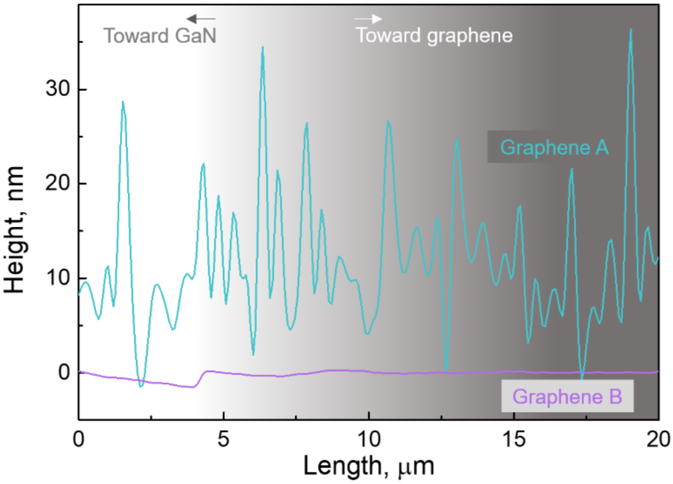

Figure 23. AFM scan line trace of Graphene A and Graphene B samples near the edge of a graphene sheet. The edge zone is around 5 µm into the scan. Note: different measurement units are marked on the axes.

Next, all three samples were subjected to further investigation. Raman spectroscopy was chosen as one of the most widely used techniques to confirm the presence and evaluate the quality of graphene. To minimize the influence of GaN-related Raman modes, Graphene A and Graphene B were transferred onto a bare sapphire substrate. Graphene C was initially transferred onto GaN/sapphire template due to the high cost of the transfer. Raman spectra were measured by focusing the laser onto graphene when evaluating the Raman spectra of graphene. The separately measured Raman spectrum of bare GaN was subtracted from the Raman spectrum of graphene to reveal D mode (in the Graphene C sample only). Manipulation of spectra was necessary as second-order GaN-related peaks (in the range of approximately 1250–1500 cm^{-1}) [110,130] could have obscured the defect-related D mode of graphene.

Raman spectra of Graphene A, Graphene B, and Graphene C are represented in Figure 24. As-transferred graphene had similar spectral characteristics for all three samples. The distinctive peak of the G mode was observed at around 1585 cm^{-1}. The 2D spectral mode for Graphene A was observed at 2675.7 cm^{-1}, while Graphene B – 2678.6 cm^{-1}. The Raman feature intensity ratio (I_{2D}/I_G) for both samples was more than 2, likely indicating the presence of monolayer graphene [131].

It should be noted that defect-related D mode was observable for the Graphene A and Graphene C samples while not pronounced for the Graphene B sample. However, the intensity of this mode for wet-transferred Graphene A was relatively small compared to the G mode ($I_G/I_D = 2.8$), indicating only minor damage [115]. On the other hand, dry-transferred Graphene C exhibited the most intense D mode of all three samples in the Raman spectrum.

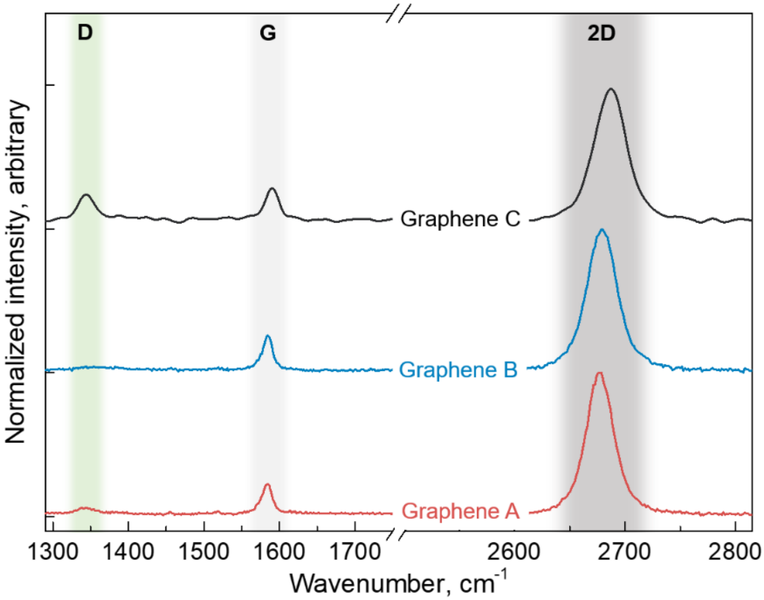

Figure 24. Raman spectra of Graphene A, Graphene B, and Graphene C samples. Graphene A and Graphene B were transferred onto sapphire substrates, while Graphene C – onto GaN; GaN spectrum was later measured separately and subtracted. All spectra were normalized and shifted vertically for clarity. Raman modes D, G, and 2D were marked accordingly.

From personal experience, dry transfer was hard to master and costly. Raman spectra revealed a likely defective layer. The success of transferring graphene without cracking the handling layer was low. Because of that, it was chosen to build the knowledge of GaN epitaxy on graphene by first adopting a cost-effective and easier-to-master wet transfer approach. AFM data and Raman spectroscopy results suggested Graphene B as the best quality sample. Therefore, the wet transfer of Graphene B was used for most of the experiments discussed further unless indicated otherwise.

LAB NOTES 1 A picture-based story of **the wet transfer of graphene** is intended to familiarize the reader with the actual work environment from the mostly first-person POV. Images are left unedited and messy intentionally. It may be used as a guide for future students to improve the transfer process.

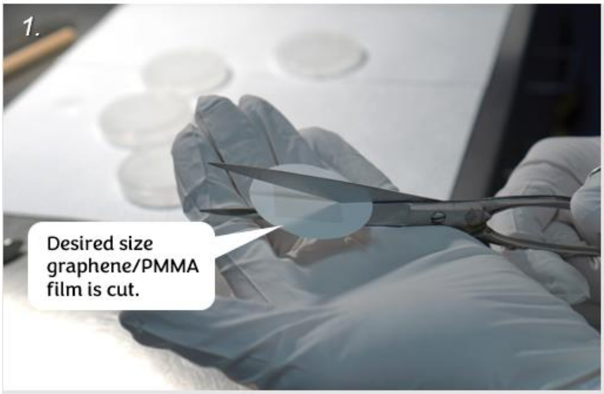

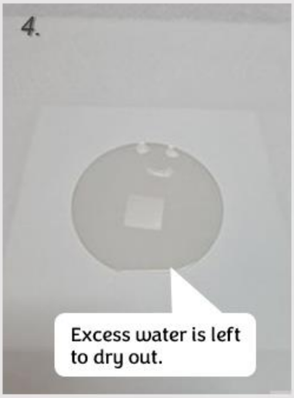

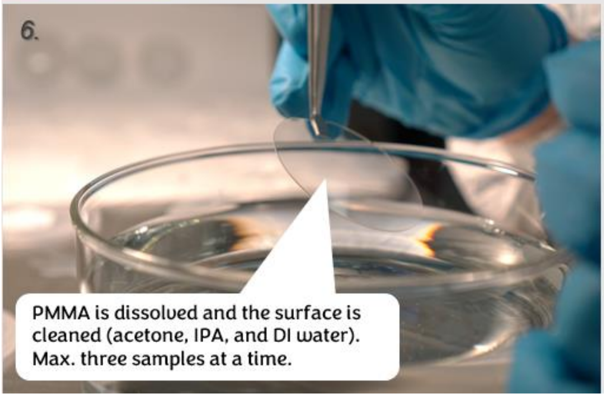

Time required*: up to 2 h of manual work, up to 2 days of vacuum storage.
Budget:** modestly expensive, likely up to a hundred euros per transfer.
Expected quality: normal.
Achieved quality*: as anticipated at first successful try.
*Process duration and transfer quality are subject to user experience.
**Expenses are subjective, based on the writer's personal experience and not intended to promote the process or product.

LAB NOTES 2 A picture-based story of **the dry transfer of graphene from SiC** is intended to familiarize the reader with the actual work environment from the first-person POV. Images are left unedited and messy intentionally. It may be used as a guide for future students to improve the transfer process.

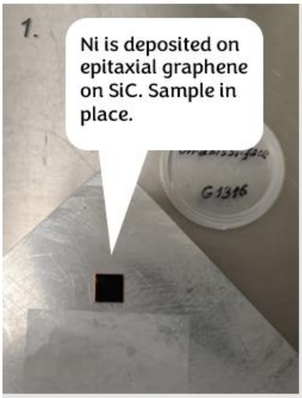

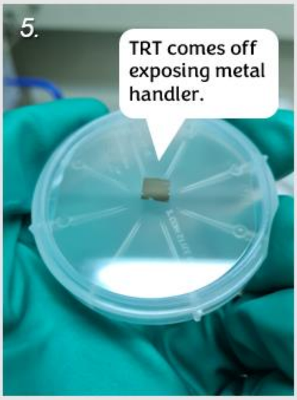

Time required*: up to 45 min, assuming metals are deposited separately.
Budget:** very expensive, likely up to seven hundred euros per transfer.
Expected quality: excellent.
Achieved quality*: lower than anticipated at first successful try.
*Process duration and transfer quality are subject to user experience.
**Expenses are subjective, based on the writer's personal experience and not intended to promote the process or product.

2.3. GaN growth on monolayer graphene

High-quality GaN epilayers are usually grown at elevated temperatures above 1000 °C. The minimum GaN growth temperature in the MOVPE process is determined mainly by ammonia decomposition efficiency and is approximately 500 °C in practical applications. On the other hand, the risk of graphene damage significantly increases as the growth temperature approaches and exceeds 1000 °C [132]. Another aspect of graphene stability to note is that graphene is placed in the atmosphere of numerous reactive species such as ammonia, hydrogen, atomic nitrogen, and others during the MOVPE process. Even the reactive species released from the template itself were shown to cause damage to the monolayer, at least to some degree [90].

As a result, it was decided first to investigate how different growth temperatures affect the graphene monolayer to mitigate the likely adverse effects of the MOVPE process. For this reason, a single-step growth profile was used to deposit GaN at various temperatures. A two-step process is used in the normal growth of GaN on a sapphire substrate by the MOVPE process. First, the buffer layer is deposited at a lower temperature (approximately 600 °C). Temperature is then ramped to over 1000 °C for coalescence and eventual high-quality film growth [2]. Possible single-step and two-step growth profiles are represented in Figure 25. In the following MOVPE growth of GaN experiments, process temperatures varied from 600 °C to 1075 °C, maintaining an H_2 as the carrier gas for MO, keeping reactor pressure of 600 mbar, and the NH_3 flow rate of 1.8 SLM.

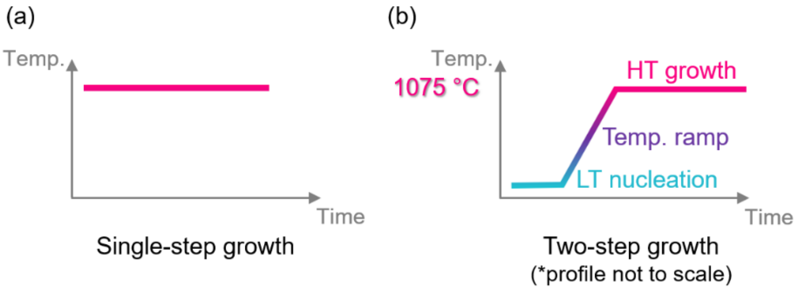

Figure 25. Growth protocols as temperature profiles: single-step growth (a) and two-step growth (b). Note: profiles are represented not to scale.

The Raman spectra were measured after the MOVPE process to assess the damage induced in graphene (Figure 26). The Raman spectrum measured after growth at 600 °C revealed a lower 2D and G feature ratio (I_{2D}/I_G) value than that measured just after the transfer – the ratio decreased from 3.0 to 1.7. An increase in temperature to 700 °C resulted in the I_{2D}/I_G also decreasing to 2.2, while a further rise in temperature to 800 °C influenced the I_{2D}/I_G value to go back to 1.8. Thus, low-temperature nucleation altered the intensity ratio of 2D and G peaks, disregarding the temperature. However, exposure to 700 °C caused the slightest change of all. The exact reason for such variation was undetermined in this work. Although, the presence of charged impurities was shown to modify the Raman spectrum of single-layer graphene even in the absence of D mode [133].

The presence of an additional defect-related Raman spectral feature, usually abbreviated D’ and expected to appear at around 1626 cm^{-1}, was also assessed [134]. D’ mode was distinguishable in the sample grown at 600 °C and resolvable in the sample grown at 800 °C. However, the D’ feature did not manifest itself in the Raman spectrum of the 700 °C grown sample. The latter observation further suggested the suitability of 700 °C to be set as the default nucleation temperature.

The growth temperature increase from 600 °C to 800 °C induced relatively small, although detectable blueshift of the G mode (from 1592 cm^{-1} to 1595 cm^{-1}) as well as the 2D mode (from 2685 cm^{-1} to 2694 cm^{-1}). The observed changes in the peak position of Raman modes could be related to the post-growth induced strain in the graphene monolayer [135]. Thermal expansion differences of the crystalline layers (both GaN epitaxial layers and sapphire substrate) were expected to cause the slight bending of the specimen.

Regarding the structure of a 2D peak, the broadening was observed as the nucleation temperature increased – the FWHM value of the 2D peak increased accordingly from 45 cm^{-1} to 70 cm^{-1}. Notably, for the 800 °C exposed sample shoulder-like feature near the 2D peak was observed. The latter finding suggested detrimental changes induced to the monolayer. Increasing the growth temperature even further to 1075 °C resulted in the lack of characteristic G and 2D modes in the Raman spectra. Even the rise of laser power in the Raman spectroscopy experiment regarding the sample grown at 1075 °C didn’t help to reveal the presence of graphene, suggesting severe or even total graphene layer damage and decomposition, which would be detrimental to the whole idea of remote epitaxy.

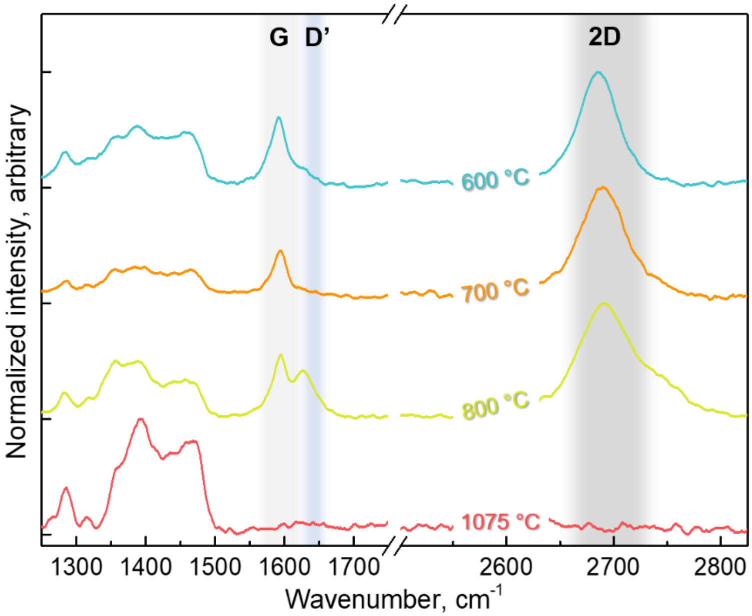

Figure 26. Raman spectra of graphene after the single-step growth. Process temperatures are indicated. Spectra are normalized and shifted vertically for clarity. Raman modes G, D', and 2D are marked accordingly. Raman spectra are adapted from the publication of the author [P1]. © IOP Publishing. Reproduced with permission. All rights reserved.

Furthermore, additional Raman spectra were acquired from multiple areas of graphene across the samples to ensure that a single measurement error was not misleading. In Figure 27, only minor variations of the same-sample Raman spectra are observed, providing additional support for the choice of 700 °C temperature as being the most suitable for the nucleation. It should be noted that Raman spectra were acquired from at least three distinct areas of graphene on most of the samples. In most cases, conclusions about the sample were made if no more than one outlier spectrum was observed. For example, the I_{2D}/I_G was less than 2 for all the measured areas in 600 °C and 800 °C grown samples, while more than 2 for all the measured regions regarding the sample exposed to 700 °C temperature.

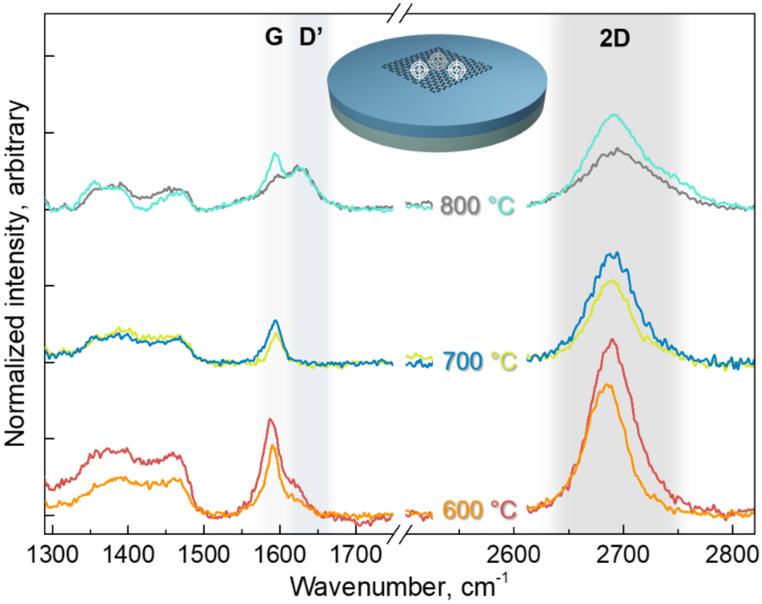

Figure 27. Raman spectra of graphene after the single-step growth. The spectra are measured in at least two arbitrary zones above graphene (as represented in the inset), in addition to the results presented in Figure 26. Corresponding growth temperatures are indicated. Spectra are normalized and shifted vertically for clarity. Raman modes G, D', and 2D are marked accordingly.

Determination of the suitable nucleation temperature led to the implementation of an entire GaN thin film growth by the MOVPE process recipe. The MOVPE process was performed by the growth of the nucleation layer at 700 °C and ramping of the temperature over the period of approximately 10 min to 1075 °C. H_2 gas was used as a carrier gas for MO. Over 2 µm of coalesced GaN film was grown at a growth temperature of 1075 °C. The reactor pressure was kept at 150 mbar, and a V/III flux ratio was set and maintained at 700. Two samples were initially fabricated – one with the GaN epilayer grown at 1075 °C for 5 min and one grown for 60 min for complete epilayer coalescence (after the nucleation at 700 °C).

Raman spectra from the samples were acquired afterward (Figure 28). Graphene Raman fingerprints of G and 2D modes were visible even over a thick (approximately 2.4 µm) GaN layer meaning that a two-step recipe prevented graphene decomposition. The relatively weak signal associated with graphene could be explained by the presence of strong second-order GaN-related Raman features in the same spectral region. Also, it was not unusual to observe (or at least display) graphene-related Raman features only after the lift-off of the epilayer, as indicated in the literature [84].

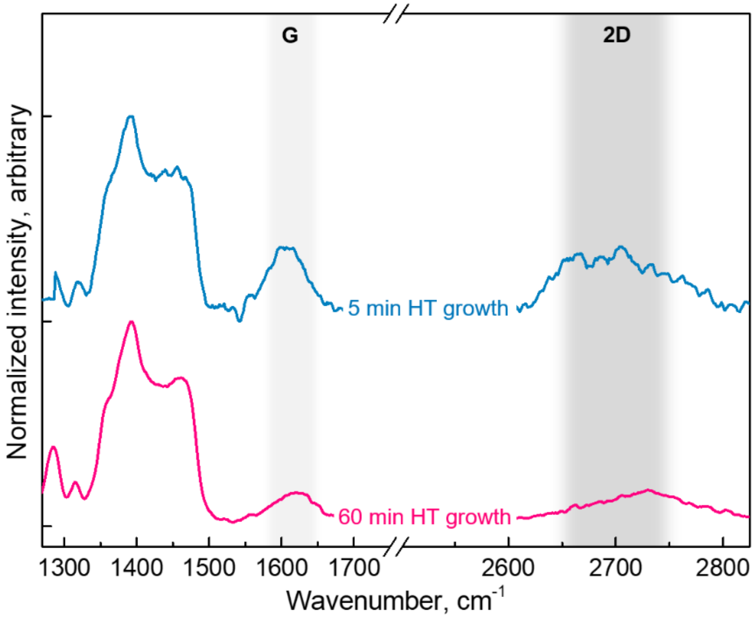

Figure 28. Raman spectra of graphene after the two-step growth, with the second step temperature of 1075 °C. Second-step growth times are indicated. Spectra are normalized and shifted vertically for clarity. Raman modes G and 2D are marked accordingly. Raman spectra are adapted from the publication of the author [P1]. © IOP Publishing. Reproduced with permission. All rights reserved.

In this work, a set of at least eight distinct samples were fabricated by adjusting different growth settings – nucleation step time, nucleation step temperature, temperature ramping to 1075 °C time, metalorganics flow during the temperature ramping step, and similar. Color-coded growth profiles are represented in Figure 29 for convenience. The influence of the variation of each growth parameter independently was not further studied in detail in this work. However, most of the samples were thoroughly investigated for generalized comparison. In this way, the recipe for the best quality epilayer was determined.

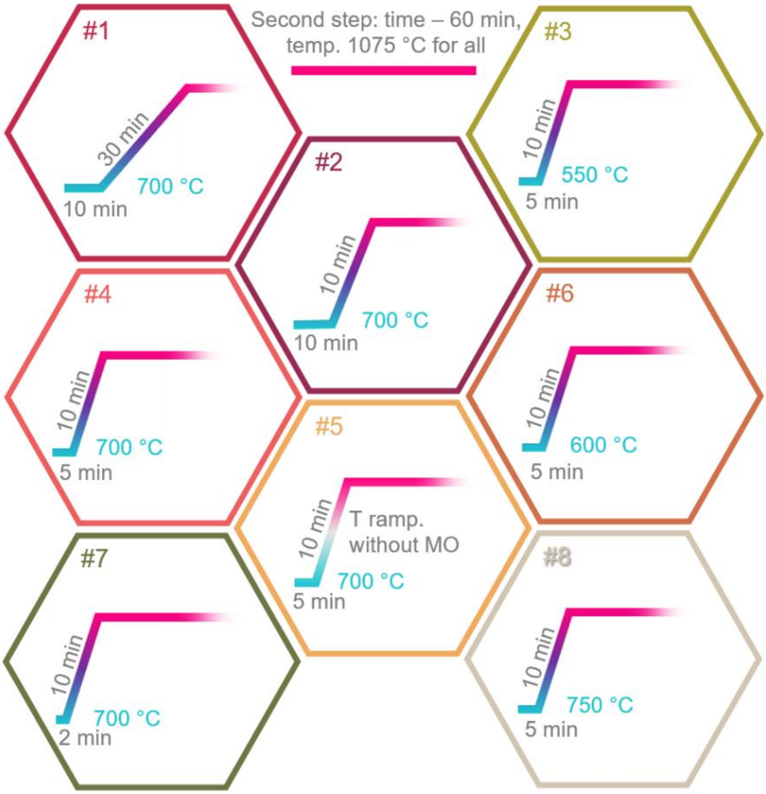

Figure 29. Color-coded (for reference in subsequent result analysis) growth profiles of a set of samples analyzed in this work.

The entire growth of GaN epilayers by the MOVPE process was *in situ* monitored using a laser reflectometry system operating at 650 nm. Representative data of the observed signal is shown in Figure 30. In the latter figure, sample A represents a complete coalescence of the GaN epilayer during the high-temperature growth step. The reflectivity signal oscillations recovered after a particular time following the temperature ramping, indicating the formation of a flat surface. Even though the low-temperature nucleation proceeded by separate island formation, manifested by initially low reflectivity signal. In contrast, Sample B represents the poor-quality sample growth, where GaN grains were formed instead of a continuous GaN epitaxial layer. In the former case, reflectivity signal oscillations were not observed during the entire MOVPE growth, and the reflectivity signal from the forming layer was constantly low.

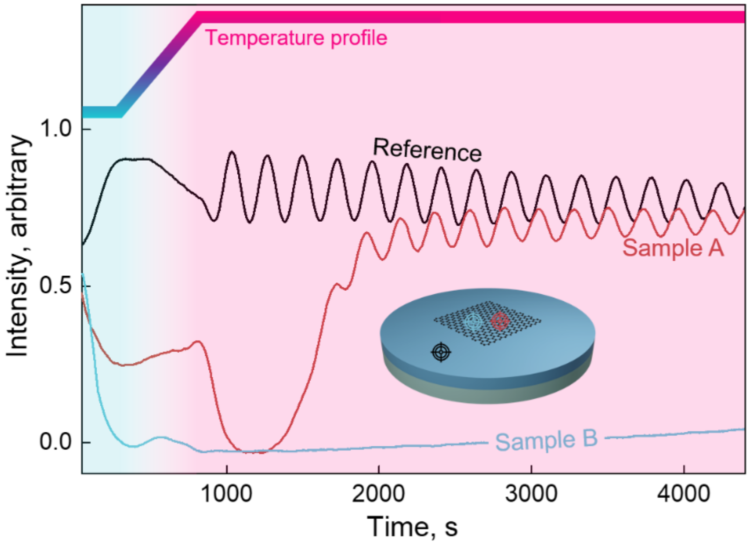

Figure 30. *In situ* reflectometry data during MOVPE growth. Reflectance evolution during low-temperature growth, temperature ramping, and high-temperature growth should be interpreted according to the temperature profile (indicated). An inset figure corresponds to the approximate points of signal measurement. Sample A represents the initial growth of seeds with subsequent layer coalescence and the formation of a high-quality film. Sample B represents the growth of grains instead of the film during the entire MOVPE process resulting in a low-quality GaN film. Reflectivity data is adapted from Supplementary material from the publication of the author [P1].

Initially, the quality of all the epilayers from a set was studied employing XRD. The measured and normalized rocking curves of the GaN (0002) reflection are represented in Figure 31 (a). The FWHM values were calculated for each rocking curve by Voigt profile fitting. A comparison of the crystalline quality of distinct samples determined utilizing XRD analysis is represented in Figure 31 (b).

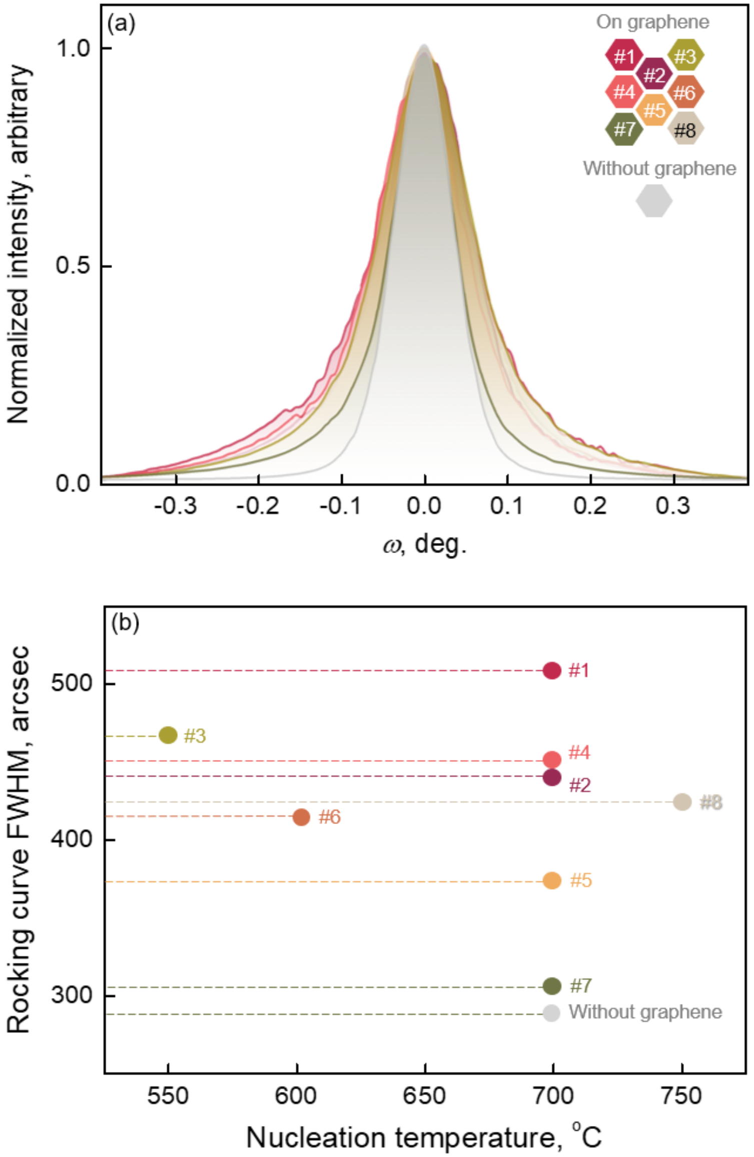

Figure 31. Normalized XRD rocking curves of the set of GaN samples grown on graphene using different process parameters (a). FWHM of rocking curves from (a) in (b). Colors in (a) and (b) correspond to the growth profiles indicated in Figure 29. XRD results are adapted from the publication of the author [P1]. © IOP Publishing. Reproduced with permission. All rights reserved.

Subsequently, the optical properties were investigated by the photoluminescence technique. Two best crystalline quality samples fabricated on monolayer graphene were chosen for in-depth analysis (Figure 32). Additionally, the photoluminescence spectrum from the epilayer grown without the monolayer was acquired for reference. All the spectra demonstrated the prominent characteristic bands of GaN – yellow PL at approximately 2.2 eV, blue PL at approximately 2.8 eV, and a near-band-edge emission at approximately 3.4 eV. The NBE emission was also slightly redshifted for both samples. The peak PL signal was observed at 3.43 eV regarding both GaN samples grown on monolayer graphene, compared to 3.44 eV concerning the sample of GaN epitaxial film fabricated onto GaN/sapphire template without graphene interlayer. The observed minor redshift was attributed to the GaN epilayer stress relaxation when the vdW surface of monolayer graphene was present beneath the epilayer [136,137]. The exact positions of the NBE band are represented in the inset of Figure 32. The yellow and blue PL bands are usually observed in PL spectra of GaN epilayers and were attributed to, for example, carbon, hydrogen, and oxygen impurities-related defects usually unavoidable in the GaN fabrication process [138–140].

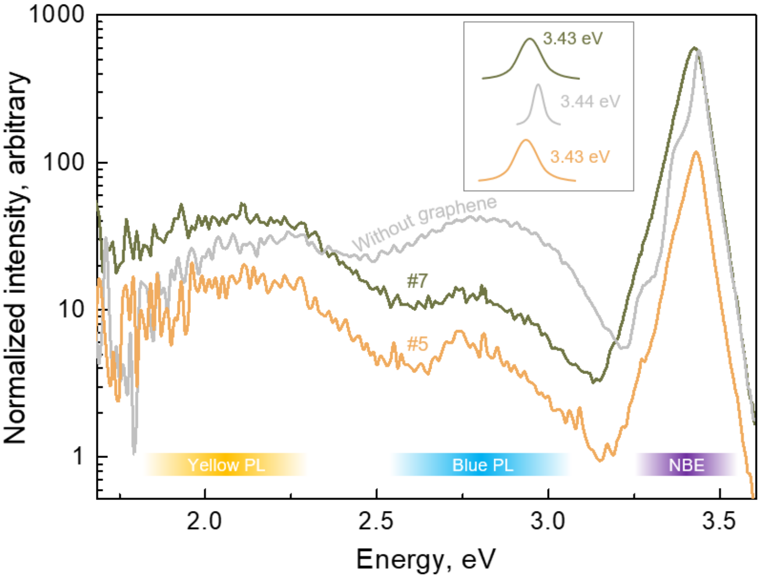

Figure 32. PL spectra of GaN epilayers grown on both the graphene and the bare GaN template (marked as reference). The colors of the spectra correspond to the growth profiles indicated in Figure 29. Inset shows a zoomed-in NBE peak. PL data is adapted from the publication of the author [P1]. © IOP Publishing. Reproduced with permission. All rights reserved.

The dynamics of GaN formation on graphene were investigated primarily by the SEM technique. After the initial low-temperature nucleation step, the seed-like formation of relatively small GaN crystals (up to 1 μm) on graphene was observed (Figure 33). SEM investigation revealed that part of GaN nuclei formed in linear structure clusters – random elongated patterns were seen, as highlighted in Figure 33 (a). The elongated groups of GaN nuclei demonstrated no in-plane alignment with one another. Such GaN nucleation behavior was attributed to graphene defects acting as the preferential nucleation sites. For example, cracks and tears of graphene induced during preparation or transfer might allow a direct link between nucleating GaN and the GaN seeding layer. Besides, CVD graphene is suspected to be composed of arbitrarily oriented domains [141], resulting in grain boundaries or wrinkles, which could act as the preferential sites for GaN to nucleate on or through them.

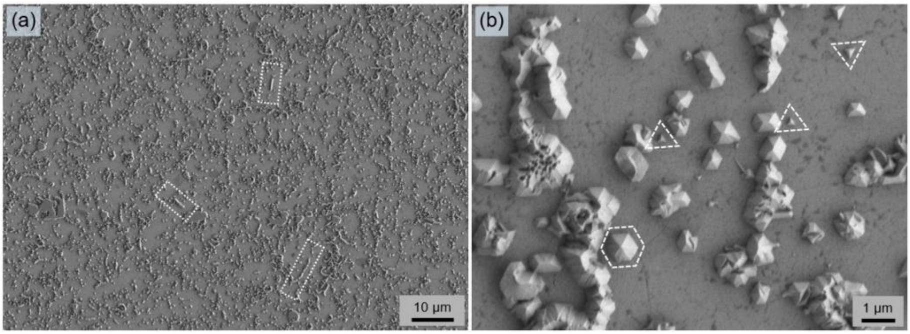

Figure 33. SEM images of the GaN nuclei formed at low temperature (700 °C). The tendency for GaN nuclei to arrange in an arbitrary elongated pattern is marked in (a) for eye guidance. The dashed figures in the zoomed-in area (b) enclose two types of GaN nuclei for eye guidance. SEM results are adapted from the publication of the author [P1]. © IOP Publishing. Reproduced with permission. All rights reserved.

Another important observation at the initial nucleation step was the formation of two different geometry nuclei – hexagonal and tetrahedral pyramid-shaped, as revealed in Figure 33 (b). The hexagonal shape of GaN nuclei is usually observed during GaN formation as wurtzite type GaN exhibits a hexagonal crystal structure. In contrast, the tetrahedral shape of GaN nuclei is less commonly observed, although reported for GaN and InN when grown on graphene [142,143]. It was argued that tetrahedral-shaped nuclei form due to the lack of a direct link to the underlying GaN through the vdW surface of graphene. Therefore, such a shape could indicate a pure remote epitaxy process of a stress-free GaN [143]. In this study, the data were insufficient to draw such a conclusion, although it cannot be dismissed either.

Both types – hexagonal and tetrahedral-shaped nuclei – were in-plane aligned to one another. Such azimuthal alignment indicated the existence of interaction between the epilayer and the seeding layer through monolayer graphene, disregarding the shape. Aligned nucleation behavior is highlighted by the dashed lines enclosing arbitrary nuclei in Figure 33 (b).

As pristine monolayer graphene has no dangling bonds, the nucleation capability on its surface may be highly suppressed. Partial coverage of GaN/sapphire template by graphene could have resulted in an epitaxial lateral overgrowth epitaxy mode meaning that graphene acted mainly as a mask. Moreover, in this study, monolayer graphene covered only a fraction of the epitaxial GaN/sapphire template, leading to an expressed concern that monolayer graphene only served as a mask allowing the overgrowth from the sides [19]. To ensure that the latter consideration was not the case, the samples covered with GaN were further investigated by SEM at the end of each of three primary stages of the growth – low-temperature nucleation, temperature ramping step, and high-temperature growth (Figure 34). It was observed that the MOVPE growth of GaN on graphene proceeded as follows: first, the nuclei developed (as discussed previously); afterward, the nuclei expanded laterally, covering most of the graphene; and finally, the entire film coalesced and formed to a high-quality GaN epitaxial layer. Thus, it was proved that epitaxy on monolayer graphene, when only part of the epitaxial substrate is covered, is not just a regular ELOG process.

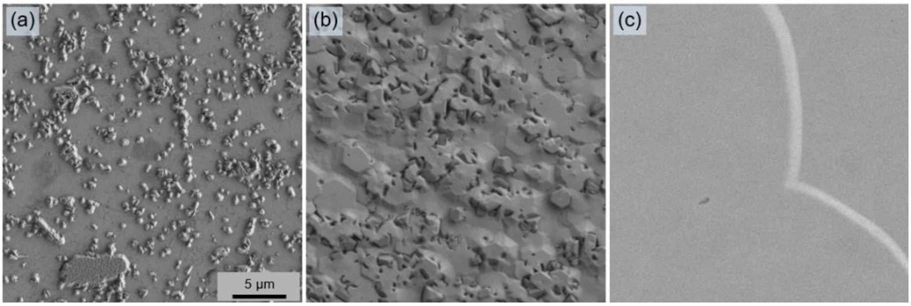

Figure 34. SEM images corresponding to the evolution of GaN on graphene monolayer during different phases of MOVPE growth. Low-temperature (700 °C) seed formation (a); 5 min growth of high-temperature (1075 °C) GaN (b); and 1 h growth of high-temperature (1075 °C) GaN (c). Arbitrary defect in (c) is left intentionally to ensure that the image is focused. All three SEM images do not necessarily correspond to the same growth protocol. SEM images are adapted from Supplementary material included in the publication of the author [P1].

Relatively thick (2.4 μm) GaN epitaxial films were grown by the MOVPE process for further analysis. The surface of the as-grown GaN epitaxial layers on graphene and on bare GaN/sapphire template was investigated by the AFM technique. AFM scan analysis revealed that GaN grown on graphene had only a slightly larger surface RMS value of 0.5 nm in the 5 µm × 5 µm scan area compared to the GaN epitaxial layer grown without the graphene interlayer (the surface RMS value of 0.2 nm of the same-size scan area). In both cases, atomic steps were seen as the surface roughness was less than 1 nm, indicating a relatively smooth GaN epilayer (Figure 35).

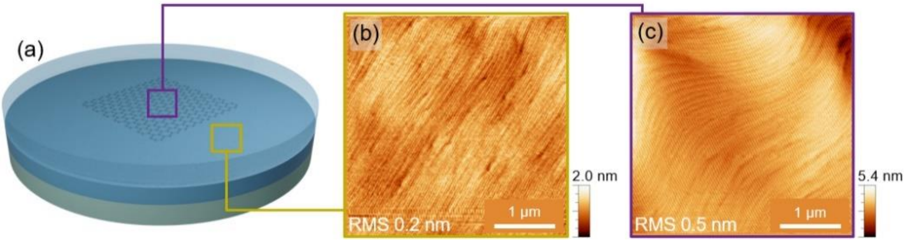

Figure 35. Schematic representation of the final sample with GaN film grown on graphene-covered GaN/Sapphire template (a). AFM scans of the different areas of the same sample after GaN film growth on bare GaN (b) and on monolayer graphene (c). Surface RMS values are indicated in each AFM scan accordingly. AFM results are adapted from the publication of the author [P1]. © IOP Publishing. Reproduced with permission. All rights reserved.

Two samples were chosen for further interlayer analysis by the TEM technique. Sample A was a fully coalesced GaN film grown at a nucleation temperature of 700 °C and Sample B – at 600 °C (other growth settings were kept unchanged). In TEM analysis, areas close to the expected monolayer were investigated thoroughly. The bright horizontal stripe observed at the expected graphene interface was attributed to the monolayer graphene for Sample A, as represented in Figure 36 (b). It should be noted that the width of the bright stripe area was arguably surpassing the thickness of a single layer of graphene. Such observation could be explained by the unintentional sample inclination, or influence of the existing off-cut angle of the substrate, as illustrated in Figure 36 (c). Another similar situation was observed in other work regarding epitaxy on graphene [137]. In any case, the graphene interface proved to be a relatively regular one. GaN crystallographic orientation (primarily *c*-direction) was preserved in an epilayer grown on the graphene monolayer, with no significant irregularities seen at the interface in Figure 36 (a). The areas of different brightness and wrinkling in the figure discussed are attributed to the periodic thickness variation of the specimen in the direction of an electron beam. The variation resulted from a particular sample preparation process, as was discussed in the subchapter Transmission and scanning electron microscopy. Thus, it was not attributed to the sample imperfections.

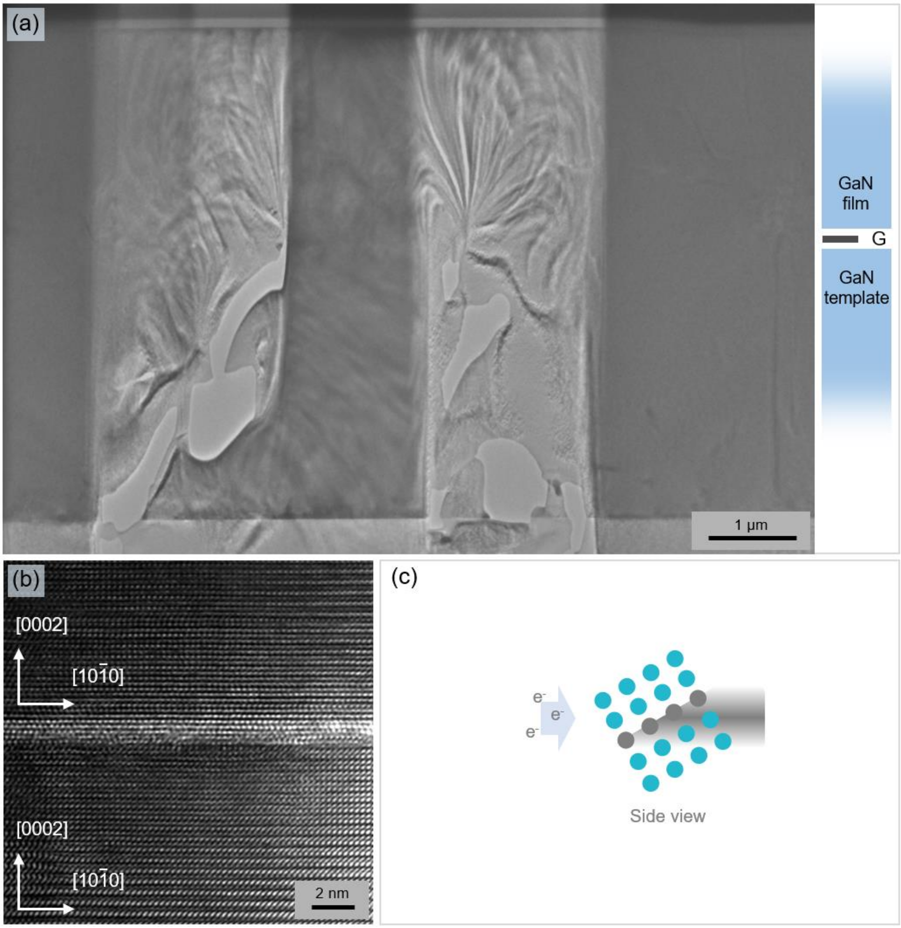

Figure 36. TEM image of GaN/graphene/GaN/sapphire structure and its schematic representation on the right (a). Zoomed-in interface of graphene with GaN epilayer grown by a two-step, 700 °C nucleation protocol (b). Determined crystallographic directions are indicated in (b). The vertical strips of different brightness in image (a) resulted from the periodic thickness variations as samples were prepared for TEM imaging. The thickness of the thickness-varying areas in (a) is approximately 50 nm. The bright horizontal strip in (b) is associated with the graphene monolayer. The apparent thickness of the graphene monolayer may be greater than that of monolayer graphene due to the unintentional sample inclination, as represented in schematics of experiment (c). TEM results are adapted from the publication of the author [P1]. © IOP Publishing. Reproduced with permission. All rights reserved.

On the other hand, Sample B demonstrated an uneven graphene interface, as shown in Figure 37 (a). Even though the largest investigated area of the sample was composed of the intended *c*-axis oriented wurtzite crystalline structure GaN, partial inclusions of cubic-phase GaN or even misoriented crystallites were also observed in the specimen under investigation, as outlined in Figure 37 (b). Hexagonal-type GaN was partially observed forming tilted in an unusual angle – *c*-axis was rotated from the template surface normal by 109°, as outlined in Figure 37 (c). Even though the misoriented crystallites were overgrown by a thick and fully coalesced GaN layer, the overall quality of the epilayer was significantly degraded. Such results agreed with the XRD data (Figure 31), indicating a significantly lower crystalline quality of 600 °C grown sample compared to 700 °C nucleation-step MOVPE grown one (306 arcsec versus 411 arcsec FWHM values of rocking curves, respectively).

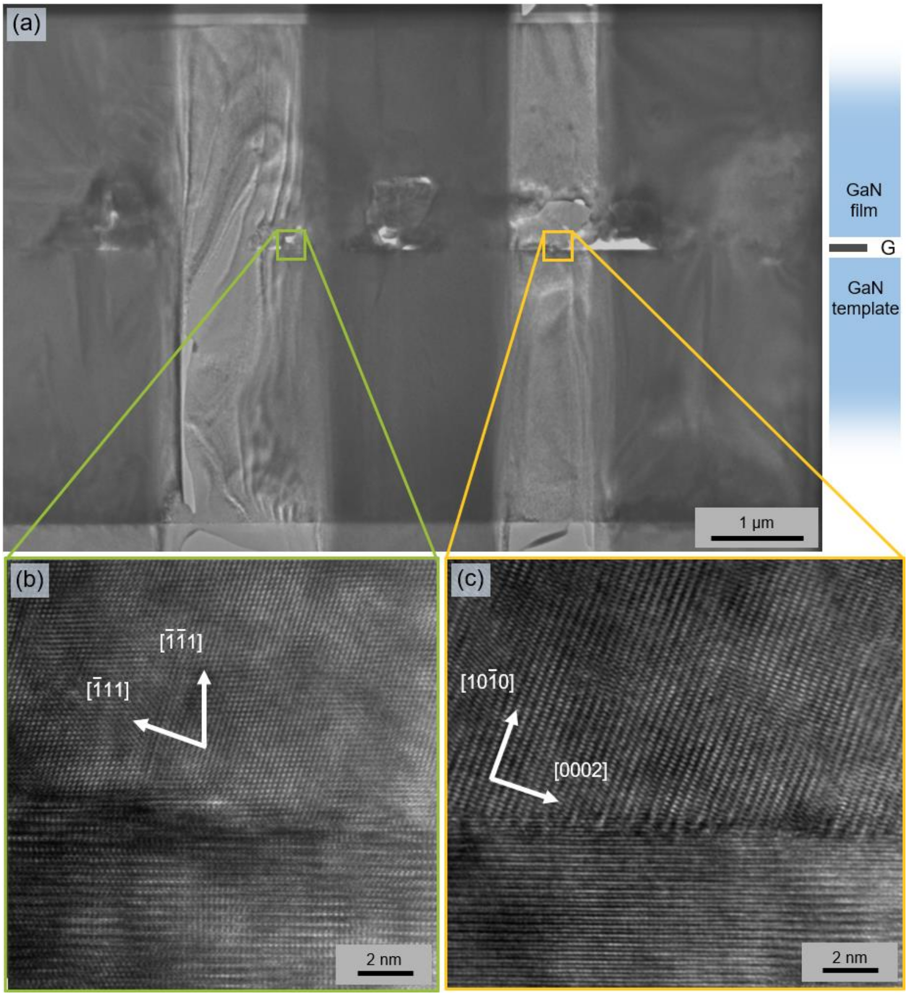

Figure 37. TEM image of GaN/graphene/GaN/sapphire structure and its schematic representation on the right (a). Zoomed-in interfaces of graphene with GaN epilayer grown by a two-step, 600 °C nucleation protocol (b) and (c). Areas of the cubic phase GaN and 109 °C tilted hexagonal GaN crystallites are shown in the colored insets, marked (b) and (c). Colored squared areas in (a) indicate approximate areas corresponding to the zoomed-in images (b) and (c). Crystallographic directions are indicated whenever determined. The vertical strips of varying brightness in image (a) resulted from the thickness variations due to sample preparation for TEM imaging. TEM results are adapted from the publication of the author [P1]. © IOP Publishing. Reproduced with permission. All rights reserved.

All the results presented in this subchapter highlighted the importance of growth optimization and proved that high-quality GaN thin films could be grown on wet-transferred monolayer graphene by applying the optimal MOVPE growth conditions. Regarding the growth temperature, it should be high enough to promote high crystalline quality GaN formation while at the same time being low enough to avoid graphene damage.

2.4. GaN membrane exfoliation

An essential step in the overall process of remote epitaxy is a thin GaN film exfoliation. In the perfect case, GaN should bond to the graphene monolayer very weakly, and its release should be immediate. However, in practice, membrane lift-off usually requires an additional stressor layer deposition. A stressor layer, in this case, provides additional lateral stress for the crystal layer onto which it is deposited, and the upward lift as the stressed metal layer tends to roll itself up. Metal-based stressor layers, such as nickel and copper, were previously implemented for the semiconductor membrane release [23,144]. If even the metal stressor layer was not enough to separate the thin membrane from the substrate, the thermal effect of dipping the structure into cold liquid nitrogen was proposed [144].

In this work, approximately 5 μm of electroplated Ni was chosen as the primary stressor layer. Two more aspects of metal electroplating had to be considered before Ni deposition. First, the surface of interest needed to be conductive. However, GaN film conductivity proved to be insufficient for Ni electroplating. Thus, an additional metal layer had to be deposited first, employing another technique. Secondly, a thin adhesive layer of titanium was proposed in literature before the deposition of Ni to form a strong bond with nitride film [12,23]. Thus, 50 nm Ti deposition by the e-beam evaporation process was chosen to proceed further. However, the choice of Ti imposed an additional hurdle, as the metal was prone to oxidation during the transfer from the e-beam evaporation apparatus to the electrolysis lab. To overcome the latter problem, an extra Au layer of 50 nm thickness was deposited by an e-beam process in a single chamber procedure consecutively after the deposition of Ti. Now, the non-oxidating Au was acting as a protective barrier for the well-adhered Ti as well as providing the conductivity necessary for Ni electrolysis.

Notably, a 2-inch wafer had to be cut into smaller samples, as graphene covered only the center part of the substrate in most cases. After the Ti and Au deposition, a 2-inch wafer was diced with an appropriate diamond scriber by hand. It was essential to first sputter the Ti and Au metal layers as dicing exposed the edges of the GaN thin film. In contrast, the edges of the sample had to be left less conductive to avoid nickel electroplating from the side and further preventing the lift-off. Only after Ti and Au deposition, followed by wafer dicing, Ni stressor layer was electroplated in chemical solutions of $NiSO_4(H_2O)_6$ and $NiCl_2$. The schematic representation of GaN thin film exfoliation is shown in Figure 38, emphasizing the membrane's tendency to roll up during electroplating.

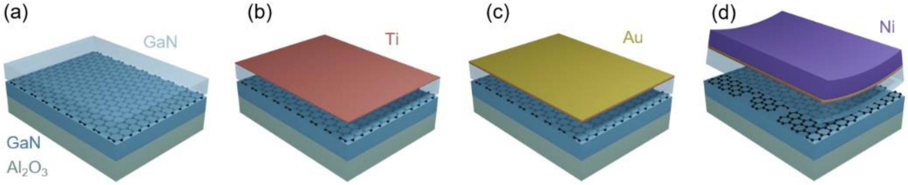

Figure 38. Schematic representation of the sample cut (a) and the deposition of metal layers for GaN exfoliation (b)–(d). The thickness of layers is not to scale. Models are adapted from the publication of the author [P2].

EDX spectra were measured to ensure that the membrane exfoliation started at the graphene interface and not, for example, at the sapphire/GaN interface. The sufficiently thick and stressed metal layers were previously shown to induce GaN spalling [145]. Both the released GaN membrane and the substrate left were investigated for the fingerprints of GaN. X-ray energies (EDX fingerprints) related to Ga and N atoms were found on both samples. The additional energy peaks were related to the metal deposited on the membrane only (Figure 39). SEM (EDX tool) software internal library was used for energy identification. EDX spectra were considered as initial proof of successful GaN exfoliation from monolayer graphene in this study.

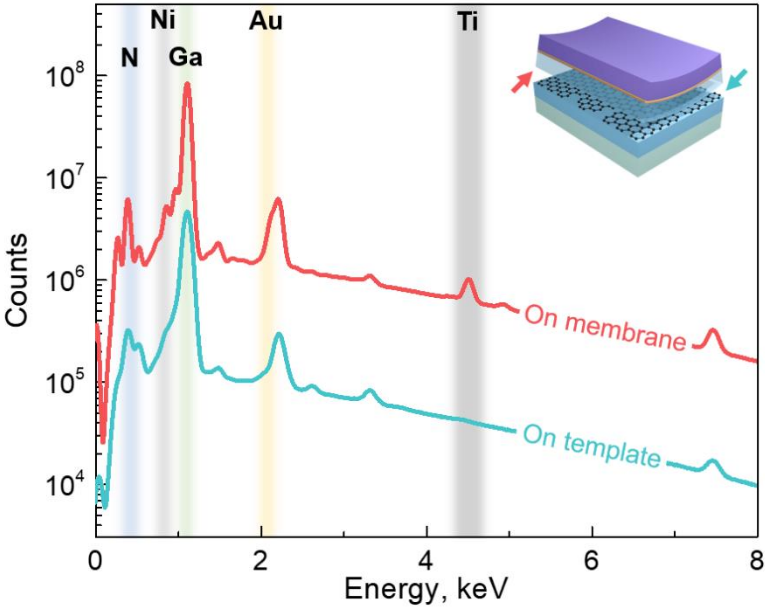

Figure 39. EDX spectra after the membrane release. Colored arrows in the inset image indicate the surfaces of EDX spectra acquisition, accordingly. Energies of N, Ni, Ga, Au, and Ti are marked accordingly. EDX results are adapted from literature [146].

Next, the GaN/sapphire template was investigated by SEM technique to evaluate exfoliation quality. The morphology of the surface of the substrate after lift-off was partially uneven, with micrometer-sized structures left, as can be seen in Figure 40 (b). Mostly regular appearance indicates that GaN lift-off was mainly successful. However, an improvement would be welcome.

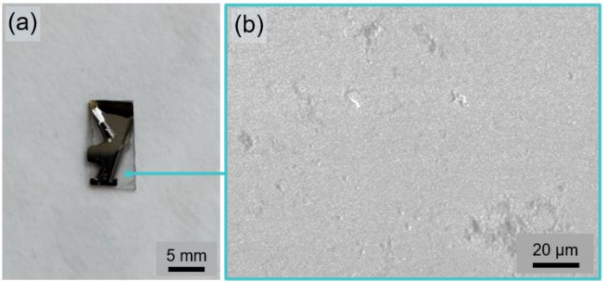

Figure 40. A picture of GaN self-exfoliation immediately after the Ni stressor deposition (a). SEM image of GaN template after the GaN membrane exfoliation (b). Partially uneven morphology can be seen. Images are adapted from the publication of the author [P2].

Finally, the quality of graphene was evaluated by Raman spectroscopy. Raman spectra, acquired from the membrane and the remaining substrate as well as from an initial sample before the growth, are shown in Figure 41. Graphene-related spectral features G and 2D were present on all samples indicating that at least a small part of graphene was also lifted-off together with the membrane. Blueshift and broadening of G and 2D modes were observed in the case of the membrane investigation. The upshift of G and 2D modes and the appearance of additional peaks (Raman shift peaks manifested at around 1449 cm^{-1} and 1732 cm^{-1}) were undetermined for this sample, as expected tensile strain was shown to result in the red-shift for graphene monolayer [135]. D' mode was observed on the substrate after exfoliation, likely due to the partial ripping of the graphene and possible adsorption of foreign materials [134]. Note that metal layers supporting the GaN membrane were not removed.

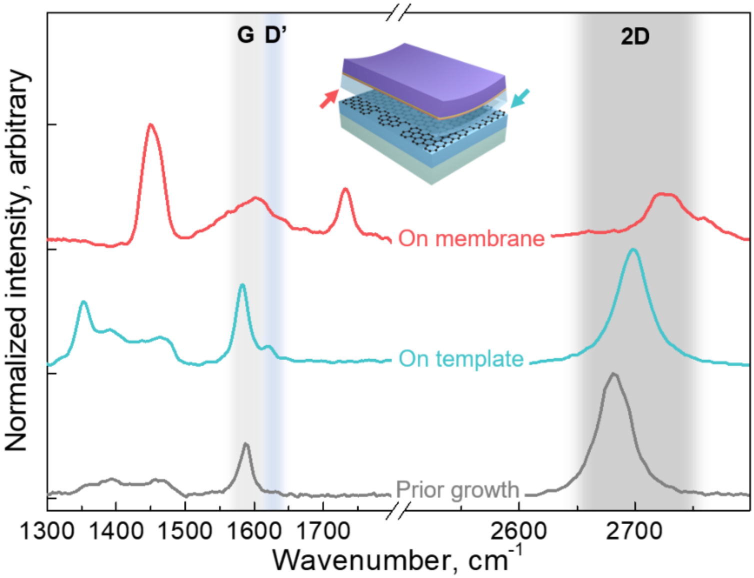

Figure 41. Raman spectra of the GaN template with monolayer graphene prior to MOVPE growth of GaN epilayer and after lift-off of GaN membrane. Colored arrows in the inset indicate the surfaces of Raman spectra measurements. Raman spectra are adapted from the publication of the author [P2].

The results presented in this subchapter demonstrate the successful GaN membrane release from the graphene interface by applying additional metal layers. However, the partial irregularities on the surface of the substrate as well as partial graphene lift-off, indicate that additional measures or improvements in the existing process should be considered to perfect the exfoliation step. The possible causes of imperfections and ways to mitigate it will be addressed in the following subchapter.

2.5. Multi-layer graphene transfer

The quality of graphene layers significantly impacts the remote epitaxy process and must be thoroughly considered [23]. However, it is hardly ever possible to achieve a perfect material crystallinity at room temperature. In addition to the intrinsic lattice disorder, extrinsic impurities are the usual side effects of the semiconductor fabrication processes. Although, defect density could be minimized by both sophisticated growth engineering techniques as well as by strict fabrication environment control. After all, the final semiconductor device characteristics partly reflect the amount of imperfections that are *good enough* for the intended device applications.

The definition of intrinsic and extrinsic defects applies to a rapidly expanding family of two-dimensional materials, with graphene at the forefront. Defects in graphene lattice are classified into several types, closely reassembling the bulk material counterparts. The main difference is that in layered materials, the defects are likely to be confined in the single atomic plane compared to three-dimensional defects in the bulk [147].

For example, point defects in graphene include Stone-Wales type lattice reconstruction, single and multiple vacancies, and native and foreign atom adsorption (adatom) [147]. The analogy of interstitial atoms straining the lattice of the bulk material is adatoms in two-dimensional materials. Such adatoms tend to form in bridge-like configurations [148], as it would require an impractical amount of energy to place an atom in the center of a hexagonal carbon ring [147]. Strained areas of graphene were also shown to include foreign adatoms [149]. In contrast to adatoms, one or several carbon atoms could be removed from the lattice of 2D material. In that case, lattice vacancies are formed. Such vacancies are mobile, able to merge with one another, and frequently induce detrimental effects on monolayer characteristics [147,150]. Impurities could also replace carbon atoms in graphene and act as dopants in the monolayer [147,151].

A pristine monolayer graphene lattice is composed of carbon atoms arranged in a hexagonal fashion. However, two neighboring hexagons could reorganize into two pentagons at an expanse of two adjacent hexagons transforming into seven-membered rings of carbon atoms [152]. Stone-Wales defects in graphene can form without any external influence and source of impurities. The high formation energy of such defects renders the formation very rare at room temperature [147]. However, the appearance of such structural defects cannot be dismissed at elevated temperatures.

The presence of grain boundaries is yet another prominent example of one-dimensional defects in graphene [147]. This defect usually arises from in-plane misoriented grain formation during the CVD process rendering graphene polycrystalline [153]. Tear in monolayer graphene is a structural imperfection of monolayer that may have played a significant role in the experiments of this work. It was shown that mechanical stress promotes crack propagation in graphene resulting in a tear [154]. “Zigzag” and “armchair” directions in a hexagonal lattice were proposed as preferential ripping directions [154]. Interestingly, grain boundaries are not necessarily the weakest links during crack formation and propagation [154].

All kinds of defects in graphene modify its electronic, photonic, thermal, and mechanical properties, usually in a detrimental way. That is especially important considering the idea of remote epitaxy. Holes and tears in monolayer graphene are of the utmost importance. Such defects directly link to the underlying substrate and allow covalent bonds of the epitaxial and seeding layers. Otherwise, graphene was shown to allow only the noticeable permeation of hydrogen atoms [63].

The wet transfer of CVD graphene, mainly used in this study, involves many processes inducing mechanical, chemical, and thermal stress to the monolayer. Although extreme care was taken during all transferring steps, there was no guarantee that a certain amount of tears were not present during the graphene transfer from metal foil to the PMMA handler at the supplier side.

The concept of “aperture-free” bilayer graphene was introduced to reduce the chance of the so-called through-hole epitaxy instead of a remote one [20]. The idea was to cover the possible tears of the first monolayer with the second monolayer. Subsequently, the defects (if any) of the second monolayer are hidden from the epilayer by the first one, considering such defects do not overlap (the probability of overlapping should be relatively small), as represented in Figure 42.

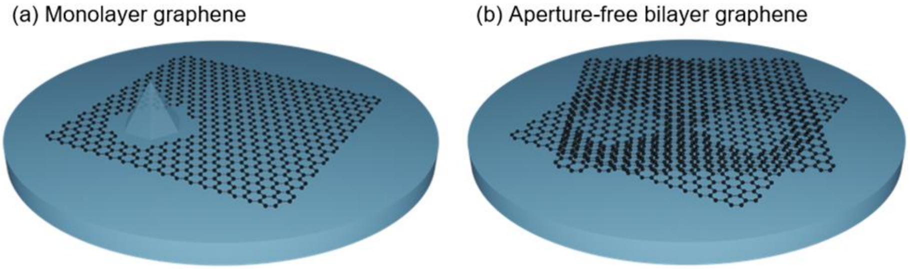

Figure 42. Schematic representation of possible epitaxy through a hole in case defective monolayer graphene is present (a) and the advantage of two defective overlapping monolayers forming an aperture-free surface (b). The model is adapted from the publication of the author [P2].

Another critical aspect is whether remote interaction is still feasible through more than a single graphene layer. Fortunately, it was previously demonstrated that for GaN remote epitaxy, using up to two dry-transferred graphene layers, is rational [14]. Even if the second monolayer weakens the remote interaction, there should be areas where only one monolayer separates the forming epitaxial layer from the seeding layer beneath through holes (or tears) in only one of the layers.

Monolayer graphene had to be wet-transferred two times to test whether two-layer graphene was suitable for remote epitaxy. The double transfer was expected to facilitate the covering of the defects of the first monolayer (Figure 43) with the second monolayer, resulting in a stack of two misoriented monolayers. Nonetheless, each transfer required separate chemical cleaning and annealing procedures that resulted in chemical, mechanical, and thermal stress to both monolayers and the GaN/sapphire template during the stack formation. Possible oxidation of GaN due to prolonged contact with air and water was yet another detrimental aspect to consider. Furthermore, contaminants could have been trapped between the layers. If, for example, PMMA was not entirely removed on monolayer graphene, temperature ramping in the hydrogen environment before MOVPE growth of GaN might have contributed to the complete removal of it. On the other hand, the second layer could have acted as a trapping layer for contaminants compromising the whole idea of remote epitaxy.

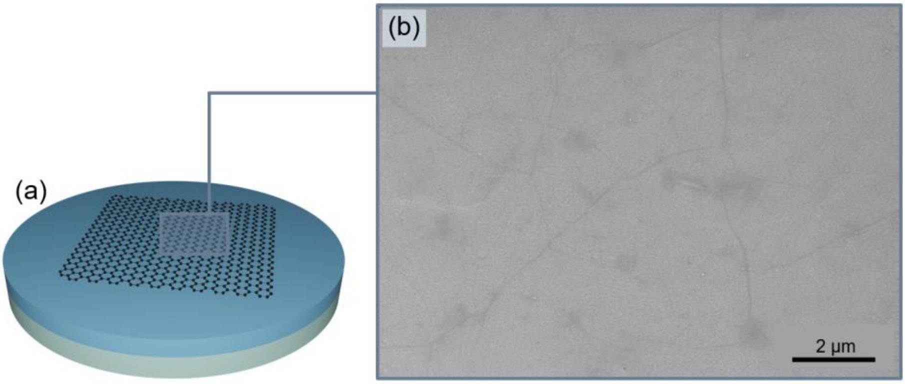

Figure 43. Schematic representation of the GaN/sapphire template with monolayer graphene on top (a) and an SEM image of monolayer graphene after the transfer procedure (b). SEM image is adapted from the publication of the author [P2].

The risk of interlayer contamination during the double-stack transfer could be mitigated using bilayer CVD graphene prepared directly by the supplier. Thus, for the following experiments, commercially available bilayer graphene was used. This type of graphene was transfer-ready and required only a single transfer process, mitigating the risk of interlayer contamination.

Initially, two types of graphene layers were used for the following experiments: a stack of two monolayers and bilayer graphene. Monolayer graphene was also used to form triple-stack graphene. Triple stack graphene was intended to be used as a reference demonstrating the non-remote epitaxy process of GaN, as three layers were confirmed to be too thick to allow remote interaction [14]. The monolayer graphene transfer procedure described in the subchapter Transfer of monolayer graphene was implemented two and three times to form the respective number of monolayer stacks.

Bilayer graphene transfer slightly differed from the monolayer one. The transfer proceeded by soaking a sponge holding the graphene with small water droplets. A thoroughly soaked PMMA/graphene structure was placed into DI water and left to a standstill for a few hours. Before the transfer, water was also left to a standstill overnight. In case air bubbles were trapped at the graphene water interface – a particular plastic slab was used for fishing graphene and re-immersing it. This step was supplier-recommended to facilitate the air bubble removal. Subsequently, graphene was transferred onto our templates and left to dry out for at least 30 min in the air. Samples were then baked in a controlled environment oven for an additional 30 min. The cleaning of PMMA continued in preheated (40 °C) acetone and IPA solutions while gently stirring from time to time by hand and rinsing the samples in DI water. As a final step, the samples were annealed for 8 h in a controlled environment oven at 300 °C in a high vacuum atmosphere. The schematic representation of four types of graphene-covered GaN/sapphire templates prepared by wet-transferring of multiple graphene layers is shown in Figure 44.

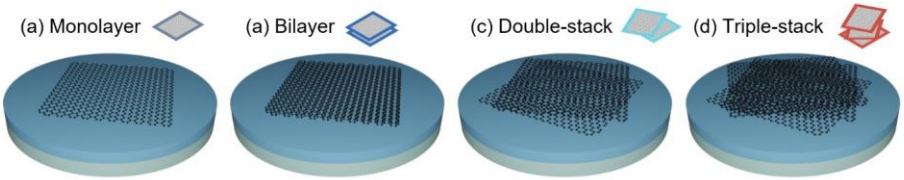

Figure 44. Schematic representation of four sets of samples used in the following experiments – monolayer graphene (a), single-transfer bilayer graphene (b), double-stack of monolayer graphene (c), and triple-stack of monolayer graphene (d). Graphical designations used in the following figures are marked accordingly. Layers are not to scale.

The transferred graphene layers were immediately investigated by Raman spectroscopy by focusing the excitation beam onto a 0.8 μm diameter spot on the overlapping areas of graphene. Three spectra per sample from different regions were typically acquired to discard possible data outliers (not shown here). The Raman spectra fingerprints of graphene – G and 2D modes – were prominent in all samples measured, confirming the successful transfer procedures of graphene (Figure 45).

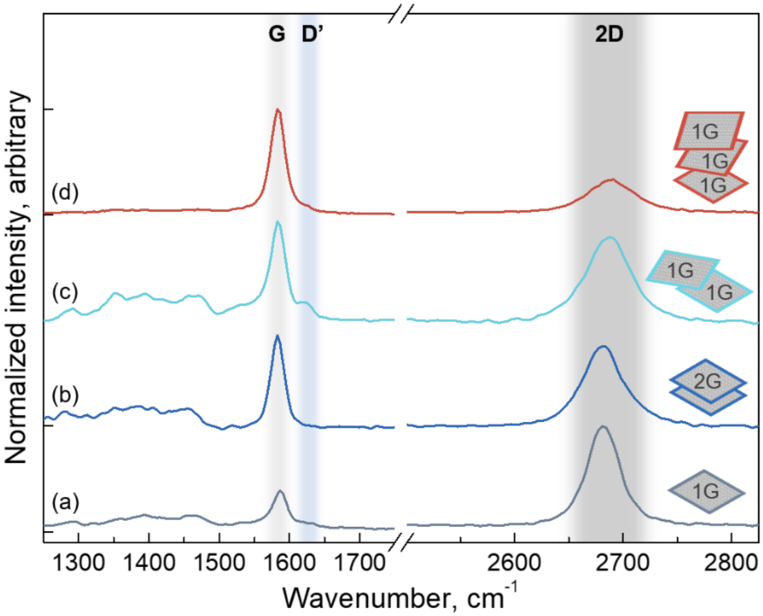

Figure 45. Raman spectra measured after the wet transfer of monolayer graphene (a), bilayer graphene (b), double-stack of monolayer graphene (c), and triple-stack of monolayer graphene (d). All the spectra are normalized and shifted vertically for clarity. Raman modes G, D’, 2D are marked accordingly. Raman spectra are adapted from the publication of the author [P2].

The G peak was observed at approximately 1586 cm^{-1} for monolayer graphene, while 2D – at approximately 2682 cm^{-1}. However, the G mode of graphene downshifted to approximately 1583–1584 cm^{-1} in case more than one monolayer was investigated.

The intensity of the D mode could still be debatable as it was partially obscured by relatively intense second-order Raman GaN peaks in the range of 1250–1500 cm^{-1} (as was discussed previously). Another defect-related mode D’ was clearly resolved in double-stack graphene. One peculiarity to note is that in the case of triple-stack graphene, only G and 2D graphene modes were visible, with no GaN peaks in the expected spectral range. This observation could be explained by the presence of a thick graphene stack mostly screening the scattering from GaN. At the same time, relatively intense scattering in the G mode region dominated the Raman spectrum. Furthermore, Raman spectra were normalized and compressed in the *y*-direction. The particular spectral range was more clearly resolved in Figure 46 by a different representation.

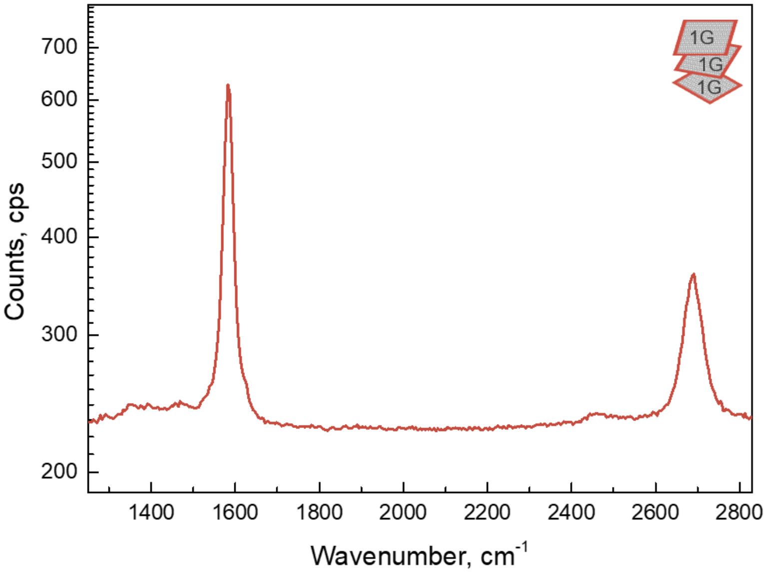

Figure 46. Raman spectrum measured after the wet-transfer of triple-stack of monolayer graphene in addition to results presented in Figure 45.

One of the features distinguishing monolayer and bilayer graphene is the composition of a 2D peak. This mode resolves in the upshift and broadening of a 2D peak for more than one graphene layer [117]. A well-investigated multi-peak structure of the broadened 2D peak may also be resolved. A 2D peak of Raman spectra of graphene was best fitted by four components in the double-stack graphene measured. The Lorentzian fit of four peaks manifested in peak wavenumbers at 2658.5 cm^{-1}, 2677.2 cm^{-1}, 2691.4 cm^{-1}, and 2706 cm^{-1}. The observation confirmed that a thicker than monolayer graphene stack was formed. The resolved structure of the 2D peak is outlined in Figure 47.

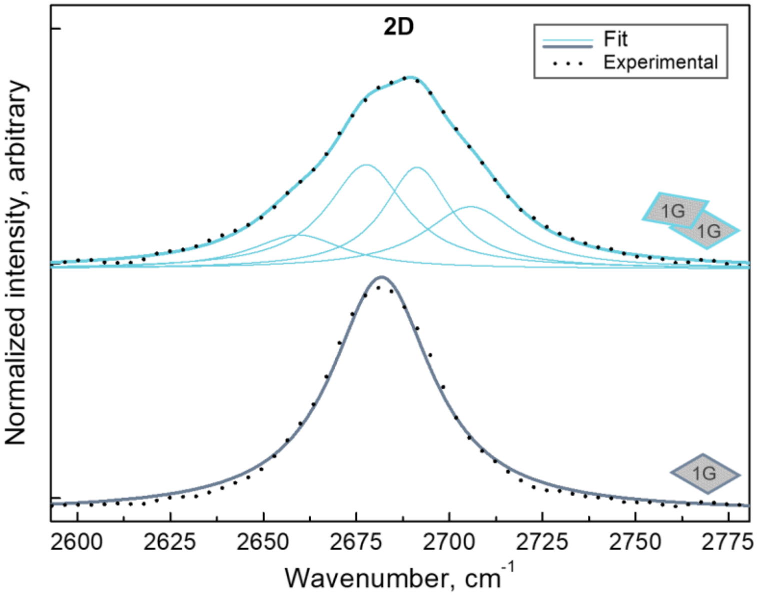

Figure 47. A zoomed-in 2D peaks of Raman spectra were measured after the transfer of monolayer graphene and a double-stack of monolayer graphene (as indicated). The Lorentz fit of the peaks and the resolved four peak composition in case two layers of graphene were present.

The appearance of four components of the 2D peak in bilayer graphene is related to the electronic band splitting, as explained in Figure 48.

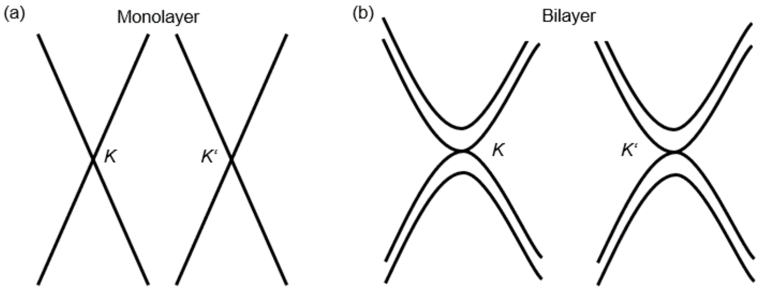

Figure 48. Simplified electron dispersion in monolayer (a) and bilayer (b) graphene in the vicinity of K. An illustration is adapted from literature [117].

The intensity ratio of 2D and G peaks of graphene (I_{2D}/I_G) was another important feature in the experimental evaluation of the number of graphene layers transferred [131]. The intensity ratio was measured being approximately 2.5, considering GaN/sapphire template covered with monolayer graphene, in agreement with an expected ratio for a monolayer

(≥ 2). Raman spectra of bilayer and double-stack graphene demonstrated the peaks' intensity ratio of approximately 0.8, while the expected value was approximately 1. In the case of triple-stack graphene, the calculated intensity ratio value of 0.3. The ratio differed from the expected value of approximately 0.6 [131]. The possible causes of such low value were attributed to the folding of the monolayers and the formation of multi-layer zones of graphene during the multiple transfers. All the calculated values of I_{2D}/I_G are graphically illustrated in a histogram in Figure 49.

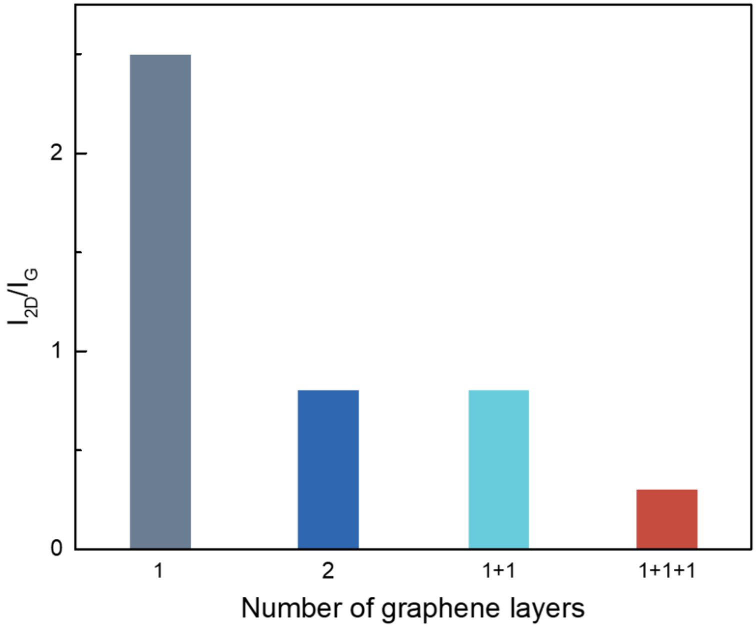

Figure 49. Illustration of the ratio of 2D and G mode intensities for corresponding graphene layers. The ratio values are calculated from the spectra presented in Figure 45.

In conclusion, the data of Raman spectroscopy were sufficiently in agreement with the expected number of graphene monolayers transferred. Thus, the samples were ready for the MOVPE growth of GaN epitaxial layers.

2.6. GaN growth on multi-layer graphene

The next step of remote epitaxy experiments was to investigate the influence of the number and the type of graphene layers on GaN nucleation. It was known from the previous experiments (outlined in subchapter GaN growth on monolayer graphene) that GaN nucleation manifests in a few distinct types of nuclei on monolayer graphene – hexagonal pyramid- and tetrahedral-shaped. Previous studies also suggested that clearly-defined and well-aligned nuclei could be observed on both monolayer and bilayer graphene [14,20]. Some authors have recently expressed concern that bilayer graphene could obstruct seed and epilayer interaction hindering remote epitaxy capabilities [19]. However, provided EBSD experimental data was arguably insufficient to neglect the interaction as GaN seed orientation homogeneity differed when bilayer and triple-layer graphene were used to cover the substrate.

As the growth of GaN epilayer is time and resource-intensive, short GaN nucleation by the MOVPE process was chosen as a viable way to test multilayer graphene suitability. A growth protocol for GaN nuclei formation at 700 °C for 5 min was implemented. Afterward, GaN nuclei were investigated using the SEM technique.

The nucleation differences were observed immediately. As expected, both regular shape and irregular shape island formations were discovered on monolayer graphene. Ordinary shape (both hexagonal pyramid- and tetrahedral-shaped) nuclei were in-plane aligned, with one of the edges (two edges in case of hexagonal shape) perpendicular to the $[11\bar{2}0]$ direction of the underlying sapphire substrate. The orientation of such nuclei was confidently resolved during SEM scanning as a round sapphire wafer had a flat perpendicular to this direction. GaN nucleation on bilayer graphene demonstrated a somewhat similar shape, characteristic of both hexagonal and triangular-based nuclei. However, nuclei size was smaller, and also a lack of irregular-shaped nuclei was observed. Finally, growth on the double- and triple-stack of graphene layers differed from growth on single-transfer graphene. Almost no regular-shaped nuclei were observed. Similarly, in-plane alignment was not manifested, suggesting a lack of remote interaction. The corresponding zoomed-in SEM images are represented in Figure 50**.**

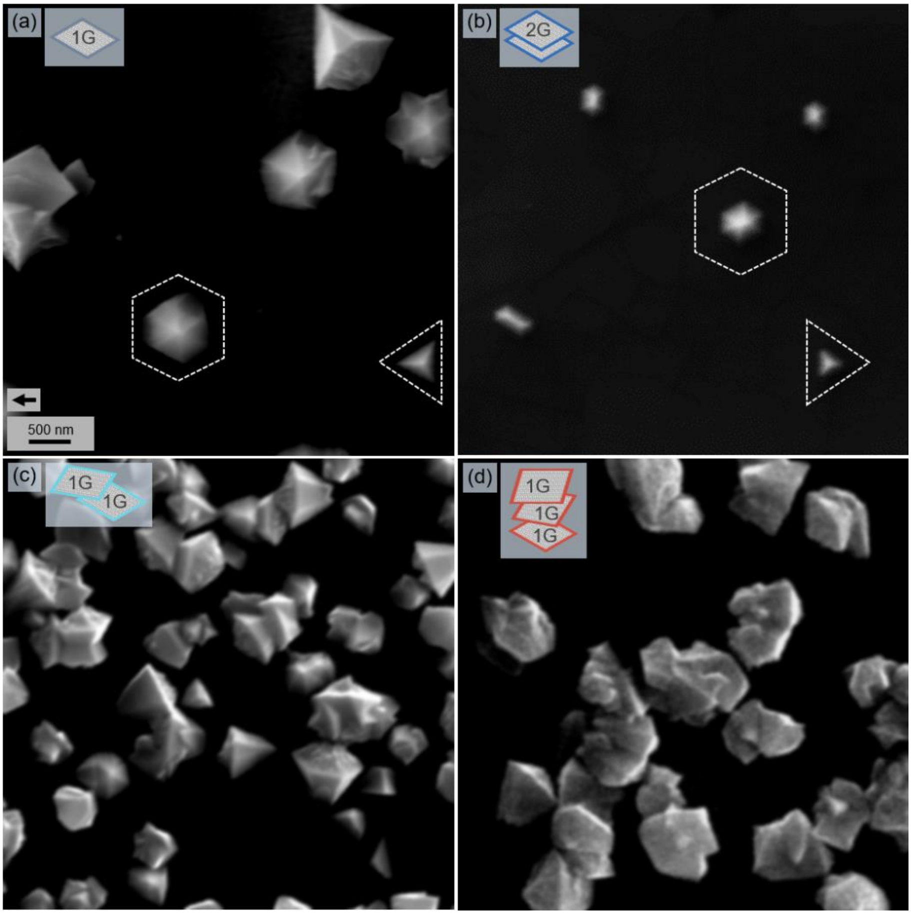

Figure 50. Zoomed-in SEM images of the GaN nuclei after the MOVPE growth of the low-temperature (700 °C) nucleation layer for 5 min. The growth was performed on: monolayer graphene (a), bilayer graphene (b), double-stack graphene (c), and triple-stack graphene (d). The scale bar in (a) is the same for all SEM images. The black arrow in an image (a) indicates $[11\bar{2}0]$ direction of an underlying sapphire substrate for all images. White dashed figures in (a) and (b) enclose two types of GaN nuclei – hexagonal pyramid- and tetrahedral-shaped seeds.

Zoomed-out SEM images around the center of the graphene area were taken to investigate nucleation density (Figure 51). Very sparse nucleation was observed on bilayer graphene, as expected. Such discovery was partially attributed to the lack of holes in aperture-free bilayer graphene. In this case, the van der Waals surface of graphene was unfavorable for GaN to nucleate on [93,155]. However, low-temperature growth characteristics on double-stacked graphene were different. GaN nucleation density was high and very similar to that of triple-stack graphene. Such a result was unanticipated initially. It could be that the double transfer of graphene significantly damaged the first layer and left the interface contaminated. The induced interface contamination negatively affected GaN growth by remote epitaxy mode.

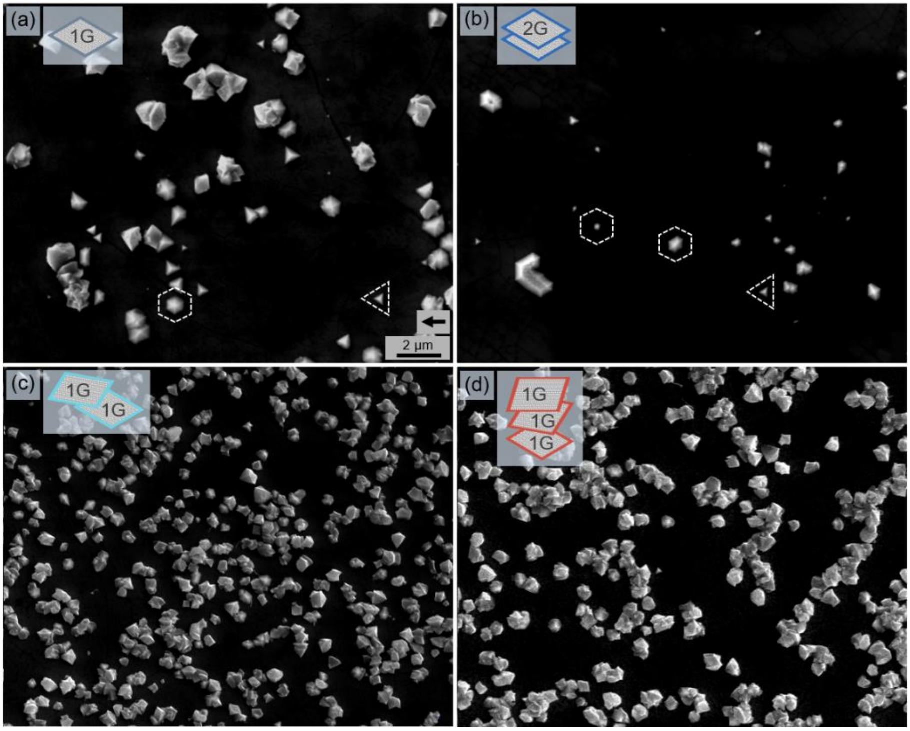

Figure 51. Zoomed-out SEM images of the GaN nuclei after the MOVPE growth of the low-temperature (700 °C) nucleation layer for 5 min. The growth was performed on: monolayer graphene (a), bilayer graphene (b), double-stack graphene (c), and triple-stack graphene (d). The scale bar in (a) is the same for all SEM images. The black arrow in an image (a) indicates $[11\bar{2}0]$ direction of an underlying sapphire substrate for all images. White dashed figures in (a) and (b) enclose two types of GaN nuclei – hexagonal pyramid- and tetrahedral-shaped seeds. SEM images are adapted from the publication of the author [P2].

Seeds on monolayer graphene covered around 12 % of the total surface area, while only 2 % on the bilayer. Thus, nucleation was significantly suppressed by an additional graphene layer on top. However, a considerably larger area on multiple transfer graphene was covered by GaN seeds exceeding 30 %, suggesting epitaxy on damaged layers (Table 1).

Table 1. Surface coverage by GaN nuclei after 5 min of growth on a different number and types of graphene layers.

Number of graphene layers	Approx. GaN nuclei coverage, %
1	12
2	2
1+1	35
1+1+1	33

The double-stack of monolayers and bilayer graphene were chosen for further investigation. These samples were expected to suit the remote epitaxy of GaN epitaxial layers on double-layer graphene. However, the nucleation differences suggested the bilayer to be the better choice. A two-step optimized growth protocol discussed in the subchapter GaN growth on monolayer graphene was used to form around 2.5 µm GaN film, starting with the nucleation at 700 °C and one hour-long MOVPE growth at 1075 °C. After the MOVPE process, the samples were immediately subjected to SEM investigation. Significant differences in GaN epilayer formation were revealed (Figure 52). GaN film on bilayer graphene was fully coalesced and relatively smooth, as demonstrated by AFM measurement (Figure 53). However, even after an hour of growth, GaN film on a double-stack of graphene only partially coalesced with no continuous epitaxial film present. The SEM findings further confirmed that bilayer graphene is more suitable for remote epitaxy growth mode than the double-stack of monolayers.

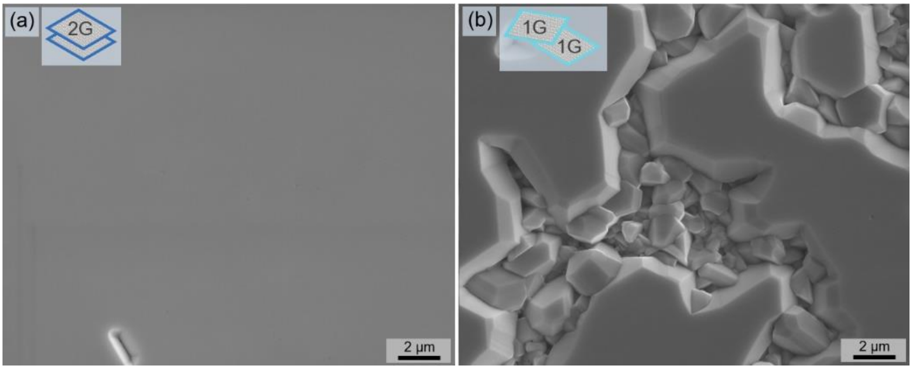

Figure 52. SEM images of GaN films grown on bilayer graphene (a) and double-stack of graphene (b). Arbitrary defect in (a) was left intentionally to ensure that the image was focused. SEM images are adapted from the publication of the author [P2].

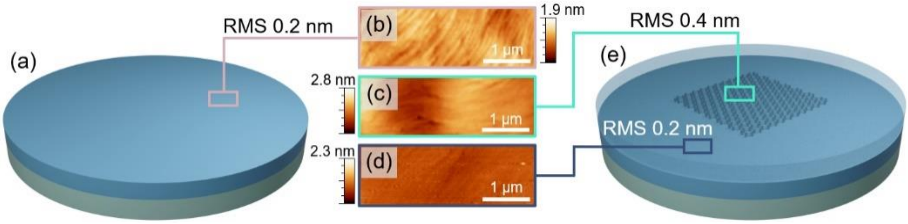

Figure 53. Schematic representation of the GaN sapphire template prior to the graphene transfer (a) as well as after the GaN membrane growth on bilayer graphene (e). Corresponding AFM scans are shown in (b)-(d). Surface RMS values are indicated in each AFM image accordingly. Part of the AFM results is adapted from the publication of the author [P2].

The bilayer graphene suitability for high-quality GaN film growth was confirmed by XRD measurements of the GaN/sapphire template and the GaN thin film on bilayer graphene. Complementary to the XRD measurements of the (0002) reflection, the rocking curves (φ-scans) of the $(1\bar{1}00)$ plane (also known as GaN *m*-plane) were measured using in-plane XRD geometry (Figure 54). Such an approach was chosen to minimize the contribution of the underlying GaN substrate and have an XRD signal solely from GaN epitaxial layer on graphene. Very similar FWHM values of both samples were obtained – 767 arcsec and 808 arcsec for the substrate and the epilayer, respectively. The finding indicated a good crystalline quality of GaN thin film grown by the MOVPE process on bilayer graphene. As continuous film did not form in the case of double-stack graphene, the corresponding sample was not included in the XRD analysis

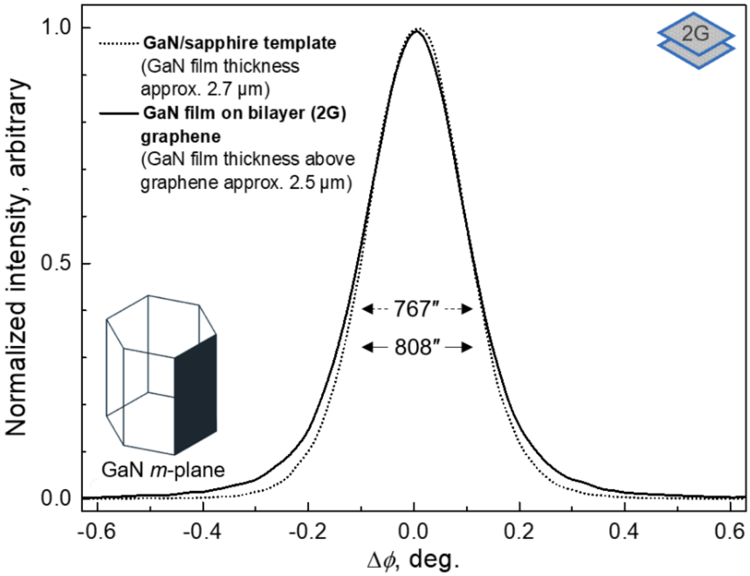

Figure 54. XRD rocking curves of $(1\bar{1}00)$ reflection (indicated in the inset) of GaN epilayer grown on bilayer graphene (marked by a solid black line) and the GaN/sapphire template (marked by a black dotted line). XRD data is adapted from the publication of the author [P2].

The last but not least measurement in comparing the bilayer graphene and the double-stacked graphene was the interface analysis by TEM – contrasting views are represented in Figure 55. The bright horizontal stripe composed of two brighter regions was seen in the sample of bilayer graphene (Figure 55 (a)). The well-defined two-layer structure was attributed to the two monolayers of graphene. Coherent atomic steps of GaN were seen in the template as well as in the epilayer on top. The GaN crystallographic direction [0002] was resolved for both the substrate and the epilayer GaN by the FFT analysis of the acquired TEM images.

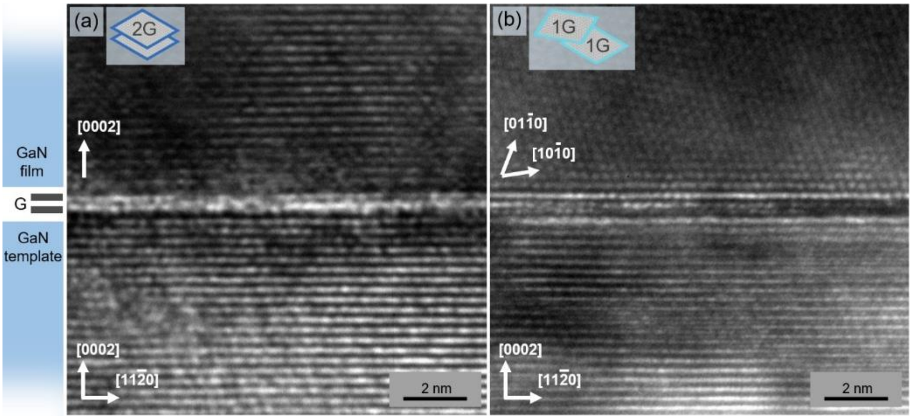

Figure 55. TEM images of GaN film grown on bilayer (a) and double-stack graphene (b) with the schematic representation of the sample on the left. Crystallographic directions are indicated where determined. TEM images are adapted from the publication of the author [P2].

However, Figure 55 (b) presented a different situation between the GaN/sapphire template and the epitaxial layer at the atomic interface. The two-layer structure was hardly resolvable within a thicker than two-layer structure interface. Coherent atomic steps in the [0002] direction were seen in the GaN/sapphire template side. However, the orientation of GaN has changed immediately after the interface suggesting the vdW growth mode instead of the remote one. This observation was in agreement with SEM images presented in Figure 50 (c) and Figure 51 (c).

All the analyzed results confirmed the wet-transferred bilayer graphene suitability for GaN growth by the MOVPE process manifesting in remote epitaxy mode when graphene was transferred in a single step. In contrast, the likely interface contamination and deterioration of double-stack graphene resulted in a van der Waals (or even another type) growth mode.

2.7. Outlook

This work provides insights and optimization strategies for GaN growth on graphene and thin membrane exfoliation. The next generation of flexible devices will likely include membranes of such inorganic materials. However, to fully implement such an approach at scale, many steps still require further optimization and scaling:

- The size of graphene coverage could be maximized. Innovative large-scale transfer methods could be one way to reduce the cost further and increase the yield [156].

- The tension of a metal stressor layer could be optimized to avoid the total roll-up of the exfoliated membrane. It could be achieved by modification of electrolytes and/or the thickness of the stressor layer.

- GaN membrane exfoliation should be demonstrated after the MOVPE process on the bilayer graphene-covered GaN/sapphire template.

CONCLUSIONS

1. GaN/sapphire template was demonstrated as a cost-effective alternative substrate for remote epitaxy of GaN by the MOVPE process.

2. It was shown that wet-transferred graphene is of sufficient quality for remote epitaxy of GaN by the MOVPE process after an appropriate PMMA removal procedure.

3. Graphene decomposition in hydrogen- and ammonia-containing atmosphere during the MOVPE process of GaN is prevented at a 700 °C or lower temperature.

4. Two-step MOVPE process of GaN on graphene-covered GaN/sapphire template with the nucleation step carried at 700 °C and followed by lateral coalescence at 1075 °C results in a high-quality GaN epitaxial layer.

5. Stack of Ti adhesive layer, Au oxidation barrier layer, and electroplated Ni stressor layer was shown to assist exfoliation of GaN membrane grown by MOVPE on graphene covered GaN/sapphire template.

6. The pristine interface of single-process wet-transferred bilayer graphene on GaN/sapphire template permits sufficient remote interaction of GaN nuclei and the seeding layer beneath bilayer graphene. At the same time, double-process wet-transferred bilayer graphene restricts the remote epitaxy of GaN by MOVPE.

REFERENCES

[1] S. Nakamura and M. R. Krames, “History of Gallium–Nitride-Based Light-Emitting Diodes for Illumination”, Proc. IEEE **101**(10), 2211–2220 (2013).

[2] S. Nakamura, “GaN Growth Using GaN Buffer Layer”, Jpn. J. Appl. Phys. **30**, L1705–L1707 (1991).

[3] S. Nakamura, N. Iwasa, M. Senoh, and T. Mukai, “Hole Compensation Mechanism of P-Type GaN Films”, Jpn. J. Appl. Phys. **31**, 1258–1266 (1992).

[4] H. Amano, N. Sawaki, I. Akasaki, and Y. Toyoda, “Metalorganic vapor phase epitaxial growth of a high quality GaN film using an AlN buffer layer”, Appl. Phys. Lett. **48**(5), 353–355 (1986).

[5] B. N. Pushpakaran, A. S. Subburaj, and S. B. Bayne, “Commercial GaN-Based Power Electronic Systems: A Review”, J. Electron. Mater. **49**(11), 6247–6262 (2020).

[6] A. Chen, “Gallium nitride is the silicon of the future”, theverge.com, accessed April 22, 2022, at https://www.theverge.com/2018/11/1/18051974/gallium-nitride-anker-material-silicon-semiconductor-energy.

[7] S. Xu, A. Jayaraman, and J. A. Rogers, “Skin sensors are the future of health care”, Nature **571**(7765), 319–321 (2019).

[8] M. Kim, J.-H. Seo, U. Singisetti, and Z. Ma, “Recent advances in free-standing single crystalline wide band-gap semiconductors and their applications: GaN, SiC, ZnO, β-Ga_2O_3, and diamond”, J. Mater. Chem. C **5**(33), 8338–8354 (2017).

[9] A. K. Geim and I. V. Grigorieva, “Van der Waals heterostructures”, Nature **499**(7459), 419–425 (2013).

[10] A. Smith, “Speed read: a chip off the old block”, nobelprize.org, accessed April 22, 2022, at https://www.nobelprize.org/prizes/physics/2010/speedread.

[11] J. Chu, “Not stuck on silicon”, news.mit.edu, accessed April 22, 2022, at https://news.mit.edu/2017/graphene-copy-machine-cheaper-semiconductor-wafers-0419.

[12] H. S. Kum, H. Lee, S. Kim, S. Lindemann, W. Kong, K. Qiao, P. Chen, J. Irwin, J. H. Lee, S. Xie, S. Subramanian, J. Shim, S.-H. Bae, C. Choi, L. Ranno, S. Seo, S. Lee, J. Bauer, H. Li, K. Lee, J. A. Robinson, C. A. Ross, D. G. Schlom, M. S. Rzchowski, C.-B. Eom, and J. Kim, “Heterogeneous integration of single-crystalline complex-oxide membranes”, Nature **578**(7793), 75–81 (2020).

[13] Y. Kim, S. S. Cruz, K. Lee, B. O. Alawode, C. Choi, Y. Song, J. M. Johnson, C. Heidelberger, W. Kong, S. Choi, K. Qiao, I. Almansouri, E. A. Fitzgerald, J. Kong, A. M. Kolpak, J. Hwang, and J. Kim, “Remote epitaxy through graphene enables two-dimensional material-based layer transfer”, Nature **544**(7650), 340–343 (2017).

[14] W. Kong, H. Li, K. Qiao, Y. Kim, K. Lee, Y. Nie, D. Lee, T. Osadchy, R. J. Molnar, D. K. Gaskill, R. L. Myers-Ward, K. M. Daniels, Y. Zhang, S. Sundram, Y. Yu, S. Bae, S. Rajan, Y. Shao-Horn, K. Cho, A. Ougazzaden, J. C. Grossman, and J. Kim, “Polarity governs atomic interaction through two-dimensional materials”, Nat. Mater. **17**(11), 999–1005 (2018).

[15] J. Jiang, X. Sun, X. Chen, B. Wang, Z. Chen, Y. Hu, Y. Guo, L. Zhang, Y. Ma, L. Gao, F. Zheng, L. Jin, M. Chen, Z. Ma, Y. Zhou, N. P. Padture, K. Beach, H. Terrones, Y. Shi, D. Gall, T.-M. Lu, E. Wertz, J. Feng, and J. Shi, “Carrier lifetime enhancement in halide perovskite via remote epitaxy”, Nat. Commun. **10**(1), 4145 (2019).

[16] Y. Alaskar, S. Arafin, D. Wickramaratne, M. A. Zurbuchen, L. He, J. McKay, Q. Lin, M. S. Goorsky, R. K. Lake, and K. L. Wang, “Towards van der Waals Epitaxial Growth of GaAs on Si using a Graphene Buffer Layer”, Adv. Funct. Mater. **24**(42), 6629–6638 (2014).

[17] D. Wang, Y. Lu, J. Meng, X. Zhang, Z. Yin, M. Gao, Y. Wang, L. Cheng, J. You, and J. Zhang, “Remote heteroepitaxy of atomic layered hafnium disulfide on sapphire through hexagonal boron nitride”, Nanoscale **11**(19), 9310–9318 (2019).

[18] Y. Guo, X. Sun, J. Jiang, B. Wang, X. Chen, X. Yin, W. Qi, L. Gao, L. Zhang, Z. Lu, R. Jia, S. Pendse, Y. Hu, Z. Chen, E. Wertz, D. Gall, J. Feng, T.-M. Lu, and J. Shi, “A Reconfigurable Remotely Epitaxial VO_2 Electrical Heterostructure”, Nano Lett. **20**(1), 33–42 (2020).

[19] J. Yu, L. Wang, X. Han, Z. Hao, Y. Luo, C. Sun, Y. Han, B. Xiong, J. Wang, and H. Li, “Van der Waals coherent epitaxy of GaN and InGaN/GaN multi-quantum-well via a graphene inserted layer”, Opt. Mater. Express **11**(12), 4118 (2021).

[20] J. Jeong, Q. Wang, J. Cha, D. K. Jin, D. H. Shin, S. Kwon, B. K. Kang, J. H. Jang, W. S. Yang, Y. S. Choi, J. Yoo, J. K. Kim, C.-H. Lee, S. W. Lee, A. Zakhidov, S. Hong, M. J. Kim, and Y. J. Hong, “Remote heteroepitaxy of GaN microrod heterostructures for deformable light-emitting diodes and wafer recycle”, Sci. Adv. **6**(23), eaaz5180 (2020).

[21] K. Qiao, Y. Liu, C. Kim, R. J. Molnar, T. Osadchy, W. Li, X. Sun, H. Li, R. L. Myers-Ward, D. Lee, S. Subramanian, H. Kim, K. Lu, J. A. Robinson, W. Kong, and J. Kim, “Graphene Buffer Layer on SiC as a Release Layer for High-Quality Freestanding Semiconductor Membranes”, Nano Lett. **21**(9), 4013–4020 (2021).

[22] H. Kim, C. S. Chang, S. Lee, J. Jiang, J. Jeong, M. Park, Y. Meng, J. Ji, Y. Kwon, X. Sun, W. Kong, H. S. Kum, S.-H. Bae, K. Lee, Y. J. Hong, J. Shi, and J. Kim, “Remote epitaxy”, Nat. Rev. Methods Primer **2**(1), 40 (2022).

[23] H. Kim, K. Lu, Y. Liu, H. S. Kum, K. S. Kim, K. Qiao, S.-H. Bae, S. Lee, Y. J. Ji, K. H. Kim, H. Paik, S. Xie, H. Shin, C. Choi, J. H. Lee, C. Dong, J. A. Robinson, J.-H. Lee, J.-H. Ahn, G. Y. Yeom, D. G. Schlom, and J. Kim, “Impact of 2D–3D Heterointerface on Remote Epitaxial Interaction through Graphene”, ACS Nano **15**(6), 10587–10596 (2021).

[24] A. Yoshikawa, E. Ohshima, T. Fukuda, H. Tsuji, and K. Oshima, “Crystal growth of GaN by ammonothermal method”, J. Cryst. Growth **260**(1–2), 67–72 (2004).

[25] M. T. Hardy, D. F. Feezell, S. P. DenBaars, and S. Nakamura, “Group III-nitride lasers: a materials perspective”, Mater. Today **14**(9), 408–415 (2011).

[26] J. Wang, P. Mulligan, L. Brillson, and L. R. Cao, “Review of using gallium nitride for ionizing radiation detection”, Appl. Phys. Rev. **2**(3), 031102 (2015).

[27] T. Zimmermann, M. Neuburger, P. Benkart, F. J. Hernandez-Guillen, C. Pietzka, M. Kunze, I. Daumiller, A. Dadgar, A. Krost, and E. Kohn, "Piezoelectric GaN sensor structures", IEEE Electron Device Lett. **27**(5), 309–312 (2006).

[28] J. Chen, S. K. Oh, H. Zou, S. Shervin, W. Wang, S. Pouladi, Y. Zi, Z. L. Wang, and J.-H. Ryou, "High-Output Lead-Free Flexible Piezoelectric Generator Using Single-Crystalline GaN Thin Film", ACS Appl. Mater. Interfaces **10**(15), 12839 (2018).

[29] K. Yuk, G. R. Branner, and C. Cui, "Future directions for GaN in 5G and satellite communications", 2017 IEEE 60th International Midwest Symposium on Circuits and Systems (MWSCAS), IEEE, 803–806 (2017).

[30] L. Keesey, "NASA studies space applications for GaN crystals", nasa.gov, accessed March 20, 2022, at https://www.nasa.gov/feature/goddard/2018/nasa-studies-space-applications-for-gan-crystals.

[31] C. M. Furqan, M. U. Khan, M. Awais, F. Jiang, J. Bae, A. Hassan, and H.-S. Kwok, "Humidity sensor based on Gallium Nitride for real time monitoring applications", Sci. Rep. **11**(1), 11088 (2021).

[32] D. Gajula, I. Jahangir, and G. Koley, "High Temperature AlGaN/GaN Membrane Based Pressure Sensors", Micromachines **9**(5), 207 (2018).

[33] A. Das, A. Das, L. B. Chang, C. S. Lai, R. M. Lin, F. C. Chu, Y. H. Lin, L. Chow, and M. J. Jeng, "GaN Thin Film Based Light Addressable Potentiometric Sensor for pH Sensing Application", Appl. Phys. Express **6**(3), 036601 (2013).

[34] D.-S. Lee, J.-H. Lee, Y.-H. Lee, and D.-D. Lee, "GaN thin films as gas sensors", Sens. Actuators B Chem. **89**(3), 305–310 (2003).

[35] H. Liu, Q. Hua, R. Yu, Y. Yang, T. Zhang, Y. Zhang, and C. Pan, "A Bamboo-Like GaN Microwire-Based Piezotronic Memristor", Adv. Funct. Mater. **26**(29), 5307–5314 (2016).

[36] I. Aharonovich and E. Neu, "Diamond Nanophotonics", Adv. Opt. Mater. **2**(10), 911–928 (2014).

[37] D. E. Baker, "Graphite as a neutron moderator and reflector material", Nucl. Eng. Des. **14**(3), 413–444 (1971).

[38] H. W. Kroto, J. R. Heath, S. C. O’Brien, R. F. Curl, and R. E. Smalley, “C60: Buckminsterfullerene”, Nature **318**(6042), 162–163 (1985).

[39] D.-I. Moon, B. Kim, R. Peterson, K. Badokas, M.-L. Seol, D. G. Senesky, J.-W. Han, and M. Meyyappan, “A Single Input Multiple Output (SIMO) Variation-Tolerant Nanosensor”, ACS Sens. **3**(9), 1782–1788 (2018).

[40] K. S. Novoselov, A. K. Geim, S. V. Morozov, D. Jiang, Y. Zhang, S. V. Dubonos, I. V. Grigorieva, and A. A. Firsov, “Electric Field Effect in Atomically Thin Carbon Films”, Science **306**(5696), 666–669 (2004).

[41] A. K. Geim and K. S. Novoselov, “The rise of graphene”, Nat. Mater. **6**(3), 183–191 (2007).

[42] A. Peigney, Ch. Laurent, E. Flahaut, R. R. Bacsa, and A. Rousset, “Specific surface area of carbon nanotubes and bundles of carbon nanotubes”, Carbon **39**(4), 507–514 (2001).

[43] PDF document “Laws of the Game 20/21”, fifa.com, accessed July 29, 2022, at https://digitalhub.fifa.com/m/5371a6dcc42fbb44/original/d6g1medsi8jrrd3e4imp-pdf.pdf.

[44] M. Berger, “Graphene – all you need to know”, nanowerk.com, accessed April 25, 2022, at https://www.nanowerk.com/what_is_graphene.php.

[45] P. R. Wallace, “The Band Theory of Graphite”, Phys. Rev. **71**(9), 622–634 (1947).

[46] H.-P. Boehm, “Graphene-How a Laboratory Curiosity Suddenly Became Extremely Interesting”, Angew. Chem. Int. Ed. **49**(49), 9332–9335 (2010).

[47] “Graphene – the perfect atomic lattice”, nobelprize.com, accessed May 26, 2022, at https://www.nobelprize.org/prizes/physics/2010/press-release.

[48] Information on website, graphene-flagship.eu, accessed April 05, 2022, at https://graphene-flagship.eu.

[49] K. S. Novoselov, A. K. Geim, S. V. Morozov, D. Jiang, M. I. Katsnelson, I. V. Grigorieva, S. V. Dubonos, and A. A. Firsov, “Two-dimensional gas of massless Dirac fermions in graphene”, Nature **438**(7065), 197–200 (2005).

[50] K. I. Bolotin, K. J. Sikes, Z. Jiang, M. Klima, G. Fudenberg, J. Hone, P. Kim, and H. L. Stormer, “Ultrahigh electron mobility in suspended graphene”, Solid State Commun. **146**(9–10), 351–355 (2008).

[51] Y. Wu, K. A. Jenkins, A. Valdes-Garcia, D. B. Farmer, Y. Zhu, A. A. Bol, C. Dimitrakopoulos, W. Zhu, F. Xia, P. Avouris, and Y.-M. Lin, “State-of-the-Art Graphene High-Frequency Electronics”, Nano Lett. **12**(6), 3062–3067 (2012).

[52] A. Ambrosetti and P. L. Silvestrelli, “Trends in the Change in Graphene Conductivity upon Gas Adsorption: The Relevance of Orbital Distortion”, J. Phys. Chem. Lett. **11**(7), 2737–2741 (2020).

[53] R. R. Nair, P. Blake, A. N. Grigorenko, K. S. Novoselov, T. J. Booth, T. Stauber, N. M. R. Peres, and A. K. Geim, “Fine Structure Constant Defines Visual Transparency of Graphene”, Science **320**(5881), 1308–1308 (2008).

[54] Y. Zhang, T.-T. Tang, C. Girit, Z. Hao, M. C. Martin, A. Zettl, M. F. Crommie, Y. R. Shen, and F. Wang, “Direct observation of a widely tunable bandgap in bilayer graphene”, Nature **459**(7248), 820–823 (2009).

[55] F. Bonaccorso, Z. Sun, T. Hasan, and A. C. Ferrari, “Graphene photonics and optoelectronics”, Nat. Photonics **4**(9), 611–622 (2010).

[56] F. Valorosi, E. De Meo, T. Blanco-Varela, B. Martorana, A. Veca, N. Pugno, I. A. Kinloch, G. Anagnostopoulos, C. Galiotis, F. Bertocchi, J. Gomez, E. Treossi, R. J. Young, and V. Palermo, “Graphene and related materials in hierarchical fiber composites: Production techniques and key industrial benefits”, Compos. Sci. Technol. **185**, 107848 (2020).

[57] C. Lee, X. Wei, J. W. Kysar, and J. Hone, “Measurement of the Elastic Properties and Intrinsic Strength of Monolayer Graphene”, Science **321**(5887), 385–388 (2008).

[58] PDF document, “Scientifc background on the Nobel prize in physics 2010”, nobelprize.org, accessed May 02, 2022, at www.nobelprize.org/uploads/2018/06/advanced-physicsprize2010.pdf.

[59] E. Pop, V. Varshney, and A. K. Roy, “Thermal properties of graphene: Fundamentals and applications”, MRS Bull. **37**(12), 1273–1281 (2012).

[60] Wikipedia article, “Thermal conductivities of the elements (data page)” wikipedia.org, accessed May 15, 2022, at https://en.wikipedia.org/wiki/thermal_conductivities_of_the_elements_(data_page).

[61] “Graphene composites enable the aviation industry to gain altitude”, grapheneflagship.com, accessed May 2, 2022, at https://graphene-flagship.eu/graphene/news/graphene-composites-enable-the-aviation-industry-to-gain-altitude.

[62] T. Newcomb, “Graphene-enhanced foam debuts on inov-8 trail shoe”, forbes.com, accessed April 22, 2022, at https://www.forbes.com/sites/timnewcomb/2021/03/24/graphene-enhanced-foam-debuts-on-inov-8-trail-shoe.

[63] S. Hu, M. Lozada-Hidalgo, F. C. Wang, A. Mishchenko, F. Schedin, R. R. Nair, E. W. Hill, D. W. Boukhvalov, M. I. Katsnelson, R. A. W. Dryfe, I. V. Grigorieva, H. A. Wu, and A. K. Geim, “Proton transport through one-atom-thick crystals”, Nature **516**(7530), 227–230 (2014).

[64] P. Z. Sun, Q. Yang, W. J. Kuang, Y. V. Stebunov, W. Q. Xiong, J. Yu, R. R. Nair, M. I. Katsnelson, S. J. Yuan, I. V. Grigorieva, M. Lozada-Hidalgo, F. C. Wang, and A. K. Geim, “Limits on gas impermeability of graphene”, Nature **579**(7798), 229–232 (2020).

[65] X.-Y. Wang, A. Narita, and K. Müllen, “Precision synthesis versus bulk-scale fabrication of graphenes”, Nat. Rev. Chem. **2**(1), 0100 (2018).

[66] M. Yi and Z. Shen, “A review on mechanical exfoliation for the scalable production of graphene”, J. Mater. Chem. A **3**(22), 11700–11715 (2015).

[67] C. K. Chua and M. Pumera, “Chemical reduction of graphene oxide: a synthetic chemistry viewpoint”, Chem Soc Rev **43**(1), 291–312 (2014).

[68] Y. Hernandez, V. Nicolosi, M. Lotya, F. M. Blighe, Z. Sun, S. De, I. T. McGovern, B. Holland, M. Byrne, Y. K. Gun'Ko, J. J. Boland, P. Niraj, G. Duesberg, S. Krishnamurthy, R. Goodhue, J. Hutchison, V. Scardaci, A. C. Ferrari, and J. N. Coleman, "High-yield production of graphene by liquid-phase exfoliation of graphite", Nat. Nanotechnol. **3**(9), 563–568 (2008).

[69] X. Chen, L. Zhang, and S. Chen, "Large area CVD growth of graphene", Synth. Met. **210**, 95–108 (2015).

[70] W. Norimatsu and M. Kusunoki, "Epitaxial graphene on SiC{0001}: advances and perspectives", Phys. Chem. Chem. Phys. **16**(8), 3501 (2014).

[71] D. V. Badami, "X-Ray studies of graphite formed by decomposing silicon carbide", Carbon **3**(1), 53–57 (1965).

[72] J. Kim, H. Park, J. B. Hannon, S. W. Bedell, K. Fogel, D. K. Sadana, and C. Dimitrakopoulos, "Layer-Resolved Graphene Transfer via Engineered Strain Layers", Science **342**(6160), 833–836 (2013).

[73] X. Li, W. Cai, J. An, S. Kim, J. Nah, D. Yang, R. Piner, A. Velamakanni, I. Jung, E. Tutuc, S. K. Banerjee, L. Colombo, and R. S. Ruoff, "Large-Area Synthesis of High-Quality and Uniform Graphene Films on Copper Foils", Science **324**(5932), 1312–1314 (2009).

[74] X. Li, L. Colombo, and R. S. Ruoff, "Synthesis of Graphene Films on Copper Foils by Chemical Vapor Deposition", Adv. Mater. **28**(29), 6247–6252 (2016).

[75] H. M. Manasevit, "Recollections and reflections of MO-CVD", J. Cryst. Growth **55**(1), 1–9 (1981).

[76] H. M. Manasevit, "Single-crystal gallium arsenide on insulating substrates", Appl. Phys. Lett. **12**(4), 156–159 (1968).

[77] H. M. Manasevit, "The Use of Metal-Organics in the Preparation of Semiconductor Materials", J. Electrochem. Soc. **118**(4), 647–650 (1971).

[78] R. D. Dupuis and P. D. Dapkus, "Room-temperature operation of $Ga_{(1-x)}Al_xAs$/GaAs double-heterostructure lasers grown by metalorganic chemical vapor deposition", Appl. Phys. Lett. **31**(7), 466–468 (1977).

[79] C. A. Wang, “Early history of MOVPE reactor development”, J. Cryst. Growth **506**, 192 (2019).

[80] A. G. Thompson, V. S. Sundaram, G. R. Girard, and L. M. Fraas, “Growth of GaAs in a rotating disk MOCVD reactor”, J. Cryst. Growth **94**(4), 901–910 (1989).

[81] S. Nakamura, T. Mukai, M. Senoh, and N. Iwasa, “Thermal Annealing Effects on P-Type Mg-Doped GaN Films”, Jpn. J. Appl. Phys. **31**, L139–L142 (1992).

[82] “New light to illuminate the world”, nobelprize.org, accessed April 25, 2022, at https://www.nobelprize.org/prizes/physics/2014/press-release.

[83] J. Randall Creighton, G. T. Wang, and M. E. Coltrin, “Fundamental chemistry and modeling of group-III nitride MOVPE”, J. Cryst. Growth **298**, 2–7 (2007).

[84] J. Kim, C. Bayram, H. Park, C.-W. Cheng, C. Dimitrakopoulos, J. A. Ott, K. B. Reuter, S. W. Bedell, and D. K. Sadana, “Principle of direct van der Waals epitaxy of single-crystalline films on epitaxial graphene”, Nat. Commun. **5**(1), 4836 (2014).

[85] D. Liang, T. Wei, J. Wang, and J. Li, “Quasi van der Waals epitaxy nitride materials and devices on two dimension materials”, Nano Energy **69**, 104463 (2020).

[86] D. Jang, C. Ahn, Y. Lee, S. Lee, H. Lee, D. Kim, Y.-K. Kwon, J. Choi, and C. Kim, “Thru-Hole Epitaxy: Is Remote Epitaxy Really Remote?”, ArXiv 2110.01429 Cond-Mat (2021).

[87] F. Liu, Z. Zhang, X. Rong, Y. Yu, T. Wang, B. Sheng, J. Wei, S. Zhou, X. Yang, F. Xu, Z. Qin, Y. Zhang, K. Liu, B. Shen, and X. Wang, “Graphene-Assisted Epitaxy of Nitrogen Lattice Polarity GaN Films on Non-Polar Sapphire Substrates for Green Light Emitting Diodes”, Adv Funct Mater **30**(22), 2001283 (2020).

[88] S.-H. Bae, H. Kum, W. Kong, Y. Kim, C. Choi, B. Lee, P. Lin, Y. Park, and J. Kim, “Integration of bulk materials with two-dimensional materials for physical coupling and applications”, Nat. Mater. **18**(6), 550–560 (2019).

[89] T. Li, C. Liu, Z. Zhang, B. Yu, H. Dong, W. Jia, Z. Jia, C. Yu, L. Gan, B. Xu, and H. Jiang, "Understanding the Growth Mechanism of GaN Epitaxial Layers on Mechanically Exfoliated Graphite", Nanoscale Res. Lett. **13**(1), 130 (2018).

[90] J. Park, J. Lee, M. Park, J. Min, J. Lee, X. Yang, S. Kang, S. Kim, W. Jeong, H. Amano, and D. Lee, "Influence of Temperature-Dependent Substrate Decomposition on Graphene for Separable GaN Growth", Adv. Mater. Interfaces **6**(18), 1900821 (2019).

[91] A. Koma, "Van der Waals epitaxy—a new epitaxial growth method for a highly lattice-mismatched system", Thin Solid Films **216**(1), 72–76 (1992).

[92] M. Yen, Y. Bitla, and Y.-H. Chu, "van der Waals heteroepitaxy on muscovite", Mater. Chem. Phys. **234**, 185–195 (2019).

[93] C.-J. Shih, Q. H. Wang, S. Lin, K.-C. Park, Z. Jin, M. S. Strano, and D. Blankschtein, "Breakdown in the Wetting Transparency of Graphene", Phys. Rev. Lett. **109**(17), 176101 (2012).

[94] S. Wang, Y. Zhang, N. Abidi, and L. Cabrales, "Wettability and Surface Free Energy of Graphene Films", Langmuir **25**(18), 11078–11081 (2009).

[95] Y. Qu, Y. Xu, B. Cao, Y. Wang, J. Wang, L. Shi, and K. Xu, "Long-Range Orbital Hybridization in Remote Epitaxy: The Nucleation Mechanism of GaN on Different Substrates *via* Single-Layer Graphene", ACS Appl. Mater. Interfaces **14**(1), 2263–2274 (2022).

[96] H. Volkmann, "Ernst Abbe and His Work", Appl. Opt. **5**(11), 1720 (1966).

[97] N. Gleichmann, "SEM vs TEM", technologynetworks.com, accessed May 16, 2022, at https://www.technologynetworks.com/analysis/articles/sem-vs-tem-331262.

[98] A. Nanakoudis, "SEM: types of electrons and the information they provide", thermofisher.com, accessed May 16, 2022, at https://www.thermofisher.com/blog/microscopy/sem-signal-types-electrons-and-the-information-they-provide.

[99] R. Tomašiūnas, "Šiuolaikinės Mikroskopijos Metodai Medžiagotyrai", Vilnius: Progretus (2008), 36–38, 75–78 p., ISBN 978-9955-781-08-0.

[100] T. Ishitani, “Improvements in performance of focused ion beam cross-sectioning: aspects of ion-sample interaction”, J. Electron Microsc. (Tokyo) **53**(5), 443–449 (2004).

[101] M. Schaffer, B. Schaffer, and Q. Ramasse, “Sample preparation for atomic-resolution STEM at low voltages by FIB”, Ultramicroscopy **114**, 62–71 (2012).

[102] M. Skapas, “Bi kvantinių taškų GaAsBi matricoje tyrimas peršviečiamąja elektronine mikroskopija”, doctoral thesis, Vilnius University (2019), 29–32 p.

[103] G. Binnig, C. F. Quate, and Ch. Gerber, “Atomic Force Microscope”, Phys. Rev. Lett. **56**(9), 930–933 (1986).

[104] O. Custance, R. Perez, and S. Morita, “Atomic force microscopy as a tool for atom manipulation”, Nat. Nanotechnol. **4**(12), 803–810 (2009).

[105] I. Horcas, R. Fernández, J. M. Gómez-Rodríguez, J. Colchero, J. Gómez-Herrero, and A. M. Baro, “WSXM: A software for scanning probe microscopy and a tool for nanotechnology”, Rev. Sci. Instrum. **78**(1), 013705 (2007).

[106] Information on website nanosurf.com, accessed on May 26, 2022, at https://www.nanosurf.com/en/support/afm-modes-overview/topography-and-surface-roughness-measurements.

[107] C. V. Raman and K. S. Krishnan, “A New Type of Secondary Radiation”, Nature **121**(3048), 501–502 (1928).

[108] “The Nobel Prize in Physics 1930”, nobelprize.org, accessed April 26, 2022, at https://www.nobelprize.org/prizes/physics/1930/summary.

[109] H. M. Mansour and A. J. Hickey, “Raman characterization and chemical imaging of biocolloidal self-assemblies, drug delivery systems, and pulmonary inhalation aerosols: A review”, AAPS PharmSciTech **8**(4), 140 (2007).

[110] V. Y. Davydov, M. P. Scheglov, and M. B. Smirnov, “Raman Spectroscopy as a Tool for Characterization of Strained Hexagonal GaN/$Al_xGa_{1-x}N$ Superlattices”, **234**(3), 6 (2002).

[111] N. Kokubo, Y. Tsunooka, F. Fujie, J. Ohara, S. Onda, H. Yamada, M. Shimizu, S. Harada, M. Tagawa, and T. Ujihara, "Nondestructive visualization of threading dislocations in GaN by micro raman mapping", Jpn. J. Appl. Phys. **58**(SC), SCCB06 (2019).

[112] H. J. Trodahl, F. Budde, B. J. Ruck, S. Granville, A. Koo, and A. Bittar, "Raman spectroscopy of nanocrystalline and amorphous GaN", J. Appl. Phys. **97**(8), 084309 (2005).

[113] C. Carlomagno, D. Bertazioli, A. Gualerzi, S. Picciolini, P. I. Banfi, A. Lax, E. Messina, J. Navarro, L. Bianchi, A. Caronni, F. Marenco, S. Monteleone, C. Arienti, and M. Bedoni, "COVID-19 salivary Raman fingerprint: innovative approach for the detection of current and past SARS-CoV-2 infections", Sci. Rep. **11**(1), 4943 (2021).

[114] I. B. Hutchinson, R. Ingley, H. G. M. Edwards, L. Harris, M. McHugh, C. Malherbe, and J. Parnell, "Raman spectroscopy on Mars: identification of geological and bio-geological signatures in Martian analogues using miniaturized Raman spectrometers", Philos. Trans. R. Soc. Math. Phys. Eng. Sci. **372**(2030), 20140204 (2014).

[115] A. C. Ferrari and D. M. Basko, "Raman spectroscopy as a versatile tool for studying the properties of graphene", Nat. Nanotechnol. **8**(4), 235–246 (2013).

[116] F. Tuinstra and J. L. Koenig, "Raman Spectrum of Graphite", J. Chem. Phys. **53**(3), 1126–1130 (1970).

[117] A. C. Ferrari, J. C. Meyer, V. Scardaci, C. Casiraghi, M. Lazzeri, F. Mauri, S. Piscanec, D. Jiang, K. S. Novoselov, S. Roth, and A. K. Geim, "Raman Spectrum of Graphene and Graphene Layers", Phys. Rev. Lett. **97**(18), 187401 (2006).

[118] R. Trusovas, G. Račiukaitis, G. Niaura, J. Barkauskas, G. Valušis, and R. Pauliukaite, "Recent Advances in Laser Utilization in the Chemical Modification of Graphene Oxide and Its Applications", Adv. Opt. Mater. **4**(1), 37–65 (2016).

[119] R. P. Vidano, D. B. Fischbach, L. J. Willis, and T. M. Loehr, "Observation of Raman band shifting with excitation wavelength for carbons and graphites", Solid State Commun. **39**(2), 341–344 (1981).

[120] C. Thomsen and S. Reich, "Double Resonant Raman Scattering in Graphite", Phys. Rev. Lett. **85**(24), 5214–5217 (2000).

[121] A. A. Bunaciu, V. D. Hoang, and H. Y. Aboul-Enein, “Vibrational Micro-Spectroscopy of Human Tissues Analysis: Review”, Crit. Rev. Anal. Chem. **47**(3), 194–203 (2017).

[122] B. Monemar, “Fundamental energy gap of GaN from photoluminescence excitation spectra”, Phys. Rev. B **10**(2), 676–681 (1974).

[123] B. Monemar, P. P. Paskov, J. P. Bergman, A. A. Toropov, T. V. Shubina, T. Malinauskas, and A. Usui, “Recombination of free and bound excitons in GaN” Phys. Status Solidi B **245**(9), 1723–1740 (2008).

[124] “Max von Laue – biographical”, nobelprize.org, accessed 27 April, 2022, at https://www.nobelprize.org/prizes/physics/1914/laue/biographical.

[125] “The Nobel Prize in Physics 1915”, nobelprize.org, accessed April 27, 2022, at https://www.nobelprize.org/prizes/physics/1915/summary.

[126] M. A. Moram and M. E. Vickers, “X-ray diffraction of III-nitrides” Rep. Prog. Phys. **72**(3), 036502 (2009).

[127] T. Grinys, T. Drunga, K. Badokas, R. Dargis, A. Clark, and T. Malinauskas, “Growth conditions of semi and non-polar GaN on Si with Er_2O_3 buffer layer” J. Alloys Compd. **725**, 739–743 (2017).

[128] H. Heinke, V. Kirchner, S. Einfeldt, and D. Hommel, “X-ray diffraction analysis of the defect structure in epitaxial GaN”, Appl. Phys. Lett. **77**(14), 2145–2147 (2000).

[129] D. Lu, D. I. Florescu, D. S. Lee, V. Merai, J. C. Ramer, A. Parekh, and E. A. Armour, “Sapphire substrate misorientation effects on GaN nucleation layer properties”, J. Cryst. Growth **272**(1–4), 353–359 (2004).

[130] U. Haboeck, H. Siegle, A. Hoffmann, and C. Thomsen, “Lattice dynamics in GaN and AlN probed with first- and second-order Raman spectroscopy”, Phys. Status Solidi C **0**(6), 1710–1731 (2003).

[131] Y. Bleu, F. Bourquard, A. Loir, V. Barnier, F. Garrelie, and C. Donnet, “Raman study of the substrate influence on graphene synthesis using a solid carbon source via rapid thermal annealing”, J. Raman Spectrosc. **50**(11), 1630–1641 (2019).

[132] F. Liu, M. Wang, Y. Chen, and J. Gao, “Thermal stability of graphene in inert atmosphere at high temperature”, J. Solid State Chem. **276**, 100–103 (2019).

[133] C. Casiraghi, S. Pisana, K. S. Novoselov, A. K. Geim, and A. C. Ferrari, “Raman fingerprint of charged impurities in graphene”, Appl. Phys. Lett. **91**(23), 233108 (2007).

[134] L. M. Malard, M. A. Pimenta, G. Dresselhaus, and M. S. Dresselhaus, “Raman spectroscopy in graphene,” Phys. Rep. **473**(5–6), 51–87 (2009).

[135] T. M. G. Mohiuddin, A. Lombardo, R. R. Nair, A. Bonetti, G. Savini, R. Jalil, N. Bonini, D. M. Basko, C. Galiotis, N. Marzari, K. S. Novoselov, A. K. Geim, and A. C. Ferrari, “Uniaxial strain in graphene by Raman spectroscopy: G peak splitting, Grüneisen parameters, and sample orientation,” Phys. Rev. B **79**(20), 205433 (2009).

[136] S. J. Chae, Y. H. Kim, T. H. Seo, D. L. Duong, S. M. Lee, M. H. Park, E. S. Kim, J. J. Bae, S. Y. Lee, H. Jeong, E.-K. Suh, C. W. Yang, M. S. Jeong, and Y. H. Lee, “Direct growth of etch pit-free GaN crystals on few-layer graphene,” RSC Adv. **5**(2), 1343–1349 (2015).

[137] S.-H. Bae, K. Lu, Y. Han, S. Kim, K. Qiao, C. Choi, Y. Nie, H. Kim, H. S. Kum, P. Chen, W. Kong, B.-S. Kang, C. Kim, J. Lee, Y. Baek, J. Shim, J. Park, M. Joo, D. A. Muller, K. Lee, and J. Kim, “Graphene-assisted spontaneous relaxation towards dislocation-free heteroepitaxy,” Nat. Nanotechnol. **15**, 272–276 (2020).

[138] D. O. Demchenko, I. C. Diallo, and M. A. Reshchikov, “Hydrogen-carbon complexes and the blue luminescence band in GaN”, J. Appl. Phys. **119**(3), 035702 (2016).

[139] M. A. Reshchikov, D. O. Demchenko, A. Usikov, H. Helava, and Yu. Makarov, “Carbon defects as sources of the green and yellow luminescence bands in undoped GaN”, Phys. Rev. B **90**(23), 235203 (2014).

[140] B. Wang, F. Liang, D. Zhao, Y. Ben, J. Yang, P. Chen, and Z. Liu, “Transient behaviours of yellow and blue luminescence bands in unintentionally doped GaN”, Opt. Express **29**(3), 3685 (2021).

[141] Q. Yu, L. A. Jauregui, W. Wu, R. Colby, J. Tian, Z. Su, H. Cao, Z. Liu, D. Pandey, D. Wei, T. F. Chung, P. Peng, N. P. Guisinger, E. A. Stach, J. Bao, S.-S. Pei, and Y. P. Chen, “Control and characterization of individual grains and grain boundaries in graphene grown by chemical vapour deposition”, Nat. Mater. **10**(6), 443–449 (2011).

[142] D. Dobrovolskas, A. Kadys, A. Usikov, T. Malinauskas, K. Badokas, I. Ignatjev, S. Lebedev, A. Lebedev, Y. Makarov, and G. Tamulaitis, “Luminescence of structured InN deposited on graphene interlayer”, J. Lumin. **232**, 117878 (2021).

[143] T. Journot, H. Okuno, N. Mollard, A. Michon, R. Dagher, P. Gergaud, J. Dijon, A. V. Kolobov, and B. Hyot, “Remote epitaxy using graphene enables growth of stress-free GaN”, Nanotechnology **30**(50), 505603 (2019).

[144] W. V. Lundin, E. E. Zavarin, A. V. Sakharov, D. A. Zakheim, V. Yu. Davydov, A. N. Smirnov, I. A. Eliseyev, M. A. Yagovkina, P. N. Brunkov, E. Yu. Lundina, L. K. Markov, and A. F. Tsatsulnikov, “Growth of III-N/graphene heterostructures in single vapor phase epitaxial process”, J. Cryst. Growth **504**, 1–6 (2018).

[145] S. W. Bedell, P. Lauro, J. A. Ott, K. Fogel, and D. K. Sadana, “Layer transfer of bulk gallium nitride by controlled spalling”, J. Appl. Phys. **122**(2), 025103 (2017).

[146] D. Augulis, “III grupės nitridų nuotolinė epitaksija per grafeną”, Bachelor‘s thesis, Vilnius University (2022), 38 p.

[147] F. Banhart, J. Kotakoski, and A. V. Krasheninnikov, “Structural Defects in Graphene”, ACS Nano **5**(1), 26–41 (2011).

[148] P. O. Lehtinen, A. S. Foster, A. Ayuela, A. Krasheninnikov, K. Nordlund, and R. M. Nieminen, “Magnetic Properties and Diffusion of Adatoms on a Graphene Sheet”, Phys. Rev. Lett. **91**(1), 017202 (2003).

[149] O. Cretu, A. V. Krasheninnikov, J. A. Rodríguez-Manzo, L. Sun, R. M. Nieminen, and F. Banhart, “Migration and Localization of Metal Atoms on Strained Graphene”, Phys. Rev. Lett. **105**(19), 196102 (2010).

[150] J. Kotakoski, A. V. Krasheninnikov, U. Kaiser, and J. C. Meyer, "From Point Defects in Graphene to Two-Dimensional Amorphous Carbon", Phys. Rev. Lett. **106**(10), 105505 (2011).

[151] D. Geng, S. Yang, Y. Zhang, J. Yang, J. Liu, R. Li, T.-K. Sham, X. Sun, S. Ye, and S. Knights, "Nitrogen doping effects on the structure of graphene", Appl. Surf. Sci. **257**(21), 9193–9198 (2011).

[152] J. Ma, D. Alfè, A. Michaelides, and E. Wang, "Stone-Wales defects in graphene and other planar sp^2-bonded materials", Phys. Rev. B **80**(3), 033407 (2009).

[153] L. P. Biró and P. Lambin, "Grain boundaries in graphene grown by chemical vapor deposition", New J. Phys. **15**(3), 035024 (2013).

[154] K. Kim, V. I. Artyukhov, W. Regan, Y. Liu, M. F. Crommie, B. I. Yakobson, and A. Zettl, "Ripping Graphene: Preferred Directions", Nano Lett. **12**(1), 293–297 (2012).

[155] D.-H. Mun, H. Bae, S. Bae, H. Lee, J.-S. Ha, and S. Lee, "Stress relaxation of GaN microstructures on a graphene-buffered Al_2O_3 substrate", Phys. Status Solidi RRL - Rapid Res. Lett. **8**(4), 341–344 (2014).

[156] A. Shivayogimath, P. R. Whelan, D. M. A. Mackenzie, B. Luo, D. Huang, D. Luo, M. Wang, L. Gammelgaard, H. Shi, R. S. Ruoff, P. Bøggild, and T. J. Booth, "Do-It-Yourself Transfer of Large-Area Graphene Using an Office Laminator and Water", Chem Mater **9** (2019).

AFTERWORD ON TECHNICAL DETAILS

In a galaxy far away, a stress-free civilization may live. There, life of its members might be predictable and unsurprising, with no need for soft skills to adapt swiftly nor a set of hard skills such as how to be a plumber, an electrician, a programmer, a mechanic, a designer, a salesman, a manager, an accountant, and a teacher. Most likely, the lab work there is perfectly organized and rational as well – PMMA with graphene never rolls up, samples are always in place, reactor heater functions correctly, water leak never floods the lab, SEM keeps the vacuum inside, RTA never breaks during the *mission-critical* step, metalorganics are always stock-pilled, everyone invests time in maintaining a good record of everything they and especially their colleagues do and suggest; and, of course, everyone is aware of not catching the wrong ideas and wasting time by blindly searching for erratic insights to prove them[1] or optimizing the things that shouldn't have been there in the first place[2].

Luckily, this dissertation was written here.

---

[1] Confirmation bias.

[2] Elon Musk expressed the idea that “one of the biggest traps for smart engineers is optimizing something that shouldn’t exist”.

ACKNOWLEDGMENTS

I sincerely appreciate everyone who was part of the journey, especially:

The entire Nitride technology group led by Dr. R. Tomašiūnas, with my supervisor Dr. T. Malinauskas in the forefront – you all guided me through all of this since that summer of 2013.

Dr. M. Meyyappan’s group at NASA Ames – you showed me the fantastic world of carbon allotropes and set up a Silicon Valley mindset that is yet to bloom.

Dr. J. Kim’s group at MIT – your pioneering research sparked this thesis, and the advice on the challenging experiments was especially valuable.

The fellow students and colleagues from Graphene Flagship events – exchange of ideas while rowing in a lake in the Nordics, learning to ski in the Alps, and getting ready for the Finnish sauna were something else.

The Lindau Nobel Laureate Meeting participants – hitting the dance floor with Dr. Donna Strickland, having dinner with Dr. Dan Shechtman, and engaging in a deep discussion with Dr. Wolfgang Ketterle, among all the other bright Laureates, revealed a novel dimension of academic life.

My students – you revived the joy of learning once again.

My co-authors – this work was possible only because of your skills.

Fellow doctoral candidates – you inspired me not to lag behind, even without knowing it.

The administration of VU FNI – someone had to approve those purchases of graphene.

My dear friend, since the early days, Ramunė – now the initially missed commas are in place.

My mum and dad – you were always there, and you know it all.

DISERTACIJOS SANTRAUKA LIETUVIŲ KALBA

ĮVADAS

Galio nitridas – vienas svarbiausių III-grupės nitridų puslaidininkių – sudaro šiuolaikinių apšvietimo technologijų pagrindą. Be to, sparčiai besiplečianti baterijų įkrovimo technologijų [6], 5G ryšio [29] ir įvairių lanksčių prietaisų [28] industrija netruko atrasti GaN pranašumų. Visgi, naujiems taikymams neišvengiamai reikia inovatyvių gamybos metodų ir konkurencingos kainos. Metalorganinio nusodinimo iš garų fazės epitaksija yra vienas labiausiai paplitusių III-grupės nitridų gamybos metodų. Šiuo būdu gaminami nitridų sluoksniai formuojami ant įvairių padėklų. Populiariausiu pasirinkimu iki dabar išlieka safyras. Savieji tūriniai padėklai vis dar yra brangus pasirinkimas (Pav. 1), nors ir leidžiantis pasiekti geriausią kokybę.

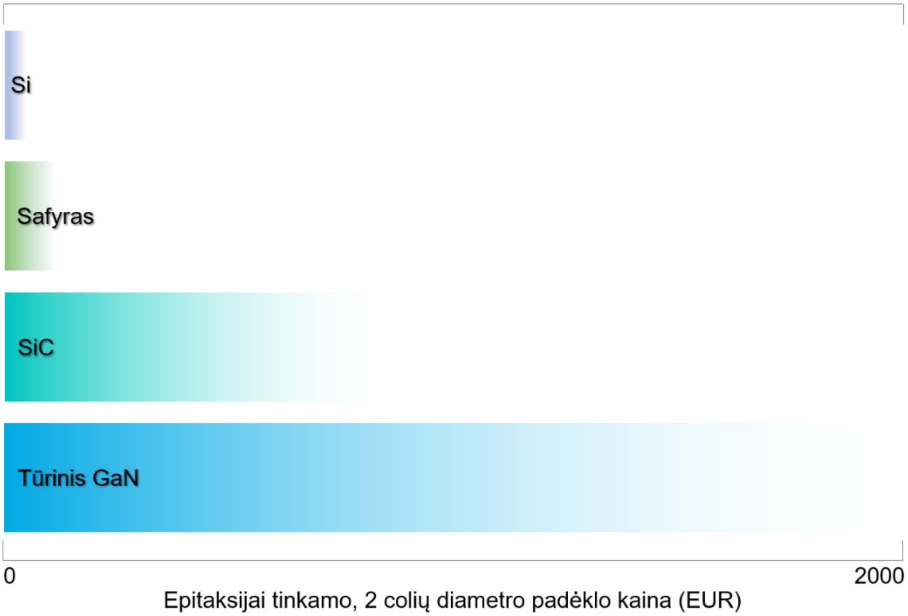

Pav. 1 Kai kurių komerciškai prieinamų, GaN kristalinių sluoksnių formavimui naudojamų 2 colių (5,08 cm) diametro padėklų orientacinė kaina 2022 metų pavasarį. Tikslios kainos ir tiekėjai neatskleidžiami dėl komercinių pasiūlymų konfidencialumo.

Pastaba. Santraukoje lietuvių kalba cituojami šaltiniai pateikiami ankstesniame šios disertacijos skyriuje anglų kalba References.

Vienas naujausių gamybos kaštų mažinimo ir inovatyvių pritaikymų sprendimų – nuotolinė epitaksija – pristatyta 2017-aisiais ir intensyviai tyrinėjama Kim *et al.* darbuose pastaruosius metus [21,23,84,88,137]. Nuotolinės epitaksijos technologija pagrįsta kristalinio sluoksnio formavimusi ant grafenu padengtų padėklų [13]. Esant pakankamai stipriam padėklo kovalentinio ryšio poliškumui grafeno paviršiuje vyraujančios van der Waals jėgos pilnai neekranuoja padėklo potencialo, todėl epitaksinis sluoksnis, auginamas per grafeną, išlaiko padėklo orientaciją bei išvengia kokybę bloginančių įtempimų [14]. Dėl kovalentinių ryšių stokos epitaksinis sluoksnis susiformuoja silpnai prikibęs prie padėklo/grafeno struktūros, todėl gali būti santykinai lengvai nuimtas. Taigi, bent trys nuotolinės epitaksijos siūlomi privalumai tampa akivaizdūs (Pav. 2):

1. Epitaksinis padėklas gali būti grąžinamas atgal į gamybą po epitaksinio sluoksnio nukėlimo, taip taupant medžiagas ir sumažinant gamybos kaštus.

2. Užaugintas epitaksinis sluoksnis yra aukštos kristalinės kokybės, kadangi epitaksija valdoma tūrinio, savojo padėklo potenciniu lauku.

3. Nukelti ploni epitaksiniai sluoksniai tampa lanksčiomis puslaidininkėmis membranomis, atveriančiomis kelią naujų prietaisų gamybai.

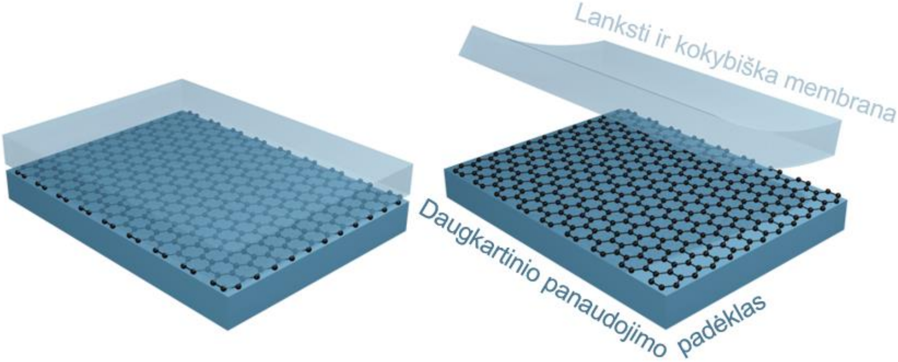

Pav. 2 Iliustracijoje pavaizduoti nuotolinės epitaksijos ant monosluoksniu grafenu padengto tūrinio, savojo padėklo privalumai: lanksti, kokybiška puslaidininkės medžiagos membrana ir padėklo daugkartinio panaudojimo galimybė.

DARBO NAUJUMAS IR TIKSLAI

Šiuo metu yra pademonstruota mokslinių darbų, pritaikančių nuotolinę epitaksiją skirtingų medžiagų formavimui [15–18], bei panaudojančių įvairius padėklus [19–21]. Visgi, galio nitrido nuotolinės epitaksijos procesas reikalauja papildomo optimizavimo. Pagrindinės problemos – galimas grafeno suirimas aukštoje temperatūroje (> 1000 °C), reikalingoje MOVPE proceso metu [90], bei neatmestinas GaN formavimasis per monosluoksnyje esančias skyles ar grafeno įplyšimus [20]. Be to, GaN epitaksijoje dažniausiai naudojami tūriniai GaN padėklai yra labai brangūs (apie 10 kartų aukštesnės kainos lyginant su GaN/safyras ruošiniais). O sausai perkeliamas epitaksinis grafenas taip pat yra labai brangus ir kol kas parduodamas tik gana mažo ploto.

Pagrindinis šio darbo tikslas buvo pademonstruoti GaN nuotolinę epitaksiją MOVPE metodu ant šlapiai perkeltu grafenu padengtų GaN/safyras ruošinių.

Tikslui nuosekliai pasiekti buvo iškelti šie uždaviniai:

1. GaN/safyras ruošinių gaminimas ir išbandymas GaN nuotolinei epitaksijai ant grafeno.

2. Grafeno perkėlimas šlapiuoju būdu kaip alternatyva brangiam sausai perkeltam epitaksiniam grafenui. Perkelto grafeno tyrimas.

3. Optimalios MOVPE proceso auginimo temperatūros ir auginimo protokolo parinkimas GaN epitaksijai.

4. Užauginto GaN epitaksinio sluoksnio nukėlimas nuo padėklo.

5. Galimybės naudoti daugiau negu vieną grafeno sluoksnį įvertinimas GaN nuotolinei epitaksijai ant GaN/safyras padėklų.

DARBO STRUKTŪRA

Disertacija anglų kalba sudaryta iš: įvado, darbo tikslo ir naujumo aprašymo, darbo struktūros apžvalgos, pagrindinių darbo teiginių, publikacijų, konferencijų ir mokymų sąrašo, autoriaus ir kolegų konkretaus indėlio aprašymo, darbe naudotų medžiagų ir eksperimentinės įrangos apžvalgos, nuoseklaus eksperimentinių rezultatų aprašymo ir interpretavimo, komentaro dėl ateities perspektyvų ir išvadų. Darbe taip pat pateikiamas trumpas autoriaus komentaras bei padėka, literatūros sąrašas, santrauka lietuvių kalba ir publikacijų kopijos (esant galimybei). Disertacijos santrauka lietuvių kalba didžiąja dalimi išlaiko aprašymo anglų kalba struktūrą, tačiau tekste pateikiamos tik esminės idėjos ir iliustracijos.

Šis darbas parengtas pagal dvi Badokas *et al.* publikacijas [P1] ir [P2], išspausdintas recenzuojamuose mokslo žurnaluose ir pateiktas šio darbo pabaigoje (pagal galimybes). Šioje disertacijoje didžiąją dalimi atkartojami publikacijose aprašyti rezultatai papildant juos naujais duomenimis ir/arba papildoma analize. Dalis šio darbo rezultatų ir iš jų išplaukiančių išvadų taip pat buvo paskelbti bakalauro studento D. Augulio bakalauro studijų praktikos ataskaitoje ir baigiamajame darbe, kurio vadovu darbų rengimo metu buvo K. Badokas. Visų autorių indėliai nurodyti atitinkamame šio darbo skyriuje.

Leidimas naudoti publikacijoje [P1] paskelbtus rezultatus buvo gautas iš leidėjo *IOP Publishing*. Publikacija [P2] paskelbta atviros prieigos žurnale, dėl to joje paskelbti rezultatai šiame darbe naudojami vadovaujantis *Creative Commons Attribution License (CC BY)* licencija be atskiro leidimo, tačiau laikantis citavimo taisyklių.

GINAMIEJI TEIGINIAI

1. GaN/safyras ruošinys su šlapiai perkeltu grafenu yra tinkamas GaN nuotolinei epitaksijai MOVPE metodu ir užaugintos membranos nukėlimui.

2. Dvipakopis MOVPE auginimo procesas, susidedantis iš GaN nukleacijos 700 °C temperatūroje ir koalescencijos 1075 °C temperatūroje leidžia užauginti aukštos kokybės GaN epitaksinį sluoksnį ant grafenu padengto GaN/safyras ruošinio ir išsaugoti šlapiai perkeltą grafeną.

PUBLIKACIJOS, KONFERENCIJOS IR MOKYMAI

Šio darbo autorius visos savo mokslinės karjeros metu paskelbė arba prisidėjo prie 12 recenzuojamų publikacijų, įtrauktų į *WoS*, paskelbimo. Taip pat pats pristatė arba reikšmingai prisidėjo prie bent 30 žodinių ir stendinių pranešimų įvairiose konferencijose ir renginiuose. Pačios svarbiausios publikacijos, pranešimai ir tarptautiniai mokymai, paskelbti ar įvykę nuo 2018 iki 2022 metų, yra išvardinti šiame skyriuje.

Į šį darbą įtraukti straipsniai

[P1] K. Badokas, A. Kadys, D. Augulis, J. Mickevičius, I. Ignatjev, M. Skapas, B. Šebeka, G. Juška ir T. Malinauskas, „MOVPE growth of GaN via graphene layers on GaN/sapphire templates“, Nanomaterials **12**(5), 785 (2022).

[P2] K. Badokas, A. Kadys, J. Mickevičius, I. Ignatjev, M. Skapas, S. Stanionytė, E. Radiunas, G. Juška ir T. Malinauskas, „Remote epitaxy of GaN via graphene on GaN/sapphire templates“, J. Phys. D **54**, 205103 (2021).

Su šiuo darbu tiesiogiai nesusiję straipsniai

[p1] D. Dobrovolskas, A. Kadys, A. Usikov, T. Malinauskas, K. Badokas, I. Ignatjev, S. Lebedev, A. Lebedev, Y. Makarov ir G. Tamulaitis, „Luminescence of structured InN deposited on graphene interlayer“, J. Lumin. **232**, 117878 (2021).

[p2] V. Novickij, R. Stanevičienė, R. Gruškienė, K. Badokas, J. Lukša, J. Sereikaitė, K. Mažeika, N. Višniakov, J. Novickij ir E. Servienė, „Inactivation of bacteria using bioactive nanoparticles and alternating magnetic fields“, Nanomaterials **11**(2), 342 (2021).

[p3] T. Čeponis, K. Badokas, L. Deveikis, J. Pavlov, V. Rumbauskas, V. Kovalevskij, S. Stanionyte, G. Tamulaitis ir Eugenijus Gaubas, „Evolution of scintillation and electrical characteristics of AlGaN double-response sensors during proton irradiation“, Sensors **19**(15), 3388 (2019).

[p4] D.-I. Moon, B. Kim, R. Peterson, K. Badokas, M.-L. Seol, D. G. Senesky, J.-W. Han ir M. Meyyappan, „A single input multiple output (SIMO) variation-tolerant nanosensor“, ACS Sens. **3**(9), 1782–1788 (2018).

Su šiuo darbu susiję konferencijų pranešimai

[C1] K. Badokas, A. Kadys, D. Augulis, J. Mickevičius, I. Ignatjev, M. Skapas, B. Šebeka, G. Juška ir T. Malinauskas, „GaN epitaxy on graphene-covered substrate“, Graphene Week, Miunchenas, Vokietija, 2022 m. rugsėjo mėn. 5–9 d., stendinis pranešimas, pristatytas K. Badoko.

[C2] K. Badokas, D. Augulis, A. Kadys, J. Mickevičius, I. Ignatjev, B. Šebeka, M. Skapas, G. Juška ir T. Malinauskas, „MOVPE of GaN on graphene-covered GaN/sapphire templates“, Open Readings, Vilnius, Lietuva, 2022 m. kovo mėn. 15–18 d., žodinis pranešimas (nuotoliniu būdu), pristatytas K. Badoko.

[C3] D. Augulis, K. Badokas, A. Kadys, B. Šebeka, I. Ignatjev, J. Mickevičius ir T. Malinauskas, „Exfoliation of GaN thin films grown by MOVPE via graphene“, Open Readings, Vilnius, Lietuva, 2022 m. kovo mėn. 15–18 d., stendinis pranešimas, pristatytas D. Augulio, kuriam vadovavo K. Badokas.

[C4] K. Badokas, A. Kadys, D. Augulis, I. Ignatjev, G. Juška, J. Mickevičius ir T. Malinauskas, „MOVPE epitaxy of group III nitrides via few-layer graphene on GaN/sapphire templates“, MRS Fall Meeting, Bostonas, Masačiusetsas, JAV, virtualus renginys, 2021 m. lapkričio mėn. 29–gruodžio mėn. 8 d., žodinis pranešimas (nuotoliniu būdu), pristatytas K. Badoko.

[C5] K. Badokas, A. Kadys, D. Augulis, I. Ignatjev, G. Juška, J. Mickevičius ir T. Malinauskas, „Remote epitaxy of GaN via few-layer graphene“, Advanced Materials and Technologies, Palanga, Lietuva, 2021 m. rugpjūčio mėn. 23–27 d., žodinis ir stendinis pranešimai, pristatyti K. Badoko, laimėtas geriausio pranešimo apdovanojimas.

[C6] D. Augulis, K. Badokas, A. Kadys, S. Strumskis, I. Ignatjev, G. Juška, J. Mickevičius ir T. Malinauskas, „The influence of graphene surface treatment on remote epitaxy of gallium nitride“, Open Readings, Vilnius, Lietuva, 2021 m. kovo mėn. 16–19 d. stendinis pranešimas, pristatytas D. Augulio, kuriam vadovavo K. Badokas.

[C7] K. Badokas, A. Kadys, T. Grinys, M. Kolenda, S. Stanionytė, M. Skapas, J. Mickevičius ir T. Malinauskas, „Remote epitaxy of GaN via graphene, APROPOS 17, 2020 m. rugsėjo mėn. 30 d.–lapkričio mėn. 1 d., Vilnius, Lietuva, kviestinis pranešimas, kuriame svarbiausius doktorantūros rezultatus pristatė vadovas dr. T. Malinauskas.

[C8] K. Badokas, A. Kadys, I. Ignatjev, G. Juška, J. Mickevičius, P. Ščajev ir T. Malinauskas, „Galio nitrido MOCVD epitaksija per grafeną“, LNFK-43, 2019 m. lapkričio mėn. 3–5 d., Kaunas, Lietuva, žodinis pranešimas, pristatytas K. Badoko.

[C9] K. Badokas, A. Kadys, I. Ignatjev, G. Juška, J. Mickevičius, P. Ščajev ir T. Malinauskas, „Graphene as an interlayer for MOCVD epitaxy of GaN“, Graphene Week, 2019 m. rugsėjo mėn. 23–27 d., Helsinkis, Suomija, stendinis pranešimas, pristatytas K. Badoko.

[C10] K. Badokas, A. Kadys, I. Ignatjev, G. Juška, J. Mickevičius, P. Ščajev ir T. Malinauskas, „MOCVD epitaxy of GaN via graphene“, Advanced Materials and Technologies, 2019 m. rugpjūčio mėn. 19–23 d., Palanga, Lietuva, stendinis pranešimas, pristatytas K. Badoko.

[C11] K. Badokas, A. Kadys, T. Grinys, M. Kolenda, S. Stanionytė, M. Skapas, J. Mickevičius ir T. Malinauskas, „MOCVD epitaxy of GaN via graphene“, EW-MOVPE 18, 2019 m. balandžio mėn. 16–19 d., Vilnius, Lietuva, stendinis pranešimas, pristatytas K. Badoko, taip pat reikšmingai prisidėjusio prie pačios konferencijos organizavimo.

[C12] K. Badokas, A. Kadys ir T. Malinauskas, „MOCVD epitaxy of group-III nitrides via graphene“, Graphene Study (Winter edition), 2019 m. kovo mėn. 3–8 d., Obergurgl, Austrija, stendinis pranešimas, pristatytas K. Badoko.

[C13] K. Badokas, „Group-III nitrides and graphene: an introduction“, EUIMWP PhD and ECI meeting under COST Action, 2019 m. sausio mėn. 31–vasario mėn. 1 d., Liubliana, Slovėnija, žodinis pranešimas, pristatytas K. Badoko.

[C14] K. Badokas ir T. Malinauskas, „MOCVD growth of III-nitride semiconductors by van der Waals epitaxy via graphene“, Graphene Study (Summer edition), 2018 m. liepos mėn. 1–6 d., Hindås, Švedija, stendinis pranešimas, pristatytas K. Badoko.

Su šiuo darbu nesusiję konferencijų pranešimai

[c1] K. Badokas, T. Malinauskas, D. Paipulas, A. Kadys, T. Grinys ir E. Gaubas, „GaN p-i-n diodes for radiation detection“, IWN, 2018 m. lapkričio mėn. 11–16 d., Kanadzava, Japonija, stendinis pranešimas, pristatytas K. Badoko.

Su šiuo darbu susiję mokymai

[W1] Graphene Study (Winter edition), 2019 kovo mėn. 3–8 d., Obergurgl, Austrija.

[W2] Graphene Study (Summer edition), 2018 liepos mėn. 1–6 d., Hindås, Švedija.

Su šiuo darbu nesusijusios mokslinės išvykos ir mokymai

[w1] 69-tasis Lindau Nobelio premijos laureatų susitikimas, tarptautinis renginys, 2019 m. birželio mėn. 30 d.–liepos mėn. 5 d., Lindau, Vokietija.

[w2] *LioniX* kompanijos organizuoti mokymai integruotos mikrobangų fotonikos prietaisų kūrimo tema, 2019 m. vasario mėn. 26 d.–kovo mėn. 1 d., Enschedė, Nyderlandai.

AUTORIAUS INDĖLIS

Šios disertacijos autorius buvo asmeniškai atsakingas už didžiąją dalį šiame darbe pateikiamų eksperimentinių rezultatų, jų analizę ir interpretavimą. Visgi, dalis eksperimentinių tyrimų bei rezultatų aptarimo neišvengiamai vyko bendradarbiaujant su kolegomis, kurių kiekvieno indėlis:

- Koncepcijos rengimas, tyrimų planavimas ir rezultatų interpretavimas – K. Badokas, dr. A. Kadys ir dr. T. Malinauskas.

- Grafeno perkėlimo eksperimentai – K. Badokas ir D. Augulis (vadovaujant K. Badokui).

- MOVPE auginimai – dr. A. Kadys, K. Badokas ir D. Augulis (vadovaujant dr. A. Kadžiui).

- Raman poslinkio spektrų matavimas – dr. I. Ignatjev, K. Badokas ir D. Augulis (spektrų analizė, vadovaujant K. Badokui).

- TEM matavimai – dr. M. Skapas, K. Badokas ir dr. A Selskis (bandinių paruošimas TEM matavimams).

- SEM matavimai – K. Badokas, D. Augulis (vadovaujant K. Badokui) ir E. Radiunas.

- AFM matavimai – G. Juška, D. Augulis (vadovaujant K. Badokui) ir K. Badokas (rezultatų analizė ir grafinis pateikimas).

- Metalinių sluoksnių dengimas – K. Badokas (magnetroninis dulkinimas), dr. T. Grinys (garinimas elektronų pluošteliu), dr. B. Šebeka (elektrochemija) ir D. Augulis (visi eksperimentai, vadovaujant K. Badokui).

- Krūvininkų koncentracijos nustatymas naudojant Holo efektą – dr. A. Kadys.

- XRD matavimai – dr. T. Malinauskas, dr. S. Stanionytė ir D. Augulis (vadovaujant dr. T. Malinauskui).

- Rankraščių rengimas publikacijoms – K. Badokas, dr. J. Mickevičius ir dr. T. Malinauskas.

- Fotoliuminescencijos matavimai – dr. J. Mickevičius.

1. APŽVALGA

Šiame skyriuje apžvelgtos tyrimų metu naudotų medžiagų pagrindinės savybės bei jų gamybos metodai. Taip pat aprašyta didžioji dalis naudotų eksperimentinių metodikų.

1.1. Medžiagos

Galio nitridas – vienas dažniausiai sutinkamų III-grupės nitridų puslaidininkių, turinčių tiesioginį draustinių energijų tarpą, lygų 3,4 eV. GaN sluoksniai dažniausiai formuojami MOVPE būdu užauginant viurcito tipo GaN kristalus, kurių gardelės konstantos apytiksliai: a = 3,19 Å ir c = 5,19 Å (Pav. 3). GaN emisijos spektras gali būti kontroliuojamas formuojant kvantines duobes, į kurias įterpiamas, pavyzdžiui, In. Balti šviestukai kuriami padengiant GaN šviesą emituojančius diodus atitinkamais fosforais, po sužadinimo spinduliuojančiais ilgesnių bangų spektrinėje dalyje.

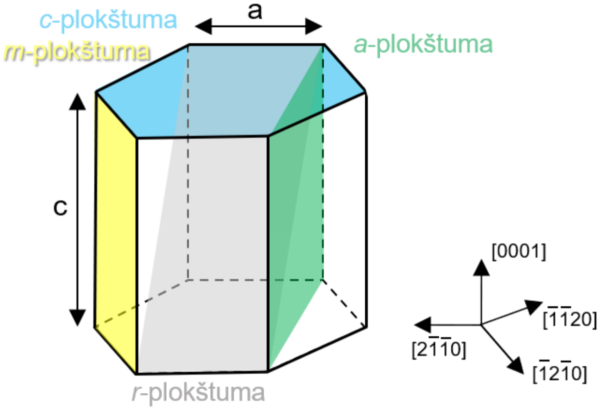

Pav. 3 Heksagoninės kristalinės struktūros GaN modelis. Kai kurios kristalinės plokštumos, kryptys ir gardelės konstantos yra atitinkamai pažymėtos.

Platus draustinių energijų tarpas leidžia panaudoti GaN didelės galios, greitaveikėje elektronikoje, taip pat prietaisuose, kurie dirba esant aukštai aplinkos temperatūrai ar radiaciniam fonui [26,29,30]. Pjezoelektrinės savybės leidžia panaudoti GaN membranas kaip jutiklius bei energijos generavimo prietaisus [27,28]. Taip pat mokslinėje literatūroje jau buvo pademonstruoti įvairūs sensoriai, sukurti GaN pagrindu – drėgmės [31], slėgio [32], pH [33] ir dujų [34]. Pigesnės gamybos technologijos išvystymas dar labiau praplėstų GaN panaudojimo galimybes tiek suteikiant GaN prietaisams naujų funkcijų, tiek ir padarant juos pigesnius, taigi labiau prieinamus vartotojams.

Grafenas – anglies alotropinė atmaina, sudaryta iš monosluoksnyje sp^2 ryšiais susijungusių anglies atomų. Grafeno struktūra pavaizduota Pav. 4. Pirmą kartą izoliuotas 2004-aisiais metais atskiriant grafeno monosluoksnį nuo grafito [40]. Išskirtinė grafeno atradimo svarba vos po šešerių metų pripažinta įteikiant fizikos srities Nobelio premiją [47], bei kiek vėliau ES paskelbiant milijardinę investiciją pavyzdinei iniciatyvai *Grafenas* [61]. Be to, sėkmingas grafeno monosluoksnio izoliavimas ir daug žadančių savybių nustatymas paskatino tyrėjus ieškoti ir kitų medžiagų, galinčių sudaryti dvimačius sluoksnius [9].

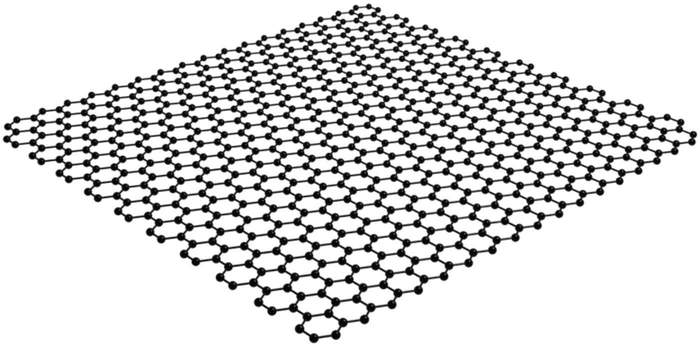

Pav. 4 Grafeno monosluoksnio struktūra.

Grafenas pasižymi ypatingomis mechaninėmis savybėmis. Nors yra labai lengvas – standartinei futbolo aikštei iškloti viensluoksniu grafeno kilimu prireiktų vos kelių gramų šios medžiagos – pasižymi stulbinamu tvirtumu [57]. Manoma, kad iš defektų neturinčio monosluoksnio grafeno pagamintas hamakas galėtų išlaikyti bent apie 4 kg masės svorį atitinkančią suaugusią katę [58]. Be to grafenas gali veikti kaip vienas ploniausių fizinių barjerų kitoms molekulėms ar atomams. Iki šiol buvo pademonstruotas tik jo laidumas vandeniliui [64]. Ši grafeno savybė labai svarbi atliekant nuotolinės epitaksijos eksperimentus šio darbo rėmuose.

Pademonstruota, kad krūvininkų judris žemoje temperatūroje, su padėklu nesusietame grafeno monosluoksnyje siekia apie 200 000 $cm^2V^{-1}s^{-1}$ [50]. Taigi grafeno elektrinės savybės leidžia tikėtis jo pritaikymų greitaveikėje elektronikoje. Tiesa, optinės grafeno savybės mažai tinkamos panaudoti grafeną šviesos emitavimui – monosluoksnis neturi draustinių energijų tarpo, tačiau gali būti panaudotas kaip detektorius (grafenas sugeria apie 2,3 % regimojo spektro spinduliuotės) [53]. Šiluminis grafeno laidumas labai didelis, lenkiantis varį, bet tik monosluoksnio plokštumoje [59].

Grafeno gamybos metodai smarkiai pažengė į priekį nuo to laiko, kai monosluoksnis buvo pirmą kartą izoliuotas nulupant jį nuo grafito lipniąja juosta. Šiuo metu grafeno, kaip ir daugumos kitų medžiagų, gamybos metodai skirstomi į sintezę iš viršaus į apačią ir iš apačios į viršų (angl. *top-down* ir *bottom-up*) [65]. Iš tūrinio grafito grafenas išskiriamas jau minėtuoju lipnios juostos būdu, kuris yra gana lėtas ir labai mažos išeigos. Kiti iš viršaus į apačią būdai – grafeno oksido išskyrimas iš oksiduoto grafito [67], bei grafeno išskyrimas skystoje fazėje [68]. Pastarieji metodai leidžia masiniu būdu gaminti grafeną, tačiau neišvengiama santykinai didelio kiekio defektų.

Būdai, leidžiantys pagaminti gana aukštos kokybės, mažai defektų turintį grafeną, yra nusodinimas iš garų fazės ir SiC karbonizacija (Pav. 5). Pastarasis metodas remiasi SiC padėklo kaitinimu aukštoje (> 1000 °C) temperatūroje [70]. Proceso metu Si atomai sublimuoja nuo pirminio padėklo paviršiaus, palikdami anglį. Esant tinkamoms sąlygoms anglies atomai paviršiuje persitvarko į heksagoninės struktūros monosluoksnį – grafeną. Šiuo būdu pagamintas grafenas yra gana brangus, tačiau aukštos kokybės, gali būti perkeliamas ant kitų padėklų panaudojant metalinius sluoksnius. Grafeno perkėlimas vyksta vadinamuoju sausuoju būdu.

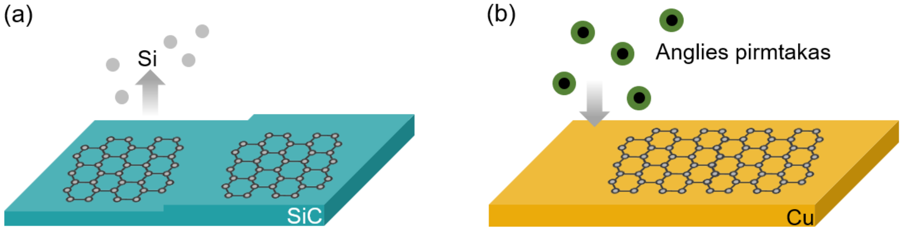

Pav. 5 Grafeno gamybos metodai: SiC karbonizacija ir grafeno susiformavimas iš paviršiuje likusios anglies (a) bei cheminis nusodinimas iš garų fazės ant metalo folijos (b).

Cheminio nusodinimo metodo esmę sudaro grafeno formavimas ant metalinių folijų iš anglies turinčių pirmtakių junginių. Praktikoje dažnai naudojamos varinės folijos – mažas anglies tirpumas varyje ir reikiamos katalitinės savybės leidžia greitai ir santykinai pigiai pagaminti didelio ploto grafeną [65,69]. Monosluoksnis gali būti perkeliamas ant kitų padėklų vadinamuoju šlapiuoju būdu: pirmiausia grafenas padengiamas laikančiuoju polimeriniu (pavyzdžiui, PMMA) sluoksniu, vario folija ištirpinama atitinkamuose tirpikliuose, vėliau grafeno ir polimero sluoksniai merkiami į vandenį ir sužvejojami ant reikiamo padėklo.

Šiame darbe buvo naudojami tiek cheminio nusodinimo būdu pagaminti, tiek ant SiC padėklų suformuoti grafeno sluoksniai, įsigyti komerciškai. Grafeno sluoksnių perkėlimo procedūros aprašytos tolesniuose šio darbo skyriuose.

1.2. Eksperimentiniai metodai

Šiame darbe GaN kristalinės struktūros formuotos metalorganinio nusodinimo iš garų fazės (sutrumpintai MOCVD arba MOVPE) metodu. Užauginti sluoksniai, taip pat ir perkeltas grafenas, buvo tiriami įvairiomis metodikomis, pavyzdžiui: skenuojančia elektronų mikroskopija (SEM), peršviečiamąja elektronų mikroskopija (TEM), atominių jėgų mikroskopija (AFM), Raman sklaidos spektroskopija, matuojant ir analizuojant fotoliuminescencijos (PL) spektrus bei pasitelkiant Rentgeno spindulių difrakcijos (XRD) metodą.

GaN sluoksniai ant grafenu padengtų padėklų auginti *AIXTRON* dušo galvutės tipo MOVPE reaktoriumi. Pati MOVPE technologija jau skaičiuoja ne vieną dešimtmetį, per kurį buvo intensyviai tobulinama [75–78]. Didžiausias proveržis pritaikant GaN epitaksinių sluoksnių augimą didelio masto apšvietimo ir elektronikos pramonėje įvyko praėjusio amžiaus aštuntojo dešimtmečio pabaigoje ir devintojo dešimtmečio pradžioje. Sėkmingas dvipakopio recepto kristalinių sluoksnių auginimui sukūrimas, inovacijos reaktoriaus dizaino srityje bei *p*-tipo GaN sluoksnio pademonstravimas [2–4] iš dalies lėmė apšvietimo technologijų revoliuciją ir prieš beveik dešimtmetį buvo pripažintas fizikos srities Nobelio premija [82].

Inžinerine prasme MOVPE reaktorius yra sudėtingas įrenginys, sudarytas iš daugybės komponentų. Esminės dalys yra: kaitinamas padėklų laikiklis (angl. *susceptor*), aušinama dušo galvutė, lazerinė *in situ* proceso stebėjimo sistema, dujų tiekimo ir srautų kontrolės posistemės bei specialios metalorganikos laikymo talpos – vadinamieji barbotavimo indai (angl. *bubblers*). Proceso metu, pagal iš anksto numatytą receptą, elektroninės reaktoriaus kontrolės sistemos parenka įvairius proceso parametrus ir preciziškai juos kontroliuoja. Taip suformuojamos iš anksto numatytos struktūros, tačiau esant reikalui operatorius dalį procesų gali valdyti realiu laiku. GaN kristalinių sluoksnių auginimui šiame darbe pirmtakėmis medžiagomis buvo pasirinktos: trimetil galis (TMG) – galio šaltinis, ir amoniakas – azoto šaltinis. Vandenilis buvo naudojamas kaip metalorganiką nešančiosios dujos.

Kristalų auginimas ant dvimačių medžiagų yra gana nauja tema. Įprastos epitaksijos sąlygomis augantis sluoksnis suformuoja kovalentinius cheminius ryšius su padėklu, ant kurio yra nusodinamas. Dėl kristalinės gardelės ir terminio plėtimosi koeficientų skirtumų užaugintas sluoksnis dažnai būna įtemptas ir/arba turintis struktūrinių defektų. Epitaksija ant dvimačių medžiagų leidžia iš dalies išvengti šių problemų, kadangi laisvųjų jungčių neturintis van der Waals paviršius nesudaro cheminių ryšių su epitaksiniu sluoksniu [13]. Tačiau cheminio ryšio trūkumas apsunkina kristalitų formavimąsi [89] bei gali lemti prastą kristalitų orientacijos išlaikymą per visą dvimatės medžiagos paviršių [14].

Kaip jau minėta Įvade, pastebėjus, kad grafenas ne visiškai ekranuoja tūrinio padėklo atomų kuriamą potencinį lauką, buvo pasiūlyta nuotolinės epitaksijos idėja [13]. Auginant tam tikras medžiagas šiuo būdu epitaksiniai sluoksniai jaučia ne tik grafeno, bet ir po juo esančio padėklo periodinį potencinį lauką, dėl to yra homogeniškai orientuojami ir užauga išlaikę monokristališkumą. Skirtingi kristalų augimo būdai iliustruoti Pav. 6.

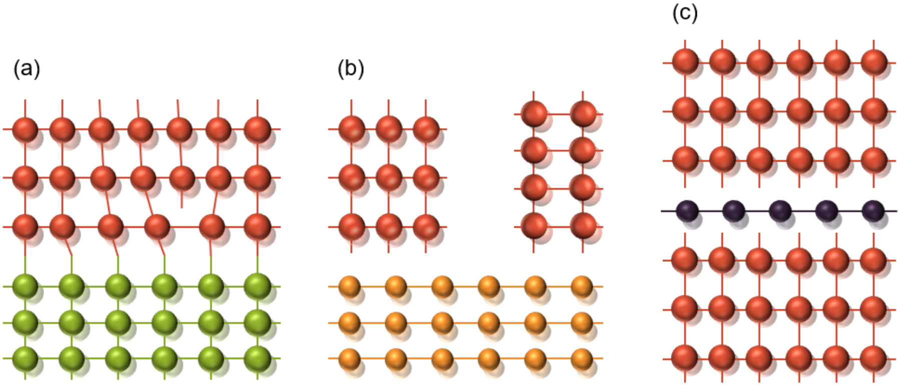

Pav. 6 Įprastas kristalo augimas suformuojant kovalentinius ryšius su padėklu (a), 3D medžiagos vdW epitaksija ant 2D medžiagų (b) ir nuotolinės epitaksijos principas, epitaksiniam sluoksniui formuojantis ant monosluoksnio grafeno (c). Iliustracija sukurta iš dalies remiantis literatūroje pateikta informacija [91,92].

Tiesa, nuotolinė epitaksija galima ne visoms medžiagų sistemoms, o tik toms, kuriose 3D medžiagos joniškumas (angl. *ionicity*) yra pakankamai didelis, o pasirinkta 2D medžiaga yra nepoliška (angl. *non-polar*). Ši sąlyga galioja GaN auginant ant grafenu padengtų GaN tūrinių padėklų [14]. Taip pat buvo pademonstruota, kad GaN nuotolinė epitaksija galima esant iki dviejų (Pav. 7) grafeno monosluoksnių, perkeltų sausuoju būdu [14,20]. Ši savybė gana svarbi praktiškai taikant nuotolinės epitaksijos idėją ir bus išsamiau aptarta tolesniame skyriuje.

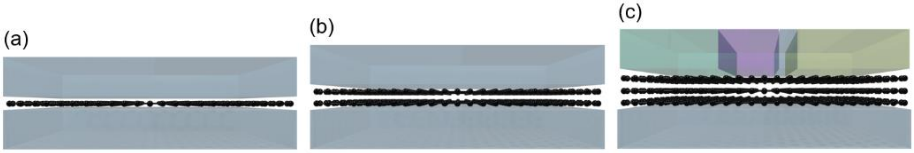

Pav. 7 GaN auginimas ant monosluoksniu, dvisluoksniu ir trisluoksniu grafenu padengtų GaN padėklų. Skirtingos spalvos iliustruoja skirtingos orientacijos GaN.

SEM ir TEM metodikos buvo skirtos netiesioginiam užaugintų GaN struktūrų ir perkelto grafeno vaizdinimui. Abi metodikos pagrįstos elektriniame lauke pagreitintų ir sufokusuotų elektronų sąveika su tiriamąja medžiaga [99]. Antrinių elektronų (angl. *secondary electrons*) SEM vaizdai leido nustatyti paviršiaus morfologiją, o TEM – atominiu tikslumu pamatyti grafeno sluoksnius, įterptus tarp GaN padėklo ir užauginto GaN epitaksinio sluoksnio.

Šiame darbe naudoti SEM mikroskopai *Apollo CamScan 300* ir *HITACHI SU8230*, veikiantys esant įvairiai elektronų pluoštą greitinančiai įtampai. TEM vaizdai atvaizduoti pasitelkiant *FEI Tecnai G2 F20 X-TWIN* įrangą. Bandiniai TEM buvo paruošti juos išpjaunant fokusuoto Ga jonų pluošto (FIB) metodu [102]. Šiam tikslui pasiekti buvo naudojama įranga *Helios NanoLab 650*.

Atominių jėgų mikroskopija nustatyta bandinių paviršiaus topografija leido įvertinti užaugintų GaN ruošinių tinkamumą tolesniam grafeno perkėlimui, nustatyti grafeno perkėlimo ir polimero nuvalymo sėkmingumą bei nustatyti užaugintų GaN epitaksinių sluoksnių šiurkštumą. AFM eksperimentams šiame darbe naudota *Nanonics MultiView 1000* matavimo sistema su CrAu lydinio adata. Bandinių paviršiaus topografiniai duomenys apdoroti ir paviršiaus aukščio nuokrypio vidutinės kvadratinės vertės (angl. *root-mean-square*) apskaičiuotos naudojantis nemokamai prieinama *WSxM* programine įranga [105].

Perkelto grafeno savybės šiame darbe buvo tiriamos Raman poslinkio spektroskopija. Ši metodika – vienas pagrindinių grafeno tyrimų būdų [115,117], leidžiantis patvirtinti sėkmingą grafeno perkėlimą, iš dalies įvertinti defektų kiekį bei nustatyti grafeno monosluoksnių skaičių. Raman poslinkio spektroskopija prieš beveik šimtmetį pademonstruota mokslininko, kurio vardu ir buvo pavadinta [107], remiasi neelastiniu žadinančios spinduliuotės išsklaidymu tiriamoje medžiagoje. Neelastinės sklaidos energija naudojama medžiagos (molekulių) specifinių vibracinių lygmenų nustatymui. Pavyzdžiui, grafeno Raman sklaidos spektre dažnai aptinkamos bent trys spektrinės smailės, vadinamos D, G ir 2D [118]. Pirmoji D smailė pasireiškia apie 1340 cm^{-1} ir yra susijusi su defektais grafeno monosluoksnyje. Taigi, eksperimentatoriai, preciziškai užauginę ir/ar perkėlę grafeną tikisi jos nepamatyti arba pastebėti mažą smailės intensyvumą palyginus su kita – G smaile. Pastaroji visada aptinkama esant grafenui (ar grafitui) ties maždaug 1588 cm^{-1}. Pati intensyviausia Raman poslinkio smailė – 2D. Ši smailė aptinkama ties maždaug 2680 cm^{-1}.

Šiame darbe naudota Raman poslinkio spektroskopijos įranga:

1. Konfokalinis Raman poslinkio vaizdinimo mikroskopas *Renishaw inVia,* veikiantis kartu su 532 nm lazeriu. Daugiau detalių galima rasti literatūroje Badokas *et al.* [P1].

2. Konfokalinis Raman poslinkio vaizdinimo mikroskopas *WITEC alpha 300R* veikiantis kartu su 532 nm lazeriu. Daugiau detalių galima rasti literatūroje Badokas *et al.* [P2].

Fotoliuminescencijos spektrų matavimai yra plačiai taikoma III-grupės nitridų (ir ne tik) tyrimo metodika. PL metodas pagrįstas medžiagos sąveika su lazerio spinduliuote ir šviesos perspinduliavimu po sužadinimo. PL spektrai gali būti naudojami draustinių energijų tarpo, įtempių, priemaišų, lemiančių medžiagos energetinių lygmenų pokyčius, nustatymui [122,123]. PL spektrams kambario temperatūroje išmatuoti šiame darbe naudoti monochromatorius *Jobin Yvon HRD-1* ir fotodaugintuvas *Hamamatsu*.

Kristalinių sluoksnių kokybei įvertinti pasitelktas Rentgeno spindulių difrakcijos metodas. Šis metodas pagrįstas monochromatinių Rentgeno spindulių difrakcija nuo atominių plokštumų ir konstruktyvia (lemiančia difrakcinius maksimumus) interferencija, kai atstumas tarp plokštumų, bangos ilgis ir kritimo bei atspindžio kampai atitinka Brego (angl. *Bragg*) difrakcijos sąlygą [126]. Kristalinei kokybei įvertinti šiame darbe pasitelkta *Rigaku SmartLab* įranga.

2. EKSPERIMENTINIAI REZULTATAI

Šiame skyriuje pateikiami pagrindiniai eksperimentiniai rezultatai. Eksperimentai didžiąja dalimi aprašyti tokia tvarka, kokia buvo atliekami darbo metu.

2.1. GaN/safyras ruošinių auginimas

Pirmieji MOVPE eksperimentai buvo skirti paruošti GaN/safyras padėklus (toliau vadinamus ruošiniais) nuotolinei epitaksijai – t. y. užauginti apie 3.1 µm storio GaN sluoksnius ant safyro padėklų. Ruošinių paviršiaus lygumas buvo svarbus parametras, kadangi būtent ant GaN paviršiaus vėliau buvo perkeliamas grafenas. MOVPE būdu užauginti dviejų tipų GaN sluoksniai: nelegiruoti (*u*GaN) ir šiek tiek Si legiruoti (*n*GaN). MOVPE auginimams naudoti 2 colių (5,08 cm) diametro, *c*-krypties orientacijos safyro padėklai, nupjauti 0,25°–0,35° link safyro kristalografinės *m*-ašies.

Krūvininkų koncentracija, nustatyta Holo efekto įtampos metodu: 10^{16} cm^{-3} ir 10^{17} cm^{-3} nelegiruotame ir Si legiruotame ruošiniuose atitinkamai. AFM metodu išmatavus ruošinių paviršiaus topografiją ir apskaičiavus aukščių RMS vertes paaiškėjo, kad šiek tiek legiruoti (*n*GaN) ruošiniai pademonstravo lygesnį paviršių (Pav. 8). *n*GaN paviršiaus aukščių RMS vertė 10 µm × 50 µm skenavime buvo 1,81 nm, tuo tarpu *u*GaN tokio paties dydžio skenavime – jau 3,81 nm. Atliekant dar mažesnio ploto skenavimą (1 µm × 5 µm) ta pati tendencija buvo išlaikyta – apskaičiuotos paviršiaus aukščių RMS vertės 0,20 nm ir 0,27 nm *n*GaN ir *u*GaN ruošiniams atitinkamai. Lygesnis *n*GaN ruošinių paviršius buvo tikėtinas remiantis MOVPE proceso GaN sluoksnių auginimų praktika, tačiau legiravimo įtakos priežastys šiame darbe išsamiai ištirtos nebuvo.

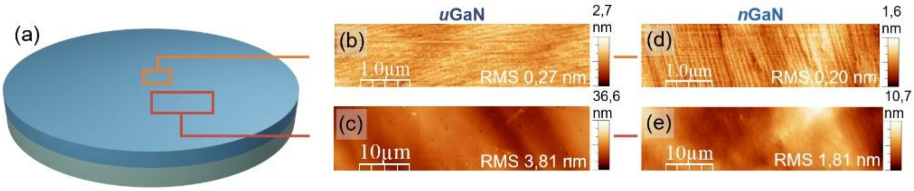

Pav. 8 GaN/safyras ruošinio struktūra (a). AFM topografiniai vaizdai atliekant skirtingų plotų skenavimus: nelegiruoto GaN paviršius (b) ir (c) bei Si legiruoto GaN paviršius (d) ir (e).

Taigi, dėl lygesnio paviršiaus dauguma šiame darbe naudotų ruošinių buvo šiek tiek Si legiruoti 2 colių diametro GaN/safyras padėklai. Susiklosčius situacijai, kai užauginti ruošiniai nebūdavo nuotolinei epitaksijai sunaudojami per kelių savaičių laikotarpį, jų paviršius *atnaujintas* užauginant papildomą 100 nm GaN sluoksnį taip iš dalies pašalinant ar uždengiant galimai susiformavusį oksido sluoksnį.

2.2. Monosluoksnio grafeno perkėlimas

Monosluoksnio grafeno perkėlimui buvo pasirinkti dviejų skirtingų tipų monosluoksniai. Šlapiajam perkėlimui (angl. *wet transfer*) naudoti Grafenas A ir Grafenas B iš dviejų skirtingų tiekėjų. Sausajam perkėlimui (angl. *dry transfer*) pasirinktas Grafenas C.

Grafeno A ir Grafeno B perkėlimo procedūros buvo labai panašios. Monosluoksniai gamintojų pateikti ant PMMA (polimetilmetakrilato) laikančiojo polimero. Grafeno monosluoksniai, kurių plotas 1 in^2 (apie 6,5 cm^2), dažnu atveju buvo žirklėmis sukarpomi į mažesnio ploto bandinius. Polimero/grafeno sluoksniai buvo merkiami į vandenį ir *sužvejojami* ant GaN/safyras ruošinių (Pav. 9). Norint atidengti grafeno monosluoksnį, PMMA polimeras buvo pašalinamas acetono ir izopropanolio (IP) pripildytose vonelėse kaitinant, vėliau nuskalaujamas dejonizuotu (DI) vandeniu. Taip pat papildomai pakaitinamas ir laikomas vakuume pernakt. Po perkėlimo grafeno sluoksniai taip pat buvo apžiūrimi optiniu mikroskopu siekiant įvertinti perkėlimo kokybę ir ruošinių tinkamumą tolesniems MOVPE eksperimentams (optinio mikroskopo nuotraukos santraukoje lietuvių kalba nepateikiamos).

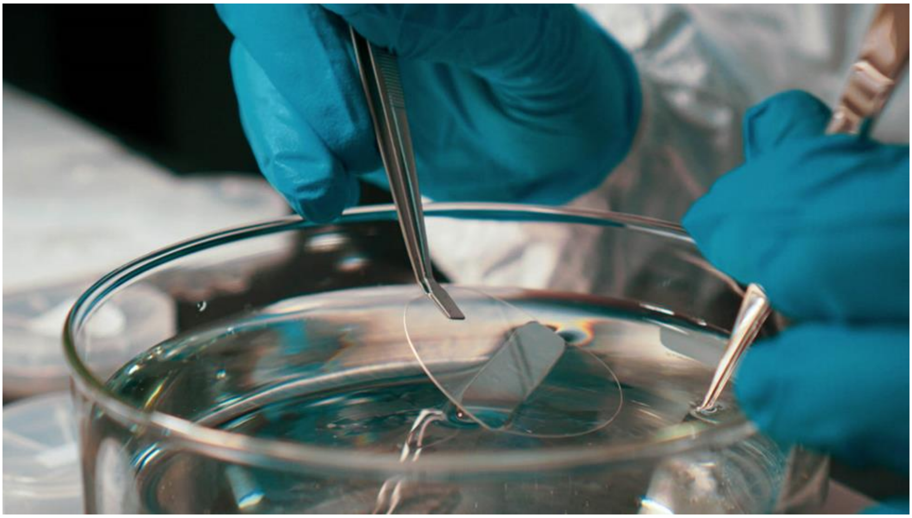

Pav. 9 Monosluoksnio grafeno ant PMMA *sužvejojimo* vandenyje procedūra, atliekama šio darbo autoriaus.

Grafeno C perkėlimo procedūra buvo brangesnė. Šis grafenas – tai epitaksinis grafenas ant SiC padėklo. Pirmasis žingsnis Grafeno C perkėlime buvo metalinių Ni sluoksnių padengimas (20 nm + 500 nm) garinimo elektronų pluošteliu ir magnetroninio dulkinimo būdais. Metaliniai sluoksniai buvo skirti grafenui nuo SiC padėklo nukelti [72]. Vėliau sekė specialios paskirties lipnios juostelės, savo lipnumą prarandančios aukštoje temperatūroje (angl. *thermal release tape*, trump. TRT), priklijavimas. Pernešus grafeno sluoksnį, šis kartu su Ni paliktas ant naujo padėklo kaitinant TRT iki 150 °C. Po TRT pašalinimo Ni sluoksnis buvo nuėsdinamas panaudojant $FeCl_3$ tirpalą. Vėliau bandinys nuplautas panaudojant šlapiajam perkėlimui aprašytą procedūrą. Išsamesnė informacija apie sausąjį grafeno perkėlimą pateikiama literatūroje [12].

Grafenas A ir Grafenas B Raman poslinkio spektroskopijos tyrimams buvo perkelti ant safyro padėklų, tuo tarpu Grafenas C – ant GaN/safyras ruošinio (dėl riboto SiC padėklų su grafenu kiekio, skirto šios disertacijos eksperimentams). Raman poslinkio spektrai pateikti Pav. 10. Visi trys perkelti grafeno monosluoksniai rodė grafenui būdingas smailes – G ir 2D. Smailių santykis I_{2D}/I_G visiems trims bandiniams taip pat buvo didesnis nei 2, indikuojantis monosluoksnio grafeno buvimą [131]. Tuo tarpu D smailė pastebėta Grafeno A ir Grafeno C perkėlimo atvejais. Kadangi ši smailė susijusi su defektais [115] ir buvo gana aiškiai išreikšta Grafeno C atveju, jo perkėlimo kokybė buvo prasčiausia. Tuo tarpu Grafeno B perkėlimas buvo geriausios kokybės, vertinant pagal Raman poslinkio spektrus.

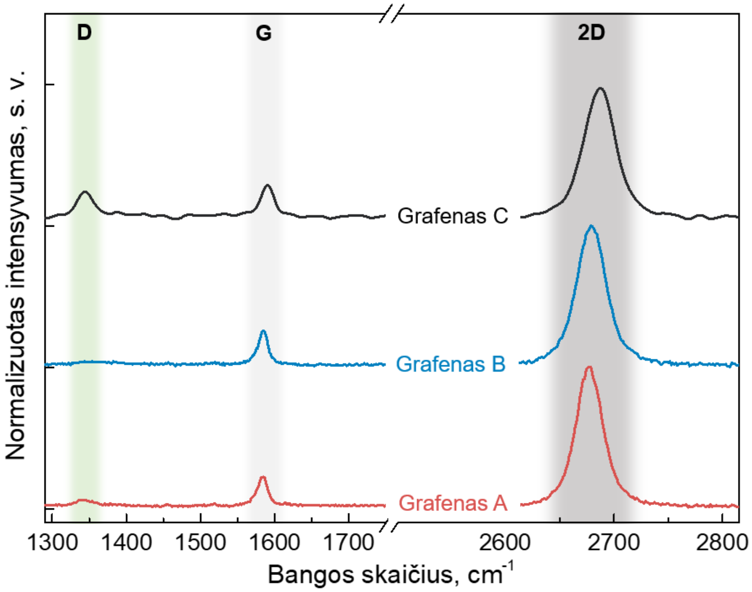

Pav. 10 Grafenu A ir Grafenu B padengtų safyro padėklų bei Grafenu C padengto GaN/safyras ruošinio Raman poslinkio spektrai. Grafeno C atveju GaN Raman poslinkio spektras išmatuotas atskirai ir atimtas. Paveikslėlyje pateikti sunormuoti ir vertikaliai išrikiuoti spektrai. Su grafenu sietinos D, G ir 2D smailės pažymėtos atitinkamai.

Grafeno A ir Grafeno B paviršiai (ypač riba ties grafeno kraštu) buvo ištirti AFM analizės metodu (rezultatai santraukoje lietuvių kalba nepateikiami). Lygesnis paviršius, taigi, tikėtina, ir geriau nusvilęs polimeras buvo Grafeno B naudojimo atveju. Dėl to tolesniems MOVPE eksperimentams buvo naudojami Grafenu B padengti GaN/safyras ruošiniai.

2.3. GaN auginimas ant monosluoksniu grafenu padengtų padėklų

Atliekant GaN auginimus MOVPE metodu įprastai naudojama aukšta temperatūra, siekianti daugiau kaip 1000 °C. Grafeno laikymas aukštos temperatūros sąlygomis [132], taip pat esant chemiškai agresyviai aplinkai (vandenilis, amoniakas, atominis azotas ir pan.) gali pažeisti monosluoksnį [90]. Taigi prieš pradedant kokybiškų epitaksinių GaN sluoksnių auginimą reikėjo nustatyti, kokiai maksimaliai GaN nukleacijos (angl. *nucleation*) temperatūrai esant grafenas išlieka nepažeistas. Atlikti keturi vienpakopiai auginimai esant skirtingoms temperatūroms: 600 °C, 700 °C, 800 °C ir 1075 °C.

Ruošiniai po nukleacijos proceso ištirti Raman poslinkio spektroskopijos metodu (Pav. 11). 600 °C, 700 °C ir 800 °C MOVPE auginimo temperatūroje grafenas išliko – buvo pastebimos su grafenu siejamos Raman poslinkio spektrinės smailės G ir 2D. Visgi, 800 °C temperatūroje laikyto grafeno Raman poslinkio spektre papildomai atsirado su defektais siejama smailė D’, susijusi su monosluoksnio kokybės suprastėjimu [134]. Tuo tarpu po GaN MOVPE auginimo tik 1075 °C (be nukleacijos žemesnėje temperatūroje) su grafenu siejamų Raman poslinkio spektro smailų buvo nematyti. Grafenas galėjo iš dalies arba net visiškai suirti 1075 °C temperatūroje esant chemiškai agresyviai aplinkai.

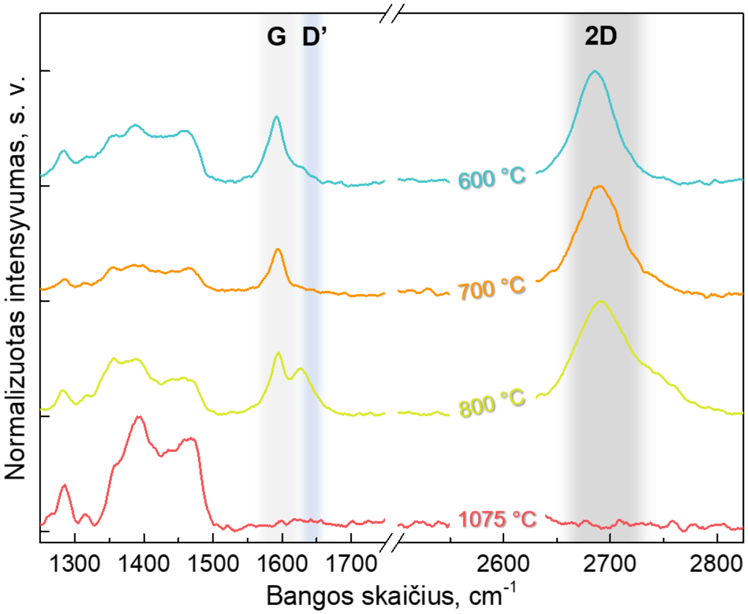

Pav. 11 Raman poslinkio spektrai MOVPE GaN auginimo skirtingose temperatūrose. Paveikslėlyje pateikti sunormuoti ir vertikaliai išrikiuoti spektrai. Su grafenu sietinos G, D’ ir 2D smailės pažymėtos atitinkamai. Raman poslinkio duomenys adaptuoti iš darbo autoriaus publikacijos [P1]. © IOP Publishing. Panaudota turint leidimą. Visos teisės saugomos.

Taigi MOVPE nuotolinės epitaksijos eksperimentams tinkamiausia maksimalia nukleacijos temperatūra pasirinkta 700 °C. Atlikti auginimai per grafeną naudojant dvipakopį (angl. *two-step*) GaN epitaksijos receptą. Šio proceso metu iš pradžių žemesnėje temperatūroje (pvz., 700 °C) suformuojamas nukleacinis sluoksnis, sudarytas daugiausiai iš GaN salų, kurios keliant temperatūrą ir tęsiant auginimą sudaro ištisinį, aukštos kokybės GaN sluoksnį. Po dvipakopio GaN epitaksinio sluoksnio auginimo Raman poslinkio spektruose jau buvo matomos su grafenu sietinos smailės (Pav. 12).

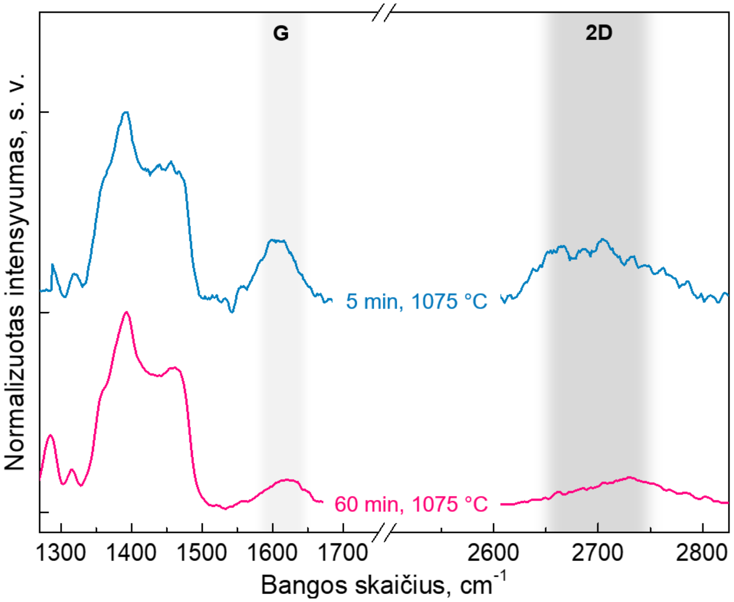

Pav. 12 Raman poslinkio spektrai po MOVPE GaN auginimo dvipakopiu receptu (nukleacijos temperatūra 700 °C). Paveikslėlyje pateikti spektrai normalizuoti ir išrikiuoti vertikaliai. Su grafenu sietinos G ir 2D smailės pažymėtos atitinkamai. Raman poslinkio duomenys adaptuoti iš darbo autoriaus publikacijos [P1]. © IOP Publishing. Panaudota turint leidimą. Visos teisės saugomos.

Bandinių rinkinys užaugintas keičiant įvairius auginimo parametrus: nukleacijos trukmę, temperatūrą (papildant aukščiau aptartus GaN epitaksinius sluoksnius), temperatūros kėlimo (iki 1075 °C) spartą, metalorganikos tiekimą temperatūros kėlimo metu. Apibendrinti GaN epitaksinių sluoksnių auginimo receptai pateikti Pav. 13. Visi šie GaN epitaksiniai sluoksniai taip pat ištirti XRD metodu matuojant ω-skenavimų pusplotį (FWHM) (XRD rezultatai santraukoje lietuvių kalba nepateikiami). Nustatytos FWHM vertės nuo 307 arcsec iki 508 arcsec.

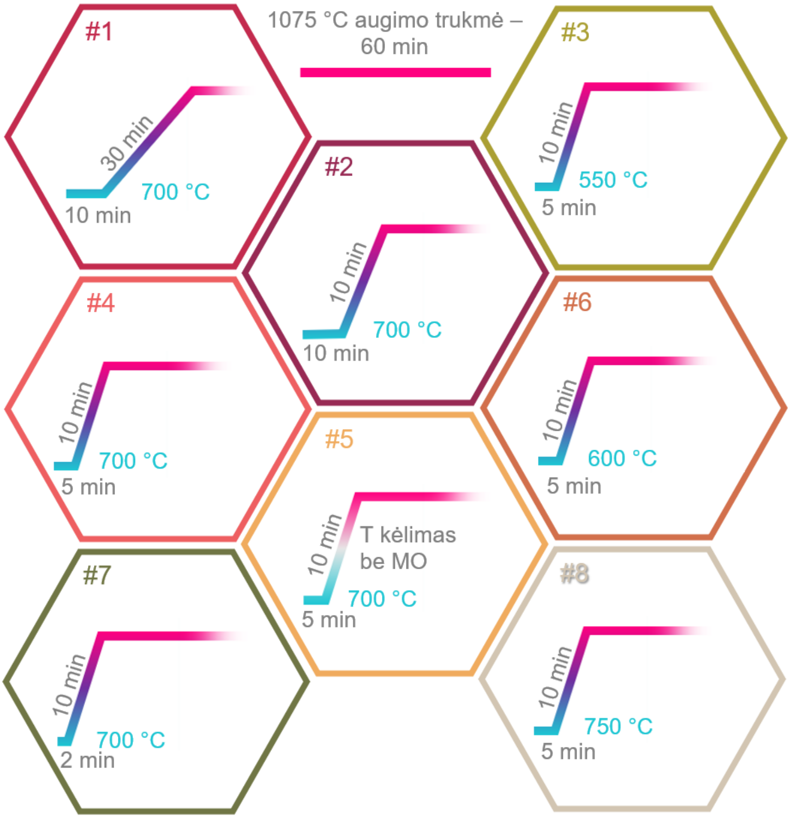

Pav. 13 Dalis GaN epitaksiniams sluoksnių ant grafenu padengtų padėklų auginti naudotų receptų su išvardintais pagrindiniais parametrais.

Geros kokybės (XRD išmatuotas ω-skenavimų pusplotis 307 arcsec) GaN epitaksinio sluoksnio ir grafenas/GaN/safyras ruošinio sandūra ištirta TEM metodu. TEM vaizduose, pateiktuose Pav. 14, matomi *c*-krypties GaN epitaksinis sluoksnis ir GaN ruošinys. Šviesesnė sritis Pav. 14 (b) priskirta grafeno monosluoksniui, tačiau jos plotis pastebimai didesnis nei tikėtasi. Šis išplatėjimas gali būti susijęs su bandinio pasvirimu, kaip pavaizduota Pav. 14 (c) ir pastebėta literatūroje [137].

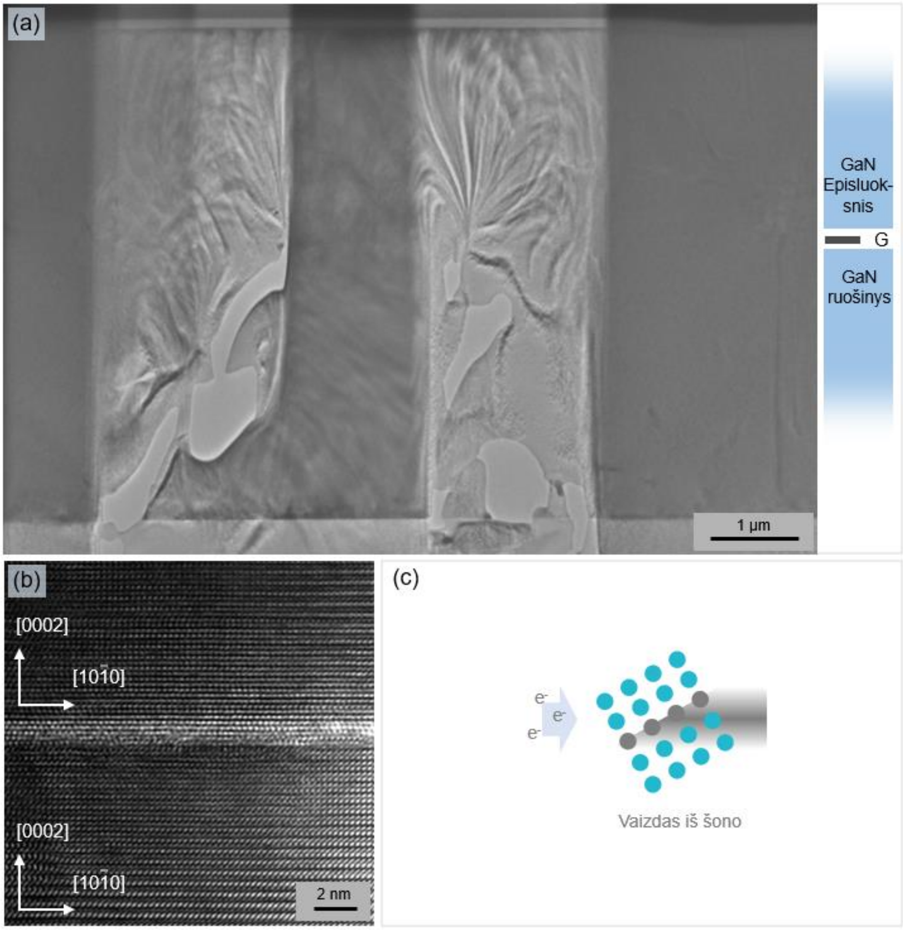

Pav. 14 TEM nuotrauka, kurioje matoma GaN/grafenas/GaN zona, bei jos schema dešinėje (a). Grafeno tarpsluoksnis bandinyje, augintame dvipakopiu būdu, naudojant 700 °C nukleacijos receptą (b). Nustatytos kristalografinės orientacijos yra pažymėtos (b). Stebimos šviesesnės, su grafenu sietinos zonos plotis gali būti paaiškintas bandinio pasvirimu (c). TEM rezultatai adaptuoti iš darbo autoriaus publikacijos [P1]. © IOP Publishing. Panaudota turint leidimą. Visos teisės saugomos.

TEM metodu ištirtas ir GaN/grafenas/GaN/safyras bandinys, kurio epitaksinio sluoksnio GaN nukleacijai buvo pasirinkta 600 °C temperatūra (rezultatai santraukoje lietuvių kalba nepateikiami). Pastaruoju atveju nepavyko aptikti tolygaus grafeno tarpsluoksnio, taip pat buvo pastebėta kitų orientacijų ir kubinės fazės GaN intarpų. Šie rezultatai pabrėžia tinkamų GaN epitaksinio sluoksnio auginimo ant grafeno sąlygų svarbą.

2.4. GaN membranos nukėlimas

GaN membranos nukėlimui nuo grafeno įprastai naudojami papildomi metaliniai sluoksniai, kai kuriais atvejais ir terminis šokas [23,144]. Šiame darbe membranos nukėlimas pademonstruotas naudojant trijų skirtingų metalų sluoksnius. Pirmasis sluoksnis – 50 nm storio titanas padengtas naudojant garinimo elektronų pluošteliu metodą (angl. *e-beam evaporation*). Antrasis sluoksnis – 50 nm storio auksas, taip pat padengtas garinimo elektronų pluošteliu metodu. Titanas pasirinktas dėl gero sukibimo su GaN, o Au sluoksnis atliko oksidacijos barjero funkciją, kadangi abu metalai padengti vakuume to paties proceso metu. Vėliau, panaudojant elektrocheminį (angl. *electroplating*) metodą, suformuotas apie 5 µm storio įtempiantis Ni sluoksnis. Ni sluoksnio formavimo metu GaN membrana savaime nusikėlė nuo grafeno (Pav. 15 intarpas). Siekiant įsitikinti, kad GaN nusikėlė būtent nuo GaN/grafenas/GaN sandūros, o ne nuo safyro arba metalinių dangų, išmatuoti EDX (angl. *energy dispersive X-ray*) spektrai (Pav. 15). EDX spektruose matyti, kad GaN liko tiek ant nukeltos struktūros, tiek ant padėklo. Taip pat išmatuoti Raman poslinkio spektrai, kuriuose stebėtos su grafenu susijusios smailės tiek ant padėklo, tiek ant nukeltos membranos (spektrai santraukoje lietuvių kalba nepateikiami). Membranos nukėlimas patvirtino sėkmingus nuotolinės epitaksijos ant grafeno eksperimentus.

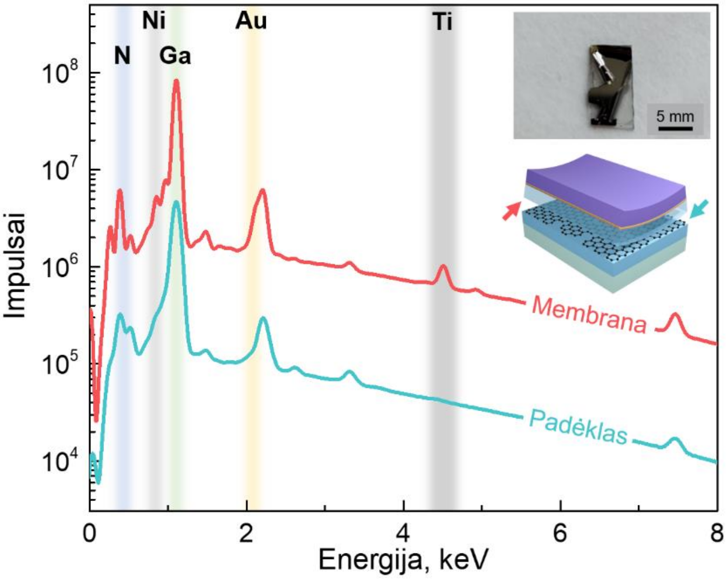

Pav. 15 Ant nukeltos membranos ir ant GaN/safyras padėklo išmatuoti EDX spektrai. Intarpe pateikta membranos nusikėlimo nuo padėklo nuotrauka ir schema. Dalis rezultatų adaptuota iš literatūros [146].

2.5. Keliasluoksnio grafeno perkėlimas

Grafeno perkėlimas yra vienas iš kritinių žingsnių, lemiančių sėkmingą nuotolinę epitaksiją [23]. Perkėlimo ir PMMA valymo metu išauga rizika pažeisti monosluoksnį. Be to kai kurie defektai [147] ir įplyšimai gali atsirasti dar grafeno gamybos metu. Trūkiai ir skylutės sudaro sąlygas besiformuojančiam epitaksiniam GaN sluoksniui sudaryti kovalentinius ryšius su padėklu, esančiu po grafeno monosluoksniu, o tai apsunkina užaugintų membranų nukėlimą. Taip pat nukėlimo metu gali būti pažeistas padėklo ir/ar membranos kristalinis paviršius.

Monosluoksnio skylių ir įtrūkių problemai spręsti buvo pasiūlytas dviejų sluoksnių grafenas (angl. *aperture-free*) [20]. Uždedant grafeno monosluoksnius vieną ant kito yra uždengiami struktūriniai defektai, esantys tik viename iš monosluoksnių (tikėtina, kad kokybiško grafeno defektų persiklojimo tikimybė yra gana maža). Ant dvisluoksnio grafeno vykdant MOCVD GaN epitaksiją galima padidinti tikimybę išvengti kovalentinių ryšių formavimosi. Be to, buvo pademonstruota, kad GaN epitaksinį sluoksnį auginant ant GaN padėklo, padengto grafenu, nuotolinė epitaksija turėtų vykti esant iki dviejų grafeno monosluoksnių [14].

Šiame darbe nustatytas šlapiuoju būdu perkelto daugiau nei vieno grafeno monosluoksnio tinkamumas nuotolinei epitaksijai. Dviejų ir trijų monosluoksnių struktūros perkeltos atliekant monosluoksnių perkėlimą ir PMMA valymą du ir tris kartus atitinkamai. Kadangi tokių procedūrų kartojimas kelis kartus gali dar labiau pažeisti monosluoksnius, taip pat perkeltas ir CVD būdu užaugintas dvisluoksnis grafenas, kuris perkeliamas šlapiąjį perkėlimą ir PMMA valymą atliekant tik vieną kartą. Po grafeno perkėlimų išmatuoti Raman poslinkio spektrai (Pav. 16). Pagal I_{2D}/I_G smailių intensyvumų santykį nustatyta, kad suformuotas atitinkamas grafeno monosluoksnių skaičius bei įvertinta jų kokybė. Su defektais siejama smailė D’ [134], buvo pastebėta tik suformavus dviejų monosluoksnių struktūrą, bet nestebima dvisluoksnį grafeną perkėlus vienu kartu.

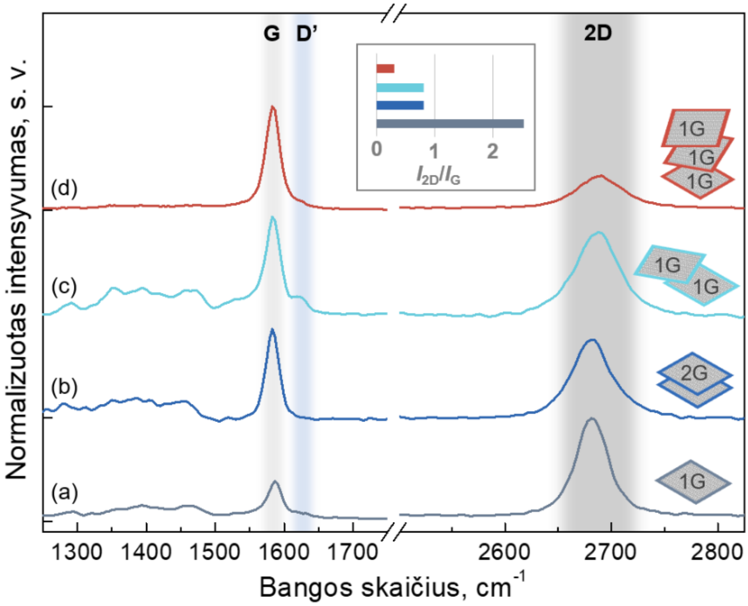

Pav. 16 Raman poslinkio spektrai, išmatuoti šlapiuoju būdu perkėlus monosluoksnį grafeną (a), dvisluoksnį grafeną (b), du grafeno monosluoksnius (c) ir tris grafeno monosluoksnius (d). Paveikslėlyje pateikti sunormuoti ir išrikiuoti vertikaliai spektrai. Intarpe pavaizduotas I_{2D}/I_G smailių santykis. Su grafenu sietinos G, D’ ir 2D smailės pažymėtas atitinkamai. Raman poslinkio duomenys adaptuoti iš darbo autoriaus publikacijos [P2].

2.6. GaN auginimas ant keliasluoksniu grafenu padengtų padėklų

GaN auginimai atlikti ant vienu, dviem ir trimis grafeno monosluoksniais padengtų GaN/safyras ruošinių. Pirmiausia ištirta GaN nukleacija (Pav. 17) receptą sustabdant po 5 min GaN auginimo 700 °C temperatūroje. Salų formavimosi dėsningumai buvo panašūs ant monosluoksnio ir dvisluoksnio grafeno, tačiau visiškai skirtingi esant dviejų monosluoksnių ir trijų monosluoksnių grafenui. Salų tankis ant dvisluoksnio grafeno buvo apie 2 %, kai tuo tarpu ant dviejų monosluoksnių – apie 35 %. Be to, ant dvisluoksnio grafeno buvo matyti dviejų tipų, taisyklingų geometrinių formų salos (tetraedrai ir heksagoninės piramidės), išlaikančios azimutinę orientaciją, taigi rodančios ryšį su padėklu (t. y. patvirtinančios nuotolinę epitaksiją). Tuo tarpu ant dviejų ir trijų monosluoksnių grafeno salos buvo netaisyklingų formų, vienos azimutinės orientacijos nepastebėta.

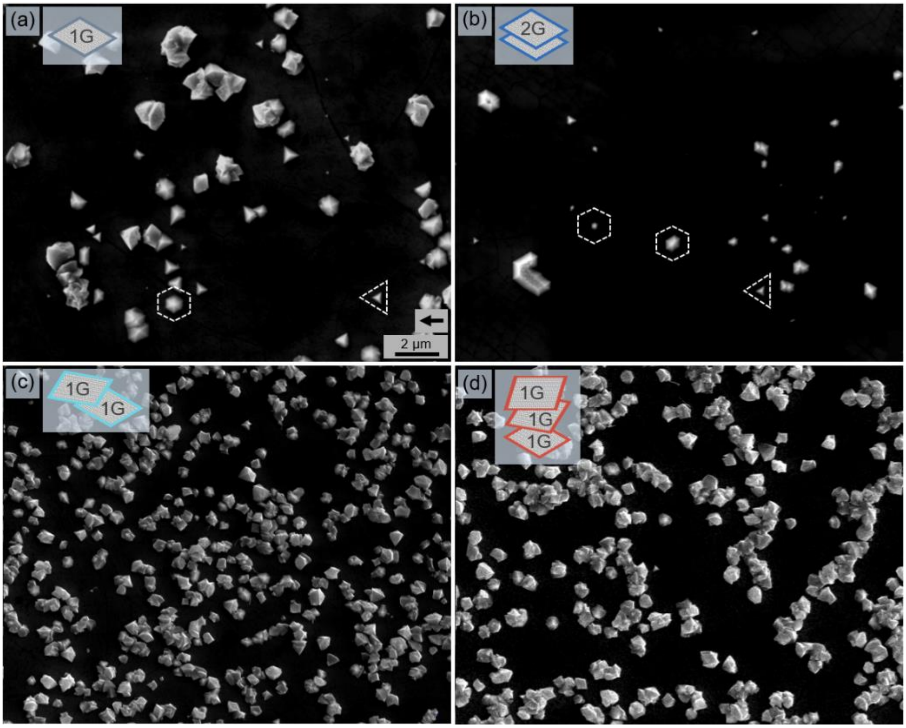

Pav. 17 GaN salų SEM nuotraukos po nukleacijos proceso, trukusio 5 min 700 °C temperatūroje. Monosluoksnis grafenas (a), dvisluoksnis grafenas (b), du grafeno monosluoksniai (c) ir trys grafeno monosluoksniai (d). Paveikslėlyje (a) nurodytas mastelis vienodas visoms nuotraukoms, o rodyklė rodo safyro padėklo kristalografinę $[11\bar{2}0]$ kryptį. Paveikslėliuose (a) ir (b) punktyrinėmis linijomis pažymėtos dviejų skirtingų tipų GaN salos. SEM vaizdai adaptuoti iš darbo autoriaus publikacijos [P2].

Ištisinį epitaksinį GaN sluoksnį pavyko užauginti ant dvisluoksnio grafeno. Šio sluoksnio kristalinė kokybė buvo labai panaši į GaN sluoksnio, užauginto ant safyro, kokybę – 808 arcsec ir 767 arcsec XRD φ-skenavimų FWHM atitinkamai. Tačiau ištisinis GaN sluoksnis nesusiformavo net per 1 h trukmės auginimą ant dviejų sluoksnių grafeno (rezultatai santraukoje lietuvių kalba nepateikiami). Ištyrus grafeno tarpsluoksnius TEM metodu pastebėtas tvarkingas dvisluoksnis grafenas, tačiau dviejų monosluoksnių sandūra nerodė aiškios dviejų sluoksnių ribos, vietomis pastebėti kitos nei padėklas (*c*-krypties) krypties GaN intarpai (Pav. 18). TEM rezultatai patvirtino SEM vaizduose (Pav. 17) pastebėtas GaN formavimosi tendencijas.

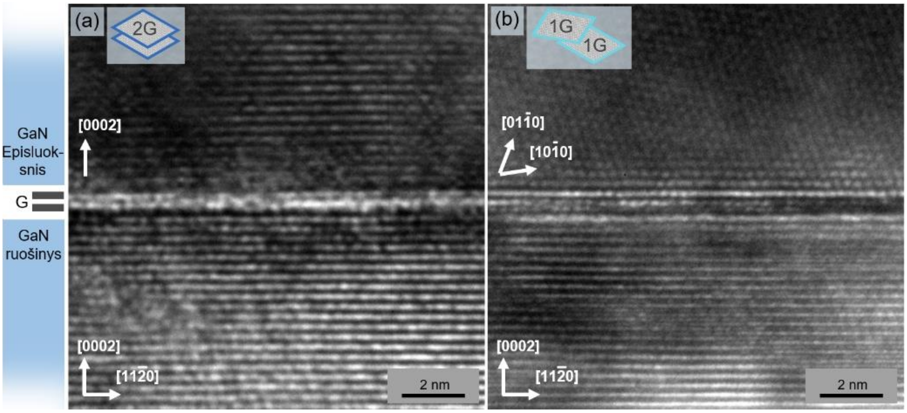

Pav. 18 TEM vaizdai ties grafeno tarpsluoksniu: dvisluoksnis grafenas (a) ir du grafeno monosluoksniai (b). Nustatytos kristalografinės GaN kryptys pažymėtos atitinkamai. TEM vaizdai adaptuoti iš darbo autoriaus publikacijos [P2].

Taigi nustatyta, kad nuotolinė GaN epitaksija galima per šlapiai perkeltą dvisluoksnį grafeną, kai šis perkeliamas naudojant tik vieną perkėlimo ir PMMA valymo procesą.

2.7. Ateities perspektyvos

Šiame darbe pateiktos įžvalgos, tikėtina, prisidės prie nuotolinės epitaksijos bei epitaksijos ant grafeno bendrąja prasme technologijų vystymo ir pritaikymo pramonei. Procesai, aprašyti šiame darbe, galėtų būti patobulinti artimiausiu metu atliekant papildomus eksperimentus:

- CVD grafenui perkelti pritaikomi nauji metodai, leidžiantys greitai, nebrangiai ir efektyviai uždengti didesnį epitaksijai skirtų GaN/safyras ruošinių plotą, pvz., naudojant laminavimo įrangą [156].

- Ni elektrolito sudėtis modifikuota sumažinant Ni sluoksnio mechaninį tempimą arba Ni dangos storis optimizuotas, taip išvengiant sunkiai kontroliuojamo membranos susivyniojimo.

- Pademonstruotas GaN membranos nukėlimas nuo daugiau nei vieno grafeno monosluoksnio, perkelto šlapiuoju būdu.

IŠVADOS

1. GaN/safyras ruošiniai yra tinkama ir ekonomiškai patraukli alternatyva GaN nuotolinei epitaksijai MOVPE metodu.

2. Šlapiuoju būdu perkeltas grafenas yra pakankamai geros kokybės, leidžiančios jį naudoti GaN nuotolinei epitaksijai MOVPE metodu.

3. Grafeno suirimo vandenilio ir amoniako aplinkoje, esančioje MOVPE proceso metu, yra išvengiama atliekant GaN nukleaciją 700 °C ir žemesnėje temperatūroje.

4. Dvipakopis MOVPE auginimo procesas, susidedantis iš GaN nukleacijos 700 °C temperatūroje ir koalescencijos 1075 °C temperatūroje, leidžia užauginti aukštos kokybės GaN epitaksinį sluoksnį ant grafenu padengto GaN/safyras ruošinio.

5. Ti, Au ir Ni sluoksniai leidžia nukelti MOVPE metodu užaugintą GaN membraną nuo grafenu padengto GaN/safyras ruošinio.

6. Vienu kartu perkeliamas dvisluoksnis grafenas yra tinkamas GaN nuotolinei epitaksijai MOVPE metodu ant GaN/safyras ruošinio. Tuo tarpu dviejų sluoksnių grafenui suformuoti naudojant dvigubą perkėlimo procesą nuotolinė GaN epitaksija nevyksta.

PUBLICATION [P1] / PUBLIKACIJA [P1]

Remote epitaxy of GaN via graphene on GaN/sapphire templates

Kazimieras Badokas, Arūnas Kadys, Jūras Mickevičius, Ilja Ignatjev, Martynas Skapas, Sandra Stanionytė, Edvinas Radiunas, Giedrius Juška, and Tadas Malinauskas

Journal of Physics D: Applied Physics **54**, 205103 (2021)

DOI:10.1088/1361-6463/abe500

Full text is available at the publisher's website /
Publikacija pasiekiama leidėjo tinklapyje

PUBLICATION [P2] / PUBLIKACIJA [P2]

MOVPE growth of GaN via graphene layers on GaN/sapphire templates

Kazimieras Badokas, Arūnas Kadys, Dominykas Augulis, Jūras Mickevičius, Ilja Ignatjev, Martynas Skapas, Benjaminas Šebeka, Giedrius Juška, and Tadas Malinauskas

Nanomaterials **12**(5), 785 (2022)

DOI:10.3390/nano12050785

nanomaterials

Article

MOVPE Growth of GaN via Graphene Layers on GaN/Sapphire Templates

Kazimieras Badokas [1,*], Arūnas Kadys [1], Dominykas Augulis [1], Jūras Mickevičius [1,*], Ilja Ignatjev [2], Martynas Skapas [2], Benjaminas Šebeka [2], Giedrius Juška [1] and Tadas Malinauskas [1]

[1] Institute of Photonics and Nanotechnology, Vilnius University, LT-10257 Vilnius, Lithuania; arunas.kadys@ff.vu.lt (A.K.); dominykas.augulis@ff.stud.vu.lt (D.A.); giedrius.juska@ff.vu.lt (G.J.); tadas.malinauskas@ff.vu.lt (T.M.)
[2] Center for Physical Sciences and Technology, LT-10257 Vilnius, Lithuania; ilja.ignatjev@ftmc.lt (I.I.); martynas.skapas@ftmc.lt (M.S.); benjaminas.sebeka@ftmc.lt (B.Š.)
* Correspondence: kazimieras.badokas@ff.vu.lt (K.B.); juras.mickevicius@ff.vu.lt (J.M.)

Abstract: The remote epitaxy of GaN epilayers on GaN/sapphire templates was studied by using different graphene interlayer types. Monolayer, bilayer, double-stack of monolayer, and triple-stack of monolayer graphenes were transferred onto GaN/sapphire templates using a wet transfer technique. The quality of the graphene interlayers was examined by Raman spectroscopy. The impact of the interlayer type on GaN nucleation was analyzed by scanning electron microscopy. The graphene interface and structural quality of GaN epilayers were studied by transmission electron microscopy and X-ray diffraction, respectively. The influence of the graphene interlayer type is discussed in terms of the differences between remote epitaxy and van der Waals epitaxy. The successful exfoliation of GaN membrane is demonstrated.

Keywords: MOVPE; remote epitaxy; gallium nitride; graphene; lift-off

Citation: Badokas, K.; Kadys, A.; Augulis, D.; Mickevičius, J.; Ignatjev, I.; Skapas, M.; Šebeka, B.; Juška, G.; Malinauskas, T. MOVPE Growth of GaN via Graphene Layers on GaN/Sapphire Templates. *Nanomaterials* **2022**, *12*, 785. https://doi.org/10.3390/nano12050785

Academic Editors: Jin-Hae Chang and Marcelo Antunes

Received: 2 February 2022
Accepted: 22 February 2022
Published: 25 February 2022

1. Introduction

In recent years, a novel approach to the growth of III-nitrides has emerged, based on 2D materials, such as graphene, as interlayers between the substrate and the epitaxial layer [1–3]. Compared to the usual buffer layers, the graphene interlayer has some advantages owing to the weak van der Waals (vdW) bond at the epilayer/graphene interface; the thermal expansion and lattice mismatch requirements are relaxed [4], resulting in reduced defect density [5–7], and the epilayer can be mechanically exfoliated and transferred to any substrate of interest [3,8,9]. Furthermore, the monolayer graphene does not completely screen the electrostatic potential of the substrate, which enables the epilayer to follow the crystalline template of the substrate [10,11]. The remote epitaxy and graphene-mediated exfoliation have been demonstrated for several material systems, including III-N [8,9,11,12], III-V [10], II-VI [9], transition metal dichalcogenides [13], perovskites [14], and other complex oxides [15].

The critical step in this approach is the graphene layer transfer. Thicker graphene interlayers allow for easier exfoliation of the grown epilayer, since the separation of films tends to occur within graphene layers [3,16] due to weaker bindings between the graphene layers than that between the graphene and the GaN [17,18]. On the other hand, to ensure interaction between the substrate and the epilayer, the graphene interlayer thickness must not exceed two monolayers [1,9,11], which restrains the graphene layer to either monolayer or bilayer thickness. Meanwhile, depending on the transfer method, cracks, wrinkles, residue, and contamination might decrease the quality of the graphene layer [19–21], and significantly affect the epilayer growth.

Generally, the transfer of the graphene layer onto the target substrate is conducted in either a wet or a dry manner. The main disadvantages of dry transfer are the appearance of cracks, due to the interaction with hard surfaces, and a relatively high material cost [19]. Cracks in the graphene layer initiate growth through holes followed by lateral overgrowth [22,23]. Therefore, we used the relatively inexpensive wet transfer method to reduce the formation of cracks. Furthermore, to minimize the impact of other graphene defects, we utilized the multiple overlapping stacks of the monolayer graphene. To evaluate the feasibility of such an approach, we compare the growth of GaN on different graphene interlayers: monolayer, bilayer, and multiple stacks of monolayer graphene.

2. Materials and Methods

The GaN layers in the studied samples were grown using a low-pressure metalorganic vapor phase epitaxy (MOVPE) in a flip-top close-coupled showerhead 3 × 2″ reactor (AIXTRON, Herzogenrath, Germany). Trimethylgallium (TMGa) and ammonia (NH_3) were used as Ga and N precursors, respectively. The epitaxy process was monitored by an in situ laser reflectometry system operating at 650 nm. Transfer-ready poly(methyl methacrylate)-coated (PMMA-coated) graphene films from two vendors were used to cover the GaN/sapphire templates. Graphene monolayers were obtained from Graphenea Inc. (San Sebastian, Spain), while the bilayer graphene was acquired from ACS Material, LLC (Pasadena, CA, USA). After the transfer, samples were annealed in an oven with a controlled environment.

The structural characterization was performed using X-ray diffraction (XRD, Rigaku SmartLab, Tokyo, Japan). The surface morphology was studied by scanning electron microscopy (SEM, CamScan Apollo 300, Cambridge, UK, now successor Applied Beams, LLC, Beaverton, OR, USA). The surface roughness was evaluated by atomic force microscopy (AFM, Nanonics MultiView 1000, Jerusalem, Israel). The freely distributed WSxM software was used to analyze AFM data [24]. The GaN–graphene interface was investigated using transmission electron microscopy (TEM, FEI Tecnai G2 F20 X-TWIN, Eindhoven, The Netherlands). Raman measurements were performed using a confocal Raman microscope (WITec alpha 300R, Ulm, Germany). The 532 nm laser excitation source, with a power of 1.5 mW, was focused on a 0.8 µm diameter spot on the sample surface. A 600 lines/mm grating was used to record the Raman spectra. The wavenumber axis was calibrated using a polystyrene standard. All the measurements were performed at room temperature.

3. Results and Discussion

The initial GaN/sapphire template was prepared by the standard MOVPE growth of the GaN layer on a 2-inch c-plane sapphire substrate (see Ref. [25] for more details). The thickness of the GaN/sapphire template was 2.7 µm; its surface was smooth with the root mean square (RMS) surface roughness value of 0.2 nm, evaluated using AFM.

3.1. Graphene Layer Transfer

Monolayer graphene pieces of size 1.3 cm × 1.3 cm were transferred onto the as-grown GaN/sapphire templates using a wet transfer procedure, described elsewhere [25]. Since graphene transfer might result in the formation of defects [19–21], the surface of the transferred graphene layer was checked by SEM. While most of the graphene layer surface was smooth, some wrinkles and possible few-layer zones were observed (Figure 1a). Since direct epitaxy through defects, such as cracks and pinholes, followed by lateral overgrowth [22,23], might significantly aggravate the epilayer exfoliation, to avoid such a growth mode, stacks of two and three graphene monolayers (double-stack and triple-stack, hereinafter) were formed by repeating the complete transfer and cleaning procedures for each monolayer. In this approach, illustrated in Figure 1b,c, overlapping stacks of the graphene monolayer cover the underlying defects, thus reducing the possibility of direct epitaxy. On the other hand, each transfer might introduce additional defects in the overlying layer.

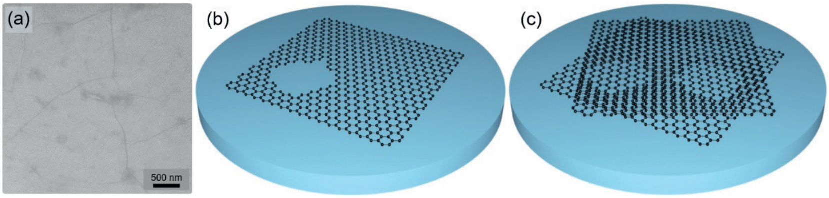

Figure 1. SEM image of monolayer graphene after the transfer procedure (**a**). Illustration of the hole in monolayer graphene (**b**), and of the holes covered by each of two overlapping graphene monolayers (**c**).

An alternative to the double-stack graphene might be the bilayer graphene. The wet transfer of bilayer graphene required additional care to prevent roll-up and air becoming trapped. First, the sponge holding the PMMA/graphene in place was soaked by placing small water droplets in the corners. The fully soaked PMMA/graphene/sponge "sandwich" was dipped into deionized water, and the PMMA/graphene was left to float freely on the water surface for a few hours. To avoid the formation of air bubbles, the deionized water was left to stand still overnight before being dipped. Next, the GaN/sapphire template was placed beneath the floating PMMA/graphene sheet, and it was attached as close as possible to the center of the template. The sample was then left to dry in the air for approximately 30 min. Afterwards, the sample was baked in an oven for 30 min at a temperature of 100 °C under N_2 atmosphere. The PMMA was removed by dipping the sample into acetone and later into isopropyl alcohol. Both solutions were preheated to 40 °C and gently stirred from time to time. Finally, the samples were annealed for 8 h at 300 °C in a vacuum.

The number and quality of graphene layers on the GaN/sapphire template were verified by Raman spectroscopy. The Raman spectra for all the studied types of graphene interlayer are presented in Figure 2. The graphene Raman fingerprints, G and 2D modes, are prominent in all spectra. The lack of an intense peak at around 1340 cm^{-1} indicated the high quality of the transferred graphene, although the defect-related D mode might be obscured by the second-order peaks of GaN in the broad range of 1250–1500 cm^{-1} [26,27]. The ratio of 2D and G peak intensities (I_{2D}/I_G), the full width at half maximum (FWHM) of a 2D peak, and the position of the 2D peak make it possible to determine the number of graphene layers with a relatively good degree of accuracy [28]. For the transferred monolayer graphene, the ratio I_{2D}/I_G was 2.5, while the position and FWHM of the 2D peak were 2682 cm^{-1} and 38 cm^{-1}, respectively, all consistent with the single graphene layer [28]. For both the double-stack and bilayer graphene, the ratio I_{2D}/I_G decreased to 0.8, and the 2D peak broadened to 48 cm^{-1}, indicating two graphene layers in the film [28]. However, there were some differences related to the main peaks: the 2D peak remained at 2681 cm^{-1}, and the G peak slightly shifted to 1583 cm^{-1} in the bilayer graphene. In contrast, the 2D peak shifted to 2687 cm^{-1}, and an additional D′ peak emerged on the shoulder of the G peak in the double-stack graphene. The broadening and the shift of the 2D peak are caused by its splitting into different subpeaks, which is explained by the evolution of the electronic bands in graphene with an increasing number of layers [29,30]. The D′ peak could be related to the defects [30], thus indicating the lower quality of the double-stack graphene compared to the bilayer graphene film. Finally, the ratio I_{2D}/I_G in the triple-stack graphene was reduced to 0.3, which is actually below the expected value of 0.6 [28], and implies layer folding and a formation of zones with a higher number of graphene layers.

3.2. Growth of GaN Epilayers

To reveal the impact of the graphene interlayer type on the formation of the initial GaN seeds, the growth of the GaN nucleation layer on the graphene-covered templates was carried out for 5 min at 700 °C without an extra recrystallization process. The selected growth conditions were based on our previous study on the remote epitaxy of GaN [25].

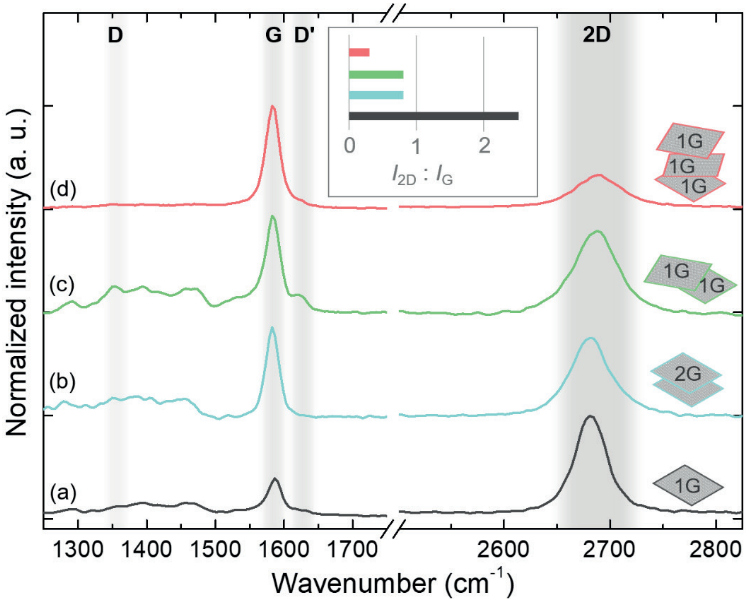

Figure 2. Raman spectra measured after the transfer of monolayer graphene (**a**), bilayer graphene (**b**), double-stack of monolayer graphene (**c**), and triple-stack of monolayer graphene (**d**). The spectra are normalized and shifted vertically for clarity. The approximate positions of the graphene Raman modes: D, D′, G, and 2D are highlighted. Inset illustrates the ratio of 2D and G mode intensities for corresponding layers.

The initial formation of GaN islands is demonstrated in the SEM images in Figure 3. A certain difference can be noticed immediately: the density of GaN seeds was much higher on the stacked graphene interlayers (Figure 3c,d). It is well known that the lack of dangling bonds and a low surface energy of graphene strongly impede the nucleation process of GaN [31,32]. Therefore, Ga or N adatoms tend to adsorb any defects, where graphene is imperfect and can supply dangling bonds; thus, preferential nucleation sites appear [33,34]. Consequently, the increased density of seeds on stacked layers can be attributed to the graphene layer damage during the transfer, especially considering that several transfers are required for the stacked graphene interlayer.

The epitaxial orientation of the GaN seeds is determined by the electrostatic interaction with the GaN template below the graphene layer [11]. Seeds with aligned crystalline planes were observed on the monolayer and bilayer graphene (Figure 3a,b); however, the GaN islands on stacked graphene seem to be oriented randomly with no specific preferred orientation (Figure 3c,d). A lack of crystalline relationship infers vdW epitaxy, when the substrate field is already screened, instead of remote epitaxy [10,11]. This is expected for the triple-stack graphene interlayer [1,9,11], while the change in the growth mechanism for the double-stack graphene could be related to the formation of zones with a higher number of graphene layers or interface contamination.

To study the difference between bilayer and double-stack graphene interlayers in more detail, the thick GaN layers of 2.5 µm were grown on both interlayer types. The optimized multi-step MOVPE protocol was used to perform nucleation at 700 °C and high-temperature growth at 1075 °C (see Ref. [25] for more details). The growth on the bilayer graphene resulted in a fully coalesced GaN film (surface roughness value of 0.4 nm); however, only a partially coalesced layer was obtained on the double-stack graphene (Figure 4).

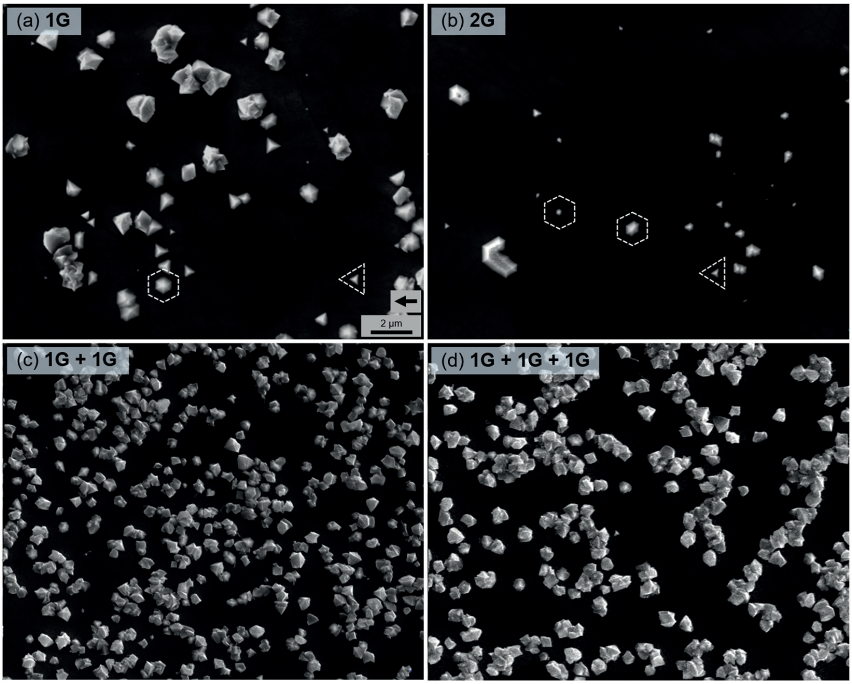

Figure 3. SEM images of the GaN nuclei after the growth of the low-temperature nucleation layer for 5 min on monolayer graphene (**a**), bilayer graphene (**b**), double-stack graphene (**c**), and triple-stack graphene (**d**). Scale bar in (**a**) is the same for all images. The black arrow in (**a**) indicates [1120] direction of an underlying sapphire substrate for all images. White dashed figures illustrate two types of GaN nuclei: hexagonal and triangular.

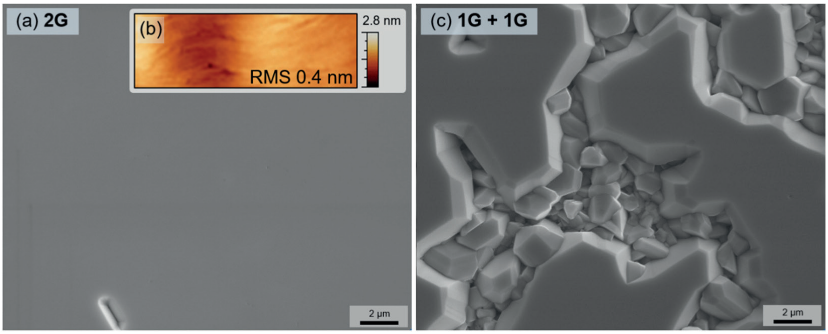

Figure 4. SEM images of the thick GaN epilayers grown on bilayer graphene (**a**) and double-stack of graphene (**c**). To assure that the image in (**a**) is in focus, an arbitrary defect is left visible. The surface morphology of GaN epilayer grown on bilayer graphene is represented by an AFM image within an area of approx. 2 μm × 5 μm (**b**).

The cross-sectional TEM images (Figure 5) of GaN epilayers revealed the contrasting interfaces in the studied samples. A well-defined two-layer structure of graphene was observed as a bright horizontal strip between the template and the epilayer in the sample with bilayer graphene (Figure 5a). The GaN epilayer on top of the graphene showed coherent atomic steps without significant disordered inclusions. Meanwhile, the double-stack graphene interlayer exhibited an uneven interface (Figure 5b), most likely due to the inner interface contamination or poor adhesion between the two graphene layers. Misoriented GaN crystallites were observed at the interface, confirming the vdW epitaxy growth mechanism, consistent with the SEM images (Figure 4a,c).

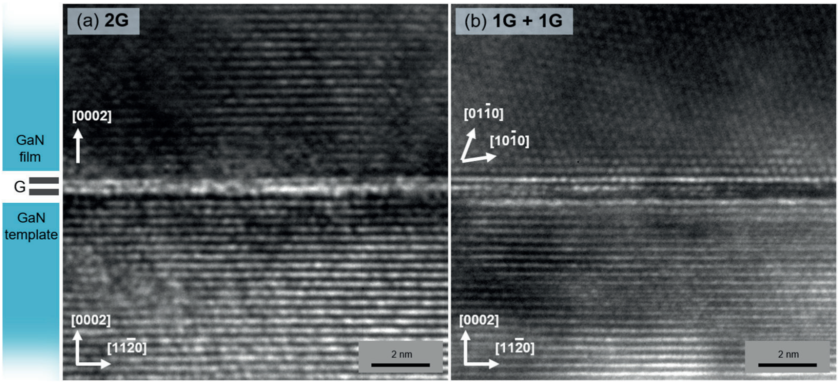

Figure 5. TEM images of GaN film grown on bilayer (**a**) and double-stack (**b**) graphene interlayers. The determined GaN directions are indicated for both the template and the epilayer.

All the presented results indicate the advantages of the single graphene transfer process. Even though multiple transfers of monolayer graphene can be used efficiently to cover the defects and holes in the underlying monolayer, each transfer increases the likelihood of a new defect formation. Eventually, it results in an uneven graphene interlayer with an uncertain thickness, which changes the growth mechanism from remote epitaxy to vdW epitaxy [1,9,11].

The structural quality of GaN epilayer grown on bilayer graphene was assessed and compared to that of the GaN/sapphire template by using XRD. To minimize the contribution of the underlying GaN template, the structural quality was evaluated using the in-plane geometry of XRD with an incident angle of 0.5 deg. The obtained rocking curves of the (1100) plane are shown in Figure 6 for both the GaN epilayer and the GaN/sapphire template. As evident, the rocking curves are very similar, with the FWHM equal to 767 and 808 arcsec for the template and epilayer, respectively. Since the broadening of the φ-scan of (1100) reflection is affected solely by the edge dislocations, which are dominant in MOVPE-grown GaN epilayers, this indicates the structural quality of the GaN layer grown on bilayer graphene as comparable to the conventional GaN layer deposited on a sapphire substrate using an optimized growth protocol.

3.3. Exfoliation of GaN Epilayer

For reliable exfoliation of thin GaN films, metal films deposited on the epilayer surface were used to generate the necessary force. The key processes are schematically presented in Figure 7a–d. First, a Ti-based adhesion layer with a thickness of 50 nm was deposited on the GaN surface by e-beam deposition. Next, a 50 nm Au protective layer was deposited using e-beam deposition. To avoid oxidation, both Ti and Au were deposited in a vacuum. Finally, a 5 μm Ni stressor layer was electroplated in a $NiSO_4(H_2O)_6$ and $NiCl_2$ solution. The combination of stresses in electroplated nickel and weak bonding to the interlayer resulted in the start of epilayer exfoliation (Figure 7f). Note that neither low-temperature thermal shock [35] nor additional handling layers [8,36] were required.

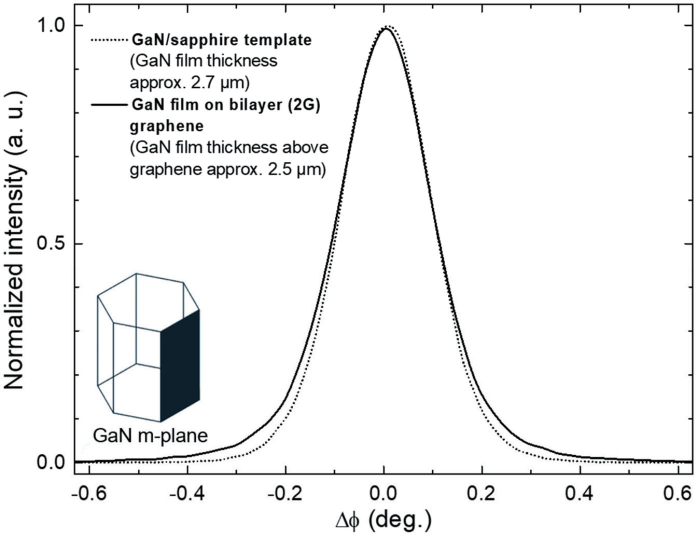

Figure 6. XRD rocking curve of (1100) plane GaN epilayer grown on bilayer graphene (solid line). For comparison, an analogous rocking curve of the GaN/sapphire template is provided (dotted line).

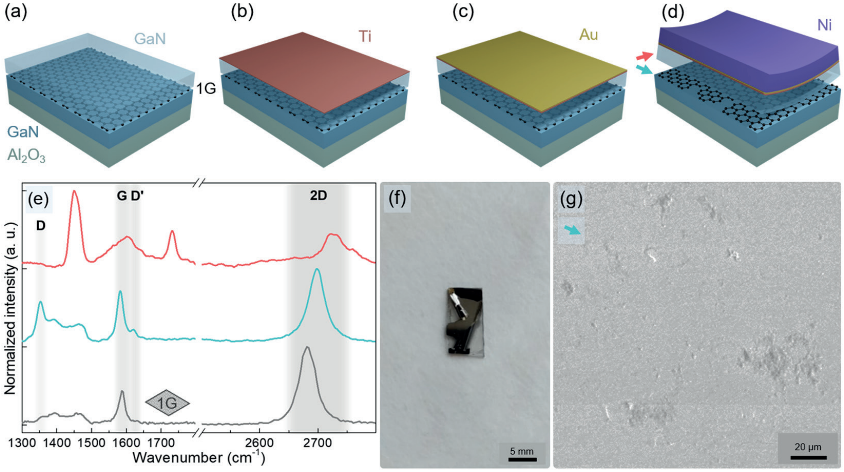

Figure 7. Schematic illustration of metal layer deposition for GaN exfoliation (**a–d**). The thickness of layers is exaggerated. Raman spectra of the template before MOVPE of GaN epilayer (grey line, **e**) and after lift-off of GaN–metal stressor stack (blue line, **e**). Colored arrows in (**d**) indicate the corresponding surfaces where Raman spectra were measured. Raman spectrum of the exfoliated GaN membrane (red line, **e**) (**f**). A stop-motion image of GaN self-exfoliation just after the Ni deposition (**f**). SEM image of graphene interlayer after the GaN epilayer exfoliation (**g**).

After the exfoliation, the presence of graphene was checked for both the GaN membrane and the remaining template. As revealed by Raman spectroscopy (Figure 7e), graphene survived on the template, although its quality was degraded, which manifested in a strong D peak as well as a visible D′ peak. Meanwhile, the graphene fingerprint peaks were also detected on the GaN membrane. This indicates that the damage to the graphene layer occurs not only during the growth of GaN epilayer [9,37], but also due to the exfoliation. The graphene interlayer was probably ripped during the exfoliation, with some flakes of graphene stuck to the GaN membrane. Furthermore, even though the overall interaction between the GaN/sapphire template and the epilayer is very weak, there might be a direct contact between the epilayer and the template through occasional holes and defects in the graphene layer, which also result in a partially damaged template, as shown in Figure 7g. Nevertheless, the successful exfoliation of the GaN epilayer proves the applicability of the presented approach. The main improvement, however, is due to the wet transfer method, while stacking of graphene monolayers requires further refinement.

4. Conclusions

GaN epilayers were grown on GaN/sapphire templates via graphene interlayers. The approach of multiple overlapping stacks of monolayer graphene was utilized to minimize the possibility of growth through holes. To evaluate the impact of interlayers on further growth, different interlayer types were studied: monolayer, bilayer, double-stack of monolayer, and triple-stack of monolayer graphene. Raman measurements revealed a small quality difference between the bilayer and the double-stack graphene, and indicated a higher than expected number of layers in triple-stack graphene. Studies of initial GaN nucleation split the interlayer influence into two groups: low density of aligned islands was observed on monolayer and bilayer graphene, and the high density of randomly oriented islands was observed on stacked graphene interlayers. The different nucleation mechanisms indicated remote and vdW epitaxy, respectively. Further growth of the thick GaN epilayer on the bilayer and double-stack graphene resulted in a high-quality and only partially coalesced GaN epilayer, respectively. Thus, the main focus should be on the graphene transfer: while multiple transfers allow the covering of holes and major defects, the single transfer process leads to a higher quality of resulting epilayer. The weak interaction between the epilayer and the underlying template allowed successful exfoliation of GaN membrane.

Author Contributions: Conceptualization, K.B., A.K. and T.M.; Funding acquisition, T.M.; Investigation, K.B., A.K., D.A., I.I., M.S., B.Š. and G.J.; Visualization, K.B.; Writing—original draft, K.B. and J.M.; Writing—review and editing, K.B., A.K., J.M. and T.M. All authors have read and agreed to the published version of the manuscript.

Funding: This research was funded by the European Social Fund according to the activity 'Improvement of researchers' qualification by implementing world-class R&D projects' of Measure No. 09.3.3-LMT-K-712 (Contract No. LMT-K-712-01-0076).

Institutional Review Board Statement: Not applicable.

Informed Consent Statement: Not applicable.

Data Availability Statement: The data that support the findings of this study are available from the corresponding author upon reasonable request.

Conflicts of Interest: The authors declare that there is no conflict of interest.

References

1. Bae, S.-H.; Kum, H.; Kong, W.; Kim, Y.; Choi, C.; Lee, B.; Lin, P.; Park, Y.; Kim, J. Integration of bulk materials with two-dimensional materials for physical coupling and applications. *Nat. Mater.* **2019**, *18*, 550–560. [CrossRef] [PubMed]
2. Yu, J.; Wang, L.; Hao, Z.; Luo, Y.; Sun, C.; Wang, J.; Han, Y.; Xiong, B.; Li, H. Van der Waals Epitaxy of III-Nitride Semiconductors Based on 2D Materials for Flexible Applications. *Adv. Mater.* **2020**, *32*, 1903407. [CrossRef]
3. Liang, D.; Wei, T.; Wang, J.; Li, J. Quasi van der Waals epitaxy nitride materials and devices on two dimension materials. *Nano Energy* **2020**, *69*, 104463. [CrossRef]
4. Alaskar, Y.; Arafin, S.; Wickramaratne, D.; Zurbuchen, M.A.; He, L.; McKay, J.; Lin, Q.; Goorsky, M.S.; Lake, R.K.; Wang, K.L. Towards van der Waals Epitaxial Growth of GaAs on Si using a Graphene Buffer Layer. *Adv. Funct. Mater.* **2014**, *24*, 6629–6638. [CrossRef]
5. Chang, H.; Liu, B.; Liang, D.; Gao, Y.; Yan, J.; Liu, Z.; Liu, Z.; Wang, J.; Li, J.; Gao, P.; et al. Graphene-induced crystal-healing of AlN film by thermal annealing for deep ultraviolet light-emitting diodes. *Appl. Phys. Lett.* **2020**, *117*, 181103. [CrossRef]
6. Chen, Z.; Liu, Z.; Wei, T.; Yang, S.; Dou, Z.; Wang, Y.; Ci, H.; Chang, H.; Qi, Y.; Yan, J.; et al. Improved Epitaxy of AlN Film for Deep-Ultraviolet Light-Emitting Diodes Enabled by Graphene. *Adv. Mater.* **2019**, *31*, 1807345. [CrossRef]

7. He, S.; Xu, Y.; Qi, L.; Li, Z.; Cao, B.; Wang, C.; Zhang, J.; Wang, J.; Xu, K. Growth of low-threading-dislocation-density GaN on graphene by hydride vapor phase epitaxy. *Jpn. J. Appl. Phys.* **2017**, *56*, 030308. [CrossRef]
8. Kim, J.; Bayram, C.; Park, H.; Cheng, C.-W.; Dimitrakopoulos, C.; Ott, J.A.; Reuter, K.B.; Bedell, S.W.; Sadana, D.K. Principle of direct van der Waals epitaxy of single-crystalline films on epitaxial graphene. *Nat. Commun.* **2014**, *5*, 4836. [CrossRef]
9. Qiao, K.; Liu, Y.; Kim, C.; Molnar, R.J.; Osadchy, T.; Li, W.; Sun, X.; Li, H.; Myers-Ward, R.L.; Lee, D.; et al. Graphene Buffer Layer on SiC as a Release Layer for High-Quality Freestanding Semiconductor Membranes. *J. Nano Lett.* **2021**, *21*, 4013–4020. [CrossRef]
10. Kim, Y.; Cruz, S.S.; Lee, K.; Alawode, B.O.; Choi, C.; Song, Y.; Johnson, J.M.; Heidelberger, C.; Kong, W.; Choi, S.; et al. Remote epitaxy through graphene enables two-dimensional material-based layer transfer. *Nature* **2017**, *544*, 340–343. [CrossRef]
11. Kong, W.; Li, H.; Qiao, K.; Kim, Y.; Lee, K.; Nie, Y.; Lee, D.; Osadchy, T.; Molnar, R.J.; Gaskill, D.K.; et al. Polarity governs atomic interaction through two-dimensional materials. *Nat. Mater.* **2018**, *17*, 999–1004. [CrossRef] [PubMed]
12. Jeong, J.; Wang, Q.; Cha, J.; Jin, D.K.; Shin, D.H.; Kwon, S.; Kang, B.K.; Jang, J.H.; Yang, W.S.; Choi, Y.S.; et al. Remote heteroepitaxy of GaN microrod heterostructures for deformable light-emitting diodes and wafer recycle. *J. Sci. Adv.* **2020**, *6*, eaaz5180. [CrossRef] [PubMed]
13. Wang, D.; Lu, Y.; Meng, J.; Zhang, X.; Yin, Z.; Gao, M.; Wang, Y.; Cheng, L.; You, J.; Zhang, J. Remote heteroepitaxy of atomic layered hafnium disulfide on sapphire through hexagonal boron nitride. *Nanoscale* **2019**, *11*, 9310. [CrossRef] [PubMed]
14. Jiang, J.; Sun, X.; Chen, X.; Wang, B.; Chen, Z.; Hu, Y.; Guo, Y.; Zhang, L.; Ma, Y.; Gao, L.; et al. Carrier lifetime enhancement in halide perovskite via remote epitaxy. *Nat. Commun.* **2019**, *10*, 4145. [CrossRef]
15. Guo, Y.; Sun, X.; Jiang, J.; Wang, B.; Chen, X.; Yin, X.; Qi, W.; Gao, L.; Zhang, L.; Lu, Z.; et al. A Reconfigurable Remotely Epitaxial VO2 Electrical Heterostructure. *Nano Lett.* **2020**, *20*, 33–42. [CrossRef]
16. Su, J.; Liang, D.; Zhao, Y.; Yang, J.; Chang, H.; Duan, R.; Wang, J.; Sun, L.; Wei, T. Freestanding GaN substrate enabled by dual-stack multilayer graphene via hydride vapor phase epitaxy. *Appl. Surf. Sci.* **2020**, *526*, 146747. [CrossRef]
17. Deng, Z.; Wang, X. Strain engineering on the electronic states of two-dimensional GaN/graphene heterostructure. *RSC Adv.* **2019**, *9*, 26024. [CrossRef]
18. Xu, Y.; Cao, B.; Li, Z.; Cai, D.; Zhang, Y.; Ren, G.; Wang, J.; Shi, L.; Wang, C.; Xu, K. Growth Model of van der Waals Epitaxy of Films: A Case of AlN Films on Multilayer Graphene/SiC. *ACS Appl. Mater. Interfaces* **2017**, *9*, 44001. [CrossRef]
19. Ullah, S.; Yang, X.; Ta, H.Q.; Hasan, M.; Bachmatiuk, A.; Tokarska, K.; Trzebicka, B.; Fu, L.; Rummeli, M.H. Graphene transfer methods: A review. *Nano Res.* **2021**, *14*, 3756–3772. [CrossRef]
20. Song, Y.; Zou, W.; Lu, Q.; Lin, L.; Liu, Z. Graphene Transfer: Paving the Road for Applications of Chemical Vapor Deposition Graphene. *Small* **2021**, *17*, 2007600. [CrossRef]
21. Kim, H.; Lu, K.; Liu, Y.; Kum, H.S.; Kim, K.S.; Qiao, K.; Bae, S.-H.; Lee, S.; Ji, Y.J.; Kim, K.H.; et al. Impact of 2D–3D Heterointerface on Remote Epitaxial Interaction through Graphene. *ACS Nano* **2021**, *15*, 10587–10596. [CrossRef]
22. Zhang, L.; Li, X.; Shao, Y.; Yu, J.; Wu, Y.; Hao, X.; Yin, Z.; Dai, Y.; Tian, Y.; Huo, Q.; et al. Improving the quality of GaN crystals by using graphene or hexagonal boron nitride nanosheets substrate. *ACS Appl. Mater. Interfaces* **2015**, *7*, 4504–4510. [CrossRef] [PubMed]
23. Lee, J.-Y.; Min, J.-H.; Bae, S.-Y.; Park, M.-D.; Jeong, W.-L.; Park, J.-H.; Kang, C.-M.; Lee, D.-S. Multiple epitaxial lateral overgrowth of GaN thin films using a patterned graphene mask by metal organic chemical vapor deposition. *J. Appl. Cryst.* **2020**, *53*, 1502–1508. [CrossRef]
24. Horcas, I.; Fernandez, R.; Gomez-Rodriguez, J.M.; Colchero, J.; Gomez-Herrero, J.; Baro, A.M. WSXM: A software for scanning probe microscopy and a tool for nanotechnology. *Rev. Sci. Instrum.* **2007**, *78*, 013705. [CrossRef] [PubMed]
25. Badokas, K.; Kadys, A.; Mickevičius, J.; Ignatjev, I.; Skapas, M.; Stanionytė, S.; Radiunas, E.; Juška, G.; Malinauskas, T. Remote epitaxy of GaN via graphene on GaN/sapphire templates. *J. Phys. D Appl. Phys.* **2021**, *54*, 205103. [CrossRef]
26. Haboeck, U.; Siegle, H.; Hoffmann, A.; Thomsen, C. Lattice dynamics in GaN and AlN probed with first- and second-order Raman spectroscopy. *Phys. Status Solidi C* **2003**, *0*, 1710–1731. [CrossRef]
27. Davydov, V.Y.; Kitaev, Y.E.; Goncharuk, I.N.; Smirnov, A.N.; Graul, J.; Semchinova, O.; Uffmann, D.; Smirnow, M.B.; Mirgorodsky, A.P.; Evarestov, R.A. Phonon dispersion and Raman scattering in hexagonal GaN and AlN. *Phys. Rev. B* **1998**, *58*, 12899. [CrossRef]
28. Bleu, Y.; Bourquard, F.; Loir, A.-S.; Barnier, V.; Garrelie, F.; Donnet, C. Raman study of the substrate influence on graphene synthesis using a solid carbon source via rapid thermal annealing. *J. Raman Spectrosc.* **2019**, *50*, 1630. [CrossRef]
29. Ferrari, A.C.; Meyer, J.C.; Scardaci, V.; Casiraghi, C.; Lazzeri, M.; Mauri, F.; Piscanec, S.; Jiang, D.; Novoselov, K.S.; Roth, S.; et al. Raman Spectrum of Graphene and Graphene Layers. *Phys. Rev. Lett.* **2006**, *97*, 187401. [CrossRef]
30. Malard, L.M.; Pimenta, M.A.; Dresselhaus, G.; Dresselhaus, M.S. Raman spectroscopy in graphene. *Phys. Rep.* **2009**, *473*, 51–87. [CrossRef]
31. Mun, D.-H.; Bae, H.; Bae, S.; Lee, H.; Ha, J.-S.; Lee, S. Stress relaxation of GaN microstructures on a graphene-buffered Al_2O_3 substrate. *Phys. Status Solidi RRL* **2014**, *8*, 341–344. [CrossRef]
32. Wang, S.; Zhang, Y.; Abidi, N.; Cabrales, L. Wettability and Surface Free Energy of Graphene Films. *Langmuir* **2009**, *25*, 11078–11081. [CrossRef] [PubMed]
33. Liu, F.; Zhang, Z.; Rong, X.; Yu, Y.; Wang, T.; Sheng, B.; Wei, J.; Zhou, S.; Yang, X.; Xu, F.; et al. Graphene-Assisted Epitaxy of Nitrogen Lattice Polarity GaN Films on Non-Polar Sapphire Substrates for Green Light Emitting Diodes. *Adv. Funct. Mater.* **2020**, *30*, 2001283. [CrossRef]

34. Al Balushi, Z.Y.; Miyagi, T.; Lin, Y.-C.; Wang, K.; Calderin, L.; Bhimanapati, G.; Redwing, J.M.; Robinson, J.A. The impact of graphene properties on GaN and AlN nucleation. *Surf. Sci.* **2015**, *634*, 81–88. [CrossRef]
35. Lundin, W.V.; Zavarin, E.E.; Sakharov, A.V.; Zakheim, D.A.; Davydov, V.Y.; Smirnov, A.N.; Eliseyev, I.A.; Yagovkina, M.A.; Brunkov, P.N.; Lundina, E.Y.; et al. Growth of III-N/graphene heterostructures in single vapor phase epitaxial process. *J. Cryst. Growth* **2018**, *504*, 1–6. [CrossRef]
36. Bedell, S.W.; Lauro, P.; Ott, J.A.; Fogel, K.; Sadana, D.K. Layer transfer of bulk gallium nitride by controlled spalling. *J. Appl. Phys.* **2017**, *122*, 025103. [CrossRef]
37. Park, J.-H.; Lee, J.-Y.; Park, M.-D.; Min, J.-H.; Lee, J.-S.; Yang, X.; Kang, S.; Kim, S.-J.; Jeong, W.-L.; Amano, H.; et al. Influence of temperature-dependent substrate decomposition on graphene for separable GaN growth. *Adv. Mater. Interfaces* **2019**, *6*, 1900821. [CrossRef]

CURRICULUM VITAE

Name	Kazimieras Badokas
Contacts	kazimieras.badokas@ff.vu.lt
Education	**2018–2022** Vilnius University, PhD, Materials Engineering
	2016–2018 Vilnius University, MSc (*Magna Cum Laude*), Optoelectronics
	2012–2016 Vilnius University, BSc, Applied Physics
Scientific career	**2020–2022** Junior researcher and lecturer at Vilnius University
	2018–2020 Research assistant at Vilnius University
	2017 Intern at NASA Ames Research Center (CA, U.S.)
	2013–2017 Engineer and technician at Vilnius University
Awards	**2019** Baltic-American Freedom Foundation grant to conduct research at MIT (MA, U.S.), canceled due to pandemic in 2020
	2018 INFOBALT award for scientific research
	2018 Lithuanian-American Innovation Award finalist, work among Top 5 Lithuanian-American innovations
	2017 Award of the President of the Republic of Lithuania for the excellence and achievements in the field of Technological science

NOTES

NOTES

NOTES

NOTES

Vilniaus universiteto leidykla
Saulėtekio al. 9, III rūmai, LT-10222 Vilnius
El. p. info@leidykla.vu.lt, www.leidykla.vu.lt
bookshop.vu.lt, journals.vu.lt
Tiražas 20 egz.